

**ASSESSMENT OF THE POTENTIAL OF ENHANCING RAINFALL THROUGH  
WEATHER MODIFICATION IN KENYA**

**NGAINA JOSHUA NDIWA**

**I56/65916/2010**

**A Dissertation submitted in partial fulfilment of the degree of Master of Science in  
Meteorology of the University of Nairobi**

**June 2012**

## DECLARATION

I hereby declare that this dissertation project is my work and has not been presented in any university or learning institution for academic award;

Sign.....

Date.....04/07/2012

**NGAINA JOSHUA NDIWA**

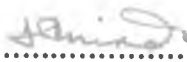
**156/65916/2010**

**Supervisors:**

Sign.....

Date.....04/07/2012

**Prof. N. J MUTHAMA**

Sign.....

Date.....04/07/2012

**Dr. J.M ININDA**

## ABSTRACT

The study assessed the potential of enhancing rainfall through weather modification. The specific objectives were aimed at determining the seasonal wind pattern; investigation of the temporal and spatial variation of atmospheric aerosols; identification of the cloud types and simulation of the effects of cloud seeding on precipitation. The study focused on enhancing rainfall during the months of October –November –December which constitute the short rain season due to the easiness of its prediction.

The datasets used included observed rainfall (1971 -2010), National centers for environmental prediction (NCEP) global wind reanalyses (1971 -2010), Moderate resolution Imaging Spectro-radiometer (MODIS) aerosol optical depth and mass concentration (2005 and 2006 October –November –December (OND), Advanced Very High Resolution Radiometer sensor (AVHRR) satellite imagery (316<sup>th</sup> Julian) and initial and boundary conditions from the Global Model for Europe (GME). Rainfall anomaly index, time series analysis, composite wind analysis, HYbrid Single-Particle Lagrangian Integrated Trajectory (HYSPLIT), object oriented image classification and Consortium Of Small scale Modelling (COSMO) model simulation were used to achieve the objective.

The 2005 and 2006 OND season were picked to represent the dry and wet years respectively during the OND season. These two years were subjected for further analysis. The pentad rainfall distribution indicated peak values mid-season during both dry and wet years. HYSPLIT backward trajectory indicated that most aerosols were continental in origin during dry year and oceanic origin during wet year. The low level winds were observed along the equator to be dominantly north easterlies with maximum wind speeds of  $4.9 \text{ ms}^{-1}$  during dry season and south-easterlies with maximum wind speeds of  $6\text{ms}^{-1}$  during the wet OND season. The aerosol optical depth (AOD550) and mass concentration were found to have higher values and highly variable during the wet rainfall season than dry rainfall season.

It was noted that strato type of clouds dominated over Lodwar, Marsabit and Wajir during dry OND season while Kakamega Kisumu and Makindu were dominated by cumulo type of clouds during wet OND season. The error matrix based on training and testing analysis showed that the overall accuracy for dry and wet OND season image classification exceeded 90% with kappa coefficient of over 0.8. COSMO Model simulation results indicated that cloud seeding with intermediate Cloud Condensation Nuclei (CCN) concentration lead to significant increase in total accumulated precipitation. However high'CCN concentration was noted to have a reduced effect on accumulate precipitation.

The study concluded that there was a possibility of enhancing rainfall through cloud seeding if adequate knowledge of dominant wind pattern; temporal and spatial variability of atmospheric aerosols and distribution of cloud types. This information would be used to form basis of feasibility and experimental studies on clouds atmosphere interaction effects on precipitation. This would go a long way towards achievement of Kenya's vision 2030.

## DEDICATION

*This study is dedicated to my Loving Parents, Mr. and Mrs. **PATRICK NGAINA***

## **ACKNOWLEDGEMENTS**

I would like to acknowledge the almighty GOD for giving me the opportunity, strength, ability and good health to carry out this research and my entire my studies.

I wish to express my sincere gratitude to my supervisors Professor Jeremiah Nzioka Muthama and Dr. Joseph Mwalichi Ininda for inculcating in me the spirit of hard work. As my supervisors, their untiring mentorship and valuable discussion made it possible to complete this work. Indeed it was an enriching experience to work them.

Special thanks go to Mr Detlev (DWD), Mr Cosmin (Romanian National Meteorological agency), Mr Sakwa and Mr.Mungai (KMD) and the entire staff of the Kenya Meteorological Department for providing the COSMO Model source codes and supporting the author in Model compilation and implementation for the study.

Special thanks are to the entire academic and technical staff at the department of Meteorology at the University of Nairobi for their continued support throughout the study.

I extent my special gratitude to my family especially my dad, mum, Judi, Ken, Susy, Vella, James, and paul for their unending moral and financial support during the course of this study. Special thanks to Mr. and Mrs. Reuben Mengich and their family for their hospitality during my this study.

Last but not least, I extent my special gratitude's to Mr. Bethwel Mutai and Mr. Paul Mining'wa for always standing by my side during both good and hard times, my friends Roonie, Reen, Ongoma, Kimchong and Niko.

MAY GOD BLESS YOU ALL

**JOSHUA NDIWA NGAINA**

**UNIVERSITY OF NAIROBI**

**JUNE 2012**

## TABLE OF CONTENTS

TITLE.....	i
DECLARATION .....	ii
ABSTRACT .....	iii
DEDICATION.....	v
ACKNOWLEDGEMENTS.....	vi
LIST OF FIGURES .....	ix
LIST OF TABLES .....	x
LIST OF ACRONYMS.....	xi
<b>CHAPTER ONE</b> .....	1
1 INTRODUCTION.....	1
1.1 Problem statement.....	2
1.2 Hypotheses of the study .....	2
1.3 Objectives of study .....	3
1.4 Justification of study .....	3
1.5 Area of study .....	4
1.5.1 Overview: Kenya.....	4
1.5.2 Physical features and climate characteristics of the area of study.....	4
<b>CHAPTER TWO</b> .....	6
2 LITERATURE REVIEW .....	6
<b>CHAPTER THREE</b> .....	14
3 DATA AND METHODOLOGY .....	14
3.1 Data.....	14
3.1.1 Rainfall data.....	14
3.1.2 NCEP global wind reanalyses datasets. ....	14
3.1.3 Daily mean atmospheric aerosol products .....	15
3.1.4 Satellite imagery .....	16
3.1.5 Global model for Europe.....	17
3.1.6 Cloud cover data.....	17
3.2 Methodology.....	18
3.2.1 Data quality control.....	18
3.2.2 Wind circulation patterns and its effects on local aerosol distribution .....	19
3.2.3 Temporal and spatial variability of atmospheric aerosols.....	20
3.2.4 Cloud type identification and image classification.....	21
3.2.5 Simulation of aerosol effects on precipitation.....	24

<b>CHAPTER FOUR</b> .....	27
4 RESULTS AND DISCUSSION .....	27
4.1 DATA QUALITY CONTROL.....	27
4.2 Wind circulation and its effects on local aerosols distribution.....	28
4.2.1 Rainfall anomaly index .....	28
4.2.2 HYbrid Single-Particle Lagrangian Integrated trajectory (HYSPLIT) analysis	31
4.2.3 Composite wind analysis.....	33
4.3 Spatial and temporal variability of aerosols over Kenya .....	35
4.3.1 Aerosol optical depth at 550 nm over Kenya .....	35
4.3.2 Aerosol mass concentration over Kenya.....	38
4.4 Clouds detection and classification.....	40
4.4.1 Image processing and cloud classification .....	40
4.4.2 Accuracy assessment.....	42
4.5 Effects of cloud seeding on precipitation .....	45
4.5.1 Simulated horizontal wind fields and accumulated precipitation.....	45
4.5.2 Assessment of effects of cloud seeding simulation .....	48
<b>CHAPTER FIVE</b> .....	49
5 SUMMARY, CONCLUSIONS AND RECOMMENDATIONS.....	49
5.1 Summary .....	49
5.2 Conclusions .....	51
5.3 Recommendations.....	51
REFERENCES .....	53
APPENDIX A: Pentad calendar .....	60
APPENDIX B: Temporal variation of atmospheric aerosols. ....	61
APPENDIX C: Procedure for obtaining precipitation simulation from COSMO Model.....	63
APPENDIX D: The INPUT_INT2LM Namelist used in this study .....	64
APPENDIX E: The runtime control parameters of the COSMO Model.....	69



## LIST OF FIGURES

Figure 1: Topographic map of Kenya (courtesy of GeoNova).....	5
Figure 2: Map of Kenya showing the area of study and rainfall stations used.....	16
Figure 3: Schematic diagram illustrating steps and type of data used in cloud classification	23
Figure 4: The principle of bi-spectral technique (Ito, 2000) .....	24
Figure 5: Analysis of variance over selected rainfall stations in Kenya .....	27
Figure 6: Time series of averaged seasonal rainfall anomaly index (1971-2010).....	29
Figure 7: Pentad rainfall during dry (2005) OND season .....	30
Figure 8: Pentad rainfall during wet (2006) OND season.....	30
Figure 9: Mean spatial distribution of rainfall during OND rainfall season .....	31
Figure 10: HYSPLIT back trajectory during dry rainfall season (15 <sup>th</sup> November 2005) .....	32
Figure 11: HYSPLIT back trajectory during wet rainfall season (15 <sup>th</sup> November 2005).....	33
Figure 12: Wind patterns at 700hPa during dry OND season (2005,1974,1998 &1975) .....	34
Figure 13: wind patterns at 700hPa during wet years (2006, 1977, 1982, 2002).....	35
Figure 14: Aerosol optical depth during dry and wet OND season over Lodwar .....	36
Figure 15: Aerosol optical depth during dry and wet OND season over Kakamega .....	36
Figure 16: Aerosol optical depth during dry and wet OND season over Dagoretti.....	37
Figure 17: Mean spatial distribution of AOD550during (a) dry and (b) wet rainfall season ..	37
Figure 18: Aerosol mass concentration during dry and wet OND season over Lodwar.....	39
Figure 19: Aerosol mass concentration during dry and wet OND season over Kakamega ....	39
Figure 20: Aerosol mass concentration during dry and wet OND season over Dagoretti .....	39
Figure 21: Mean spatial distribution of AMC during (a) dry and (b) wet rainfall season .....	40
Figure 22: Classified clouds with eCognition during the dry OND rainfall season .....	41
Figure 23: Classified clouds with eCognition during the wet OND rainfall season.....	42
Figure 24: Error Matrix based on TTA Mask for dry OND season.....	43
Figure 25: Error Matrix based on TTA Mask for wet OND season .....	44
Figure 26: Cloud type class accuracy during dry OND season .....	44
Figure 27: Cloud types accuracy during wet OND season .....	44
Figure 28: Simulated horizontal wind (m/s) and accumulated precipitation ( $\times 10^3 \text{ m}^3$ ) for low CCN concentration.....	46
Figure 29: Simulated horizontal wind (m/s) and accumulated precipitation ( $\times 10^3 \text{ m}^3$ ) for intermediate CCN concentration .....	46
Figure 30: Simulated horizontal wind (m/s) and accumulated precipitation ( $\times 10^3 \text{ m}^3$ ) for high CCN concentration.....	47
Figure 31: Time series of total accumulated precipitation for different Model runs .....	47
Figure 32: Comparison of 24 hour simulated and observed rainfall .....	48
Figure 33: Atmospheric optical depth during wet and dry OND season. ....	61
Figure 34: Atmospheric mass concentration during wet and dry OND season.....	62

## LIST OF TABLES

Table 1: List of rainfall stations and their location .....	15
Table 2: Channel of NOAA/AVHRR/3 .....	17
Table 3: Short-cut Bartlett test.....	28
Table 4: Classification of the dry, normal and wet rainfall anomaly scenarios .....	30

## LIST OF ACRONYMS

ANOVA.....	Analysis of variance
ART.....	Aerosol and Reactive Trace gases
AOD550.....	Aerosol Optical Depth measured at 550nm
AOD.....	Aerosol Optical Depth
AVHRR.....	Advanced Very High Resolution Radiometer
Cb.....	Cumulonimbus
CCN.....	Cloud Condensation Nuclei
Ci.....	Cirrus
Cg.....	Cumulonimbus congestus
COSMO.....	Consortium for Small-Scale Modeling
Cm.....	Medium level clouds
Cu.....	Cumulus
DEM.....	Digital Elevation Model
DWD.....	Deutscher Wetterdienst
ENSO.....	El Niño Southern Oscillation
FNEA.....	Fractal Net Evolution Approach
GDAS.....	Global Data Assimilation System
GME.....	Global Model for Europe
GRIB.....	Gridded Binary Data
GOK.....	Government of Kenya
HYSPLIT.....	HYbrid Single-Particle Lagrangian Integrated Trajectory
INT2LM.....	Interpolating program for COSMO Model
IPCC.....	Intergovernmental Panel on Climate Change
IR.....	Infra Red
ISDR.....	International Strategy for Disaster Management
ITCZ.....	Inter-Tropical Convergence Zone
KMD.....	Kenya Meteorological Department
LST.....	Land Surface Temperature
MAM.....	March April May
MODIS.....	Moderate resolution imaging Spectro-radiometer
NCAR.....	National Centers for Environmental Research
NIR.....	Near Infra Red
NOAA.....	National oceanic and atmospheric administration
NASA.....	National Atmospheric and Space Administration

NetCDF.....	Network Common Data Format
NWP.....	Numerical Weather Prediction
OND.....	October –November –December season
PCA.....	Principal Component Analysis
PCA –T.....	Principal Component Analysis (Temporal Mode)
POES.....	Polar Orbiting Environmental Satellites
RAI.....	Rainfall Anomaly Index
Sc.....	Strato-Cumulus
St.....	Stratus
SST.....	Sea Surface Temperature
TTA.....	Training and Testing Analysis
UTC.....	Universal Time Coordinates
WMO.....	World Meteorological Organization

## CHAPTER ONE

### 1 INTRODUCTION

The economies and livelihoods of the countries in equatorial Africa are weather dependent, whose variation affects related economic activities, such as agriculture (Centella *et al.*, 1999). The high rainfall variability implies that in some years, there is excess rainfall while in others there is rainfall deficit. In Kenya, agriculture which is mainly rain-fed and the mainstay of the economy contributes to over 26% of the gross domestic product and supports the livelihoods of about 80% of the rural population. However, the country is classified as a water-scarce country with renewable fresh water per capita at 647 m<sup>3</sup> against the United Nations recommended minimum of 1,000 m<sup>3</sup> (GOK, 2007). The intensified competition for fresh water resources by agricultural, industrial, and domestic users would lead to a sharp increase in stress on aquatic and wetland ecosystems.

The successive years of drought and flood events would continue being manifested in terms of frequent food insecurity, energy crisis, shortage of water resources and other socio economic disruptions such as transport and in insurance industry (Ininda et al, 2007). Moreover, the inadequacy of environmental water supplies in much of the world has been significantly exacerbated by declining trends in water quality due to increased pollution. By 2020, between 75 and 250 million people are projected to be exposed to an increase of water stress due to climate change (IPCC, 2007).

Most adaptation strategies have focussed on reducing the impacts of climate change such as increased frequency and magnitude of extreme events for increased resilience of the local population. These include short term, medium term and long term adaptation plans whose priorities are based on availability of required resources and capacity to implement these strategies. Other adaptation strategies locally employed are community driven initiatives involving communities or individuals making their own decisions on the best response measures based on their experience or information they receive.

For example, community initiatives included Sakai community adaptation project which identified farming community in Sakai to promote the integration of vulnerability and adaptation to climate change into sustainable development plans and planning processes and the Nganyi Community adaptation strategy that involved study of indigenous knowledge and modern-day climate change which aimed to enhance the resilience of vulnerable communities to the negative impacts of climate variability and adapt to climate change through integration of indigenous knowledge and modern-day climate risk management

science, and the development and use of innovative dissemination strategies that incorporates the indigenous knowledge and modern-day science systems (Reid, 2007). Adaptation strategies involving weather modification programs remain unexplored.

Currently, operational weather modification programs involving cloud seeding activities aimed at enhancing precipitation or mitigating hail fall exist in more than 24 countries. These include Australia, South Africa, Israel, Thailand and United States. Static, dynamic and hygroscopic cloud seeding techniques are used to modify the weather over potential regions. The commonly used seeding agents are silver-iodide, lead iodide, dry ice and hygroscopic flares (Curie et al, 2007b).

Despite the fact that rapid progress in weather modification has been made in the last three decades, fundamental issues regarding weather modification remain unresolved. These include critical uncertainties that are not yet resolved, inadequate understanding of the chain of physical processes involving cloud atmosphere interactions and limited capability to prove the success or failure of some weather modification concept. These uncertainties have resulted to critical questions regarding the seeding location, seeding time, variation of seeding amount, precipitation processes in seeded and unseeded cases and suitable seeding agents useful in practice.

### **1.1 Problem statement**

One of the consequences of climate change over Kenya is reduced rainfall over some parts of the country. This will lead to diminished water resource. The water shortage will have direct and indirect adverse impacts on national development by affecting investments in agriculture, livestock, food security, industries, tourism, infrastructure, health, shelter, transport and communication, among other sectors. This will be manifested in terms of limited socio-economic development which will hamper the achievement of the country's long term development blueprint (Vision 2030) aimed at making it a globally competitive and prosperous with a high quality of life by year 2030 (GOK, 2007). In view of this the government of Kenya has adopted weather modification as one of the strategy of achieving vision 2030. However, little research exists on weather modification over the country.

### **1.2 Hypotheses of the study**

In this study the hypotheses to be tested were that:

1. The winds pattern associated with dry and wet episodes in Kenya are not different.

2. The increased amount of rainfall observed over the area of study are not associated with dominating cumulonimbus clouds
3. The variability in total accumulated precipitation is not dependent in the concentration of cloud condensation nuclei used for seeding

### **1.3 Objectives of study**

The main objective of this study is to assess the potential of enhancing rainfall through weather modification in Kenya. To achieve this main objective, four specific objectives were pursued. These are;

1. To determine the wind circulation and its effect on local aerosol properties during the wet and dry OND season over Kenya.
2. To analyse the spatial-temporal variability of atmospheric aerosols during the wet and dry OND season over Kenya.
3. To identify and classify the dominant type of clouds during wet and dry OND season over Kenya.
4. To simulate the effects of cloud seeding on precipitation during OND season over Kenya

### **1.4 Justification of study**

Increasing demands for water make the potential for enhancing the sources, storage, and recycling of freshwater a legitimate area of study. It is estimated that global water consumption will increase by approximately 3,800 km<sup>3</sup> per year by 2025. Moreover, at least 30% of the average annual flow of a stream must remain in place if the ecological health of the streams and related ecosystems is to be maintained (Jury, 2007). Much of this water will have to be obtained from natural systems. This consumption increase will cause additional depletion of river flows in many areas, with substantial environmental consequences

The observed frequent drought conditions and the associated drop in water supply from major water towers such as Mt. Kenya and Mt. Elgon will necessitate a means of augmenting stream flows in Kenya. One possible measure to improve water supply, especially for agriculture which accounts for over 70% fresh water use is through enhance precipitation by cloud seeding. This could potentially contribute to alleviating water resource stresses and severe weather hazards given the existence of entire suite of new tools and techniques. However, few experiments have been done on weather modification in Kenya.

## **1.5 Area of study**

### **1.5.1 Overview: Kenya**

Kenya, lies between latitudes 5° North and 5° south and between longitudes 34° and 42° east. It has a land area of about 569,137 km<sup>2</sup> with great diversity of landforms such as ranging from glaciated mountain peaks with permanent snow cover. The country is split by the Great Rift Valley into the Western part which slopes down into Lake Victoria from the Mau ranges and Mount Elgon (4,300m) and the Eastern part which is dominated by Mt. Kenya and the Aberdare ranges that rise to altitudes of 5,200m and 4,000m respectively.

The Lakes occupy about 2% of total area, 18% is occupied by high potential areas while arid and semi-arid lands occupy about 80% of total land area. The major drainage basins in Kenya include the Lake Victoria, Rift Valley, Athi, Tana and Ewaso Nyiro basins and North-Eastern. Drainage is influenced by the country's topography. The main rivers drain from the central highlands into the Rift Valley and eastwards into the Indian Ocean and westwards into Lake Victoria, while those north of Mount Elgon and from the highlands along the Sudan-Ethiopian border drain mainly into Lake Turkana.

Although Kenya has numerous rivers, a comparatively small number are permanent. The major rivers include the Tana, Athi, Nzoia, Yala, Sondu, Nyando and Mara. Some of the major rivers such as Tana have been dammed upstream to provide hydroelectric power, irrigation water and water for domestic use. Kenya's lakes are categorized as fresh and saline/alkaline. Fresh water lakes include Lakes Baringo, Naivasha and Victoria (Africa's largest fresh water lake shared with Tanzania and Uganda). Most other lakes are within the Rift Valley and many of these are alkaline and valuable tourist attractions. The levels and volumes of these lakes fluctuate seasonally.

### **1.5.2 Physical features and climate characteristics of the area of study**

In Kenya, annual rainfall follows a bimodal seasonal pattern. Generally, the long rains occur in March-April-May (MAM) while the short rains occur in October-November-December (OND), but with variations. The country's climate is influenced by its equatorial location, topography, the Indian Ocean, the inter-tropical convergence zone (ITCZ) and the El Niño Southern Oscillation events. Other factors known to influence precipitation include tropical storms, easterly waves, jet streams, the continental low-level trough, and extra-tropical weather systems (Ogallo, 1989).



The influence of the ITCZ is modified by the altitudinal differences, giving rise to varied climatic regimes. There is a wide range between the maximum and minimum temperatures; from below freezing point on the snow-capped Mount Kenya to over 40<sup>0</sup>C in northwestern, northern and northeastern parts of the country. The seasonal rainfall patterns are controlled by the seasonal migration of the ITCZ. The complex topographical patterns, the existence of large lakes, variations in vegetation type and land–ocean contrasts giving rise to high spatial and temporal variation in precipitation over the region.

The ENSO events also influences the distribution of the climatological zones which changes from season to season. The Indian Ocean influences the rainfall systems of these regions. The rainfall anomalies during the El Niño years indicate that in most cases, rainfall over these zones is usually more enhanced during the El Niño episodes than during the other phases of the ENSO phenomenon. During the March-April-May season, most parts of the country tend to receive normal rainfall during El Niño years. However, the coastal areas have a tendency to receive above-normal Mean Average Monthly (MAM) rainfall during these years.



Figure 1: Topographic map of Kenya (courtesy of GeoNova)

## CHAPTER TWO

### 2 LITERATURE REVIEW

The section sought to review works in the study area including circulation patterns associated with observed rainfall, aerosols –cloud interaction and their effects on precipitation, cloud classification and identification from using satellite information and studies involving modeling of cloud –atmosphere interactions.

Aerosol particles modify atmospheric radiative fluxes and interact with clouds. As documented in the IPCC 2007 report (IPCC 2007), the global influence of natural and anthropogenic aerosols on the atmosphere is not well understood. As shown by recently published and contradictory findings the state of knowledge is even worse concerning the effects of aerosol particles on radiation, temperature, and cloud formation on the regional scale (Bell et al., 2008).

Owing to its location across the equator and along the quasi meridional western edge of the Indian Ocean, Kenya experiences a bimodal rainfall regimes referred to as “long rains” from march to may and the “short rains” from October to December. They are associated with the north south and the south north movement of ITCZ over the region (Camberlin, 1997). At the time of rainy seasons, the meridional flow corresponding to the monsoons switches to quasi easterly flow.

Okoola (1996) used both the Rainfall Anomaly Index (RAI) and Principal component analysis in temporal mode (PCA T-mode) and noted that rainfall observational network over the East African region were not uniformly distributed. Therefore, due to the unique spatial rainfall variations over the region, results from PCA T-mode were used to affirm the results from rainfall anomaly index method. The PCA T-mode was used to isolate the years with similar spatial patterns which provided time series for unique homogeneous climatologically sub regions.

Okoola (1999) studied the mid-tropospheric winds over the east African region during the March April May rainfall season established that the Wet or dry events were associated with pools of warm or cool water over the Western Indian Ocean. Furthermore, the study identified that the occurrences of anomalous rainfall in the equatorial east African region could be described or modeled in terms of 700hpa velocity winds which showed a distinctive pattern over the region.

Gatebe (1999) studied the seasonal air transport for Kenya using kinematic trajectory modeling. Significant months for trajectory analysis were determined from a classification for synoptic circulation fields. The transport corridors for Kenya were clearly bounded and well defined. It noted that air reaching the country during the OND season originated mainly from the Sahara region and northwestern Indian Ocean of the Arabian Sea in the Northern Hemisphere and Madagascan region of the Indian ocean of the Southern Hemisphere. They showed distinctive annual cycles related to north easterlies Asian monsoon and southeasterly trade winds.

Blanchard and Woodcock, (1980) found out that aerosols production as a result of natural, anthropogenic and biogenic processes from oceans and deserts formed major sources of natural aerosols. They reported that the sea-salt production rate was estimated to be 1000 to 10,000 Tg per year (or 30 to 75% of all natural aerosols). The Sub-Saharan Africa and the steppes of China were found to be the substantial sources of wind-blown dust. The source strength of these aerosols from deserts was about 2000 Tg per year and the source strength changes with desertification and changes in wind patterns.

Studies by Hobbs et al., (1997) on anthropogenic production of aerosols from biomass burning were found to be an important source of aerosol to the tropical atmosphere during certain times of year. Other anthropogenic sources included those produced from cultivation, industrial activity and transport Soot particles and fly ash injected into the atmosphere. Biogenic sources included pollens, spores, fragment of plants and animals and other microorganisms. Estimates of the annual global production rate of aerosols suggested that the forest vegetation was an important source of atmospheric particulate matter. Decaying vegetation also served as an important source of aerosol, mainly in the small particle range.

Rosenfeld et al., (2008) showed that elevated concentrations of CCN had a tendency to increase the concentration and reduce the size of the droplets in a cloud. Apart from changing the optical properties and the radiative effects of clouds on climate, it lead to the suppression of precipitation in shallow and short lived clouds and to a greater convective overturning and more precipitation in deep convective clouds. However, the responses of cloud characteristics and precipitation processes to increasing anthropogenic aerosol concentrations represented one of the largest uncertainties in the current understanding of climate change.

Maritinsson (1999) observed a significant increase in Cloud condensation nuclei (CCN) of up to  $2000 \text{ cm}^3$  with a substantial reduction of the effective droplet radius in polluted orographic clouds over a mountain ridge. Heavy smoke from forest fires in the Amazon

were observed to reduce cloud droplet size and so delayed the onset of precipitation from 1.5 kilometers above cloud base in pristine clouds to more than 5 kilometers in polluted clouds and more than 7 kilometers in pyro-clouds. Suppression of low-level rainout and aerosol washout allowed transport of water and smoke to upper levels, where the clouds appeared “smoking” as they detrained much of the pollution.

In India, several studies on aerosol distribution have been carried out. Ranjan et al., (2007) to analyzed the seasonal variability of AOD over Rajkot region and reported lower values in winter and higher values in summer, the latter being due to high wind velocities producing larger quantities of wind-driven dust particles. Dey et al., (2005) investigated the aerosol concentrations over Kanpur region and found that urban and industrial aerosols contributed more than 75% of the observed AOD during the post-monsoon and winter seasons whereas natural aerosols contributed 60% of the total AOD during the pre-monsoon and monsoon seasons. Prasad et al., (2007) examined aerosol variations over the Indo-Gangetic plain and found that the AOD was higher in the summer season than in the winter season.

Gupta et al., (2008) showed that satellite data had tremendous potential for mapping the distribution and properties of aerosols. Furthermore, it could be used to for deriving indirect estimates of particulate matter. Since ground measurements are sparse in many regions of the world, satellite data is able to serve as a surrogate measure for the monitoring of particulate matter air quality. The study noted that aerosol concentrations, particularly in Africa and Asia were continually increasing in virtually all urbanized and industrialized regions because of growing populations, rapid urbanization with consequent land use changes, increasing motorized traffic and increasing industrialization within and adjacent to urban areas.

Zhang et al., (2006c) used reflection measured by MODIS on Terra and Aqua satellites at the channels  $0.65\mu\text{m}$  and  $2.1\mu\text{m}$ . They retrieved cloud optical thickness, efficient radius and liquid water content over the Qilian Mountains of the Tibetan Plateau for the period between 2002 and 2005. They also did correlation analysis between these three parameters and 6 hr precipitation over the Qilian Mountains. Their analytical results provided important information on the water resource usage and suitability of weather modification program in west China.

Rosenfeld et al., (2005) noted that remote sensing of the seeding signature from space was very powerful. It was capable of providing near real time feedback to the targeting efficacy of the cloud seeding. Glaciated seeded tracks in super-cooled layer clouds were observed to exist for more than an hour after seeding, with a very slow spreading rate

reaching a width of less than 15 km by that time. Satellite observed signatures of glaciogenic seeding for hail prevention in Alberta, Canada, showed that seeding glaciated only portions of the convective elements

Khain et al., (2000) showed that clouds were an important part of the atmosphere and the climate system, since they determine and influence a variety of atmospheric processes states. The representation of clouds in atmospheric models has to be paid particular attention, as the formation and spatial distribution of clouds and precipitation is crucial for numerical weather prediction (NWP) as well as for climate modeling. Unfortunately, each individual cloud itself is a very complex non linear sub-system of the atmosphere and the delicate problem with cloud and precipitation modeling is to find a compromise between a very detailed but costly description in terms of spectral balance equations for the size distributions of many types of hydrometeors and a coarse but efficient parameterization in terms of equations dealing with certain integrals of the size distributions (e.g., only mass densities).

Beside observations, numerical models are important tools to improve our current understanding of the role of natural and anthropogenic aerosol particles for the state of the atmosphere. On the global scale there exist a large number of model systems and corresponding applications of models addressing the quantification of the effect of anthropogenic aerosol particles on climate change. Due to a lack of computer capacity global climate models however often include simplifications and approximations (Lohmann and Schwartz, 2009).

Zhan et al., (2005) suggested that conventional methods of assessing accuraciés which based in per-object pixel measurements considered were inadequate in assessing the quality of per object classifications because their spatial unit was no longer a pixel but an object. However, to allow comparisons between methods, certain standard procedures were followed. The study suggested other ways of assessing the accuracy of maps generated with fuzzy classification such as classification stability and best classification result. They were only used to improve the accuracy of maps generated with the object based approach.

Bruintjes, (1999) reviewed different cloud seeding methods extensively used in weather modification. These include static and dynamic mode of cloud seeding (for super cooled clouds) and hygroscopic seeding which involved modification of warm clouds. The study noted that there probably existed a spectrum of clouds that had enough liquid water to support a cloud precipitation process that could be accelerated by static, dynamic or

hygroscopic seeding. The major task lied with identifying those clouds in order to deliver the right amount of seeding material to them at the right time.

Orville (1996) reviewed the progress of cloud modeling in weather modification. The study established that the use of cloud models in hypothesis development, assessment of cloud seeding potential, and development of experimental design, operational decisions, project evaluation and understanding of seeding effects related to weather modification were very critical. Furthermore, it noted that the status of cloud-scale and Mesoscale numerical models and the capability of making pertinent observations in the atmosphere were quite advanced. These cloud models could be used to understand the results of seeding in weather modification.

Cotton and Pielke (1995) concluded that physical studies and inferences drawn from statistical seeding experiments over the last 50 years suggested that there existed a much more limited window of opportunity for precipitation enhancement by the static-mode of cloud seeding than was originally thought. The window of opportunity for cloud seeding appeared to be limited to clouds which were relatively cold-based, continental and having cloud top temperatures in the range  $-10$  to  $-25^{\circ}\text{C}$ . This explained why some cloud seeding experiments were successful while other seeding experiments yielded inferred reductions in rainfall from seeded clouds or no effect.

Mather et al. (1996b) applied a pyrotechnic method of delivering salt, based on a fog dispersal method which helped reduce a number of technical difficulties associated with preparing, handling and delivery of very corrosive salt particles. Seeding with this system was no more difficult than silver iodide flare seeding. Compared to conventional methods of salt delivery, the flares produced smaller-sized particles in the size range of  $0.5$  to  $10\mu\text{m}$ . Seeding trials with this system suggested that the pyro-techniques produced a cloud droplet spectrum that was broader and with fewer numbers, which would be expected to increase the chance for initiation of collision and coalescence processes.

Cooper et al., (1997) simulated the low-level evolution of droplet spectra in seeded and unseeded plumes. Based on a parcel ascending in the cloud updrafts, they calculated the evolution of droplet spectra by vapour deposition and collection. Their calculations were designed to emulate the effects of hygroscopic seeding with the South African flares. The calculations showed that introduction of particles in the size-range characteristic of the flares resulted in an acceleration of the collision and coalescence process. If the hygroscopic particles were approximately  $10\mu\text{m}$  in size, precipitation was initiated faster.

Furthermore, insertion of more numerous  $1\mu\text{m}$  hygroscopic particles resulted to formation of higher concentrations of drizzle.

Yin et al., (2001) used model simulations and suggested that there was a narrow window of opportunity within which seeding could be successful. This window was longer for hygroscopic seeding than for glaciogenic seeding. Thus, in addition to the size of the hygroscopic particles, the timing of seeding was crucial. Whereas seeding too early could lead to reduced rain amounts, too late seeding would cause the process to fail. It was possible that seeding reduced the rain drop size, thus increasing the evaporation below cloud base altering cold-pool and downdraft effects. This would lead to enhanced interactions and updrafts in neighbouring clouds. If seeding shifted the raindrop spectrum to larger drops, the opposite response would be expected.

Nakijima, et al., (2001) showed that for optically thick clouds, there was an expected increase in cloud albedo associated with the decrease in droplet size. For optically thinner clouds, there was an unexpected decrease of cloud albedo with decreasing droplet size. Clouds with the same vertical extent and liquid water content were observed to have higher short wave albedo over continents than over oceans. The study associated water bodies with suppressed cloud reflectivity and enhanced cloud reflectivity in polluted areas.

Li et al., (2002b) in their study in tropical oceanic convective system documented that cloud microphysical properties in deep convective regions significantly differed from those in strati-form regions. Along with the westward propagation and during the development of tropical convection, the area-mean vertical velocity profiles exhibited major ascending motion below 500mb in the left half of the cloud and the maximum ascending motion between 300 and 500mb in the right half indicating that the left half of the cloud underwent the deep convective development while the anvil cloud grew in the right half. These accounted for much larger rainfall in the left half than in the right half.

Silverman (2003) noted that the initial seeding of single clouds and subsequent single (target) cloud analyses provided statistical evidence that seeding increased rainfall. This was according to simulations using models with a detailed treatment of cloud microphysics and increased concentration of larger drops which generated an increase in graupel numbers and masses. Such increases caused more rain although it remained unclear how the clouds would be affected for the extended length of time that was suggested by some of the measurements.

Chen et al. (2005) simulated an event of cold vortex precipitation and hails in the Liaoning Province of northeast China with the three dimensional convective cloud models. It showed that the ice particles melting especially the graupels played the main role in cloud and precipitation formation. It further argued that the optimal time of silver iodide seeding was at the cloud mature stage when the convective-stratiform mixed clouds had a considerably seeding potential to enhance precipitation.

A feasibility study by Griffith et al, (2007) on operational cloud seeding program in the Salt River and the Wyoming ranges in Wyoming reported an average increase of 10% precipitation in November through March. These lead to their recommendation of these months for cloud seeding since the majority of seedable storms were present. The study further noted that a properly designed cloud seeding project could increase precipitation by more than 10% in target areas without adverse effects on surrounding areas.

A study by Curie et al, (2007) using a cloud resolving mesoscale model investigated the effects of cloud seeding by silver-iodide. When the seeding was performed at cold part of a long-lasting convective cloud to determine where, when and what amount of silver-iodide would lead to optimum effects of seeding in terms of rain precipitation enhancement and reduction of hail. They found out that the accumulated hail and rain precipitation at the surface were significantly reduced (- 6.47%) or increased (8.43%) if the seeding zone in form of a circular sector was seeded at early stage of cloud development (5.4 min of simulated time) for the largest seeding agent amount used.

Muehlbauer and Lohmann (2009) showed that the distribution of orographic precipitation strongly depended on the composition and size of the background aerosols. If these aerosols lacked sufficient giant cloud condensation nucle or efficient ice nuclei, precipitation would develop slowly and a higher fraction of the precipitation moved by the winds to the lee side of the mountain. In such a case, seeding could increase the efficiency of precipitation formation on the upwind side of the mountain.

Khain, (2009) simulated single clouds and cloud clusters and showed that depending on the cloud type, the influence of aerosol changes on cloud microphysics could affect precipitation amounts very differently. Based on the models comprehensive cloud microphysics and the used fine grid meshes such simulations were limited to small domains and short time scales. This was pointed out to the used small scales which was a major reason for differences in the net aerosol effect on the precipitation amount since macro physical buffers existed that could not be considered.



Bangert et al. (2011) used COSMO ART model to simulate the regional scale effects of the aerosol cloud interaction over Europe. It found that in the simulation of the CCN distribution, the treatment of aerosol size distribution and chemical composition was necessary and could not be replaced by correlation of CCN with either aerosol number or mass concentration. These simulations showed that the presence of CCN and clouds were closely related spatially. Furthermore, high aerosol and CCN number concentrations in the vicinity of clouds at high altitudes were found and nucleation of secondary particles enhanced above the clouds. This was attributed to an efficient formation of gaseous aerosol precursors above the cloud due to more available radiation, transport of gases in clean air above the cloud, and humid conditions.

## CHAPTER THREE

### 3 DATA AND METHODOLOGY

The data and the methods used to achieve the objectives of the present study are described in this chapter.

#### 3.1 Data

The data used in the present study include daily and monthly station rainfall totals; monthly NCEP global wind reanalyses datasets; daily atmospheric optical depth and mass concentration; satellite imagery; GME Model data; cloud cover data

The methods used included the Rainfall anomaly index, HYSPLIT backward trajectory analysis, composite wind analysis, time series analysis, object based image classification and COSMO model simulation.

##### 3.1.1 Rainfall data

The rainfall data used in this study consisted of daily and monthly records at 21 stations distributed over Kenya within the period 1971–2010 obtained from the Kenya Meteorological Department (KMD). The list of rainfall stations used in the study is shown in Table 1. Stratified sampling was used to select representative stations used for the study based on availability and continuity of the stations records. The OND monthly records referred to as “the short rains season” over Kenya were used to generate the seasonal time series for 1971–2010 from which the anomalously wet and dry years were delineated. This study used the October –November –December rainfall season due to its predictability over Kenya (Ogallo, 1989). The pentads (five day total) were calculated from the daily observations. The pentad calendar used to pick dates to be totalled is given in appendix A.

##### 3.1.2 NCEP global wind reanalyses datasets.

This wind data used in this study consisted of once-daily grid-point datasets operationally analyzed at NCEP. These NCEP analyses are produced using the four-dimensional data assimilation system. The NCEP/NCAR monthly wind data with  $2.5^{\circ} \times 2.5^{\circ}$  resolution (Kalnay et al., 1996) were adapted for the study. These wind data used were taken at 1200 UTC (3:00pm local time) when convective activities were expected to be significant over the region of study. The NCEP global reanalysis datasets used in this study were obtained

through the NOAA. The zonal and meridional wind component dataset were downloaded from the NCEP website for the period 1971 to 2010 (<ftp://ftp.cdc.noaa.gov/Datasets>).

### 3.1.3 Daily mean atmospheric aerosol products

In this study, the daily mean atmospheric aerosol products used included the aerosol optical depth measured over land at 550nm (AOD550) and aerosol mass concentration. This dataset was acquired from the MODIS Terra Level-3 daily mean data product at a spatial resolution of  $1^{\circ} \times 1^{\circ}$  over representative locations over the region of study. These products were retrieved from MODIS satellite and measured by MODIS sensor onboard the Terra satellite launched on December 18, 1999 mainly for global monitoring of the atmosphere, terrestrial ecosystems, and oceans (Savtchenko, 2004).

The period considered included selected wet and dry rainfall seasons delineated in the study. The estimated uncertainty of the MODIS AOD and mass concentration products have been reported to be  $0.05 \pm 0.15$  over land (Chu et al., 2003) and  $0.03 \pm 0.05$  over the ocean. The NASA MODIS aerosol retrieval algorithm has recently been improved and the products denoted as C005 implemented to correct systematic biases in the MODIS algorithm used previously (Remer et al., 2005). Table 1 and figure 2 shows the list of all rainfall stations and their spatial distribution used in the present study

**Table 1: List of rainfall stations and their location**

Station	Longitude	Latitude	Station	Longitude	Latitude
Colche	36.08	0.63	Marsabit	37.98	2.32
Dagoreti	36.75	-1.13	Mombasa	39.62	-4.03
Eldoret	35.28	0.58	Moyale	39.05	3.53
Garissa	39.63	-0.48	Mtwapa	39.7	-3.9
Kakamega	34.77	0.28	Nakuru	36.07	-0.28
Kisii	34.78	-0.68	Narok	35.83	-1.13
Kisumu	34.67	-0.1	Nyahururu	36.35	-0.42
Lamu	40.9	-2.27	Thika	37.1	-1.02
Lodwar	35.62	3.7	Voi	38.57	-3.4
Makindu	37.83	-2.28	Wajir	40.07	1.75
Mandera	41.87	3.93			

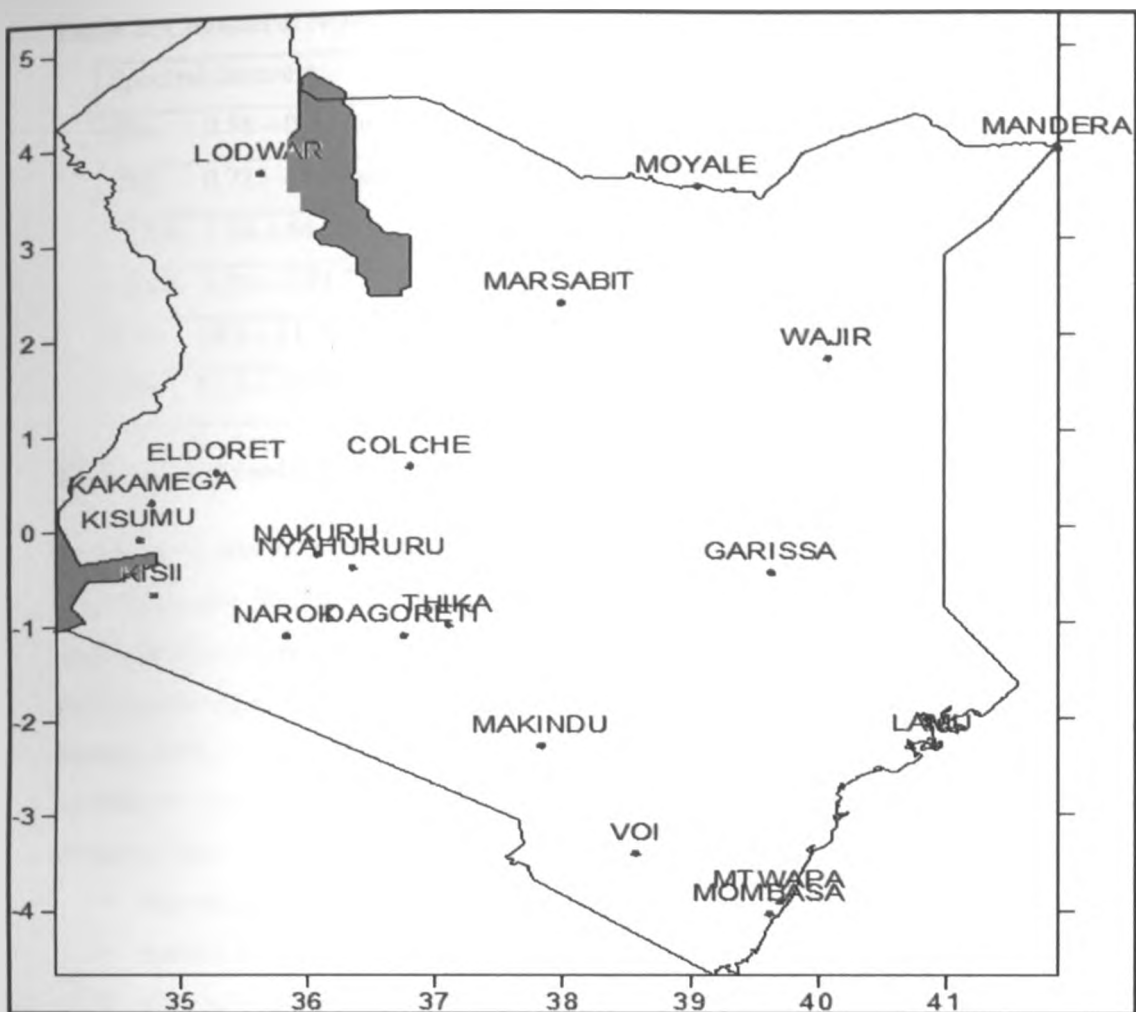


Figure 2: Map of Kenya showing the area of study and rainfall stations used

### 3.1.4 Satellite imagery

The classification of clouds was performed using daily high resolution satellite imagery (NOAA/AVHRR) for 316<sup>th</sup> Julian date observed during November during October – November –December. The images considered were for dry and wet OND rainfall seasons. The Advanced Very High Resolution Radiometer (AVHRR) sensor is carried onboard the NOAA's Polar-orbiting Operational Environmental Satellites (POES). The AVHRR/3 sensor measures atmospheric properties in six spectral bands but only five spectral bands are transmitted to the ground at any time. Other parameters such as the time codes, quality indicators, solar zenith angles, and telemetry are also appended on the images. The NOAA-18 satellite has a spatial resolution of about 1.1 km in nadir and the 6 spectral channels with the following wavelength ranges shown in table 2.

**Table 2: Channel of NOAA/AVHRR/3**

Spectral channels	Range of electromagnetic
Ch1: 0.58 – 0.68 $\mu\text{m}$	VIS (Visible)
Ch2: 0.725 – 1.70 $\mu\text{m}$	NIR (Near infrared)
Ch3A: 1.58-1.64 $\mu\text{m}$	MIR (Middle infrared – day)
Ch3B: 3.55 – 3.93 $\mu\text{m}$	MIR (Middle infrared – Night)
Ch4: 10.3 – 11.30 $\mu\text{m}$	TIR (Thermal infrared)
Ch5: 11.5 – 12.5 $\mu\text{m}$	TIR (Thermal infrared)

**3.1.5 Global model for Europe**

In this study, the initial and boundary conditions were provided by the GME global Model from Deutscher Wetterdienst (DWD) with an icosahedral model grid. The data from this model are first pre-processed to have the data in a common format which can be processed by the interpolating model (INT2LM). The GME data sets are very large. The study used a GME bitmap data, a subset that is needed to run the COSMO Model for a special domain considered. The specific characteristics of the grid of the driving model chosen for the Model domain (Mesh size: 0.0625° ~ 7 km)

- Startlat in tot latitude of lower left grid point of total input domain = 15.0 S
- startlon in tot longitude of lower left grid point of total input domain = 23.0
- dlon in longitudinal resolution of the input grid = 52.0
- dlat in latitudinal resolution of the input grid = 15.0N
- ie in tot longitudinal grid point size = 201
- je in tot latitudinal grid point size = 193
- ke in tot vertical grid point size = 316
- pollat in geographical latitude of north pole = 90.0
- pollon in geographical longitude of north pole = -180.0

**3.1.6 Cloud cover data**

Ground based cloud observations over the selected stations in the area of study were used. These stations corresponded to stations where rainfall data were obtained for both dry and wet OND season. The ground based cloud cover data were used as control points during image classification for accuracy assessment.

3.2 Methodology

Different methods were used to achieve the objectives of the study. These methods are discussed in the subsection below.

3.2.1 Data quality control

Data quality control involves estimation of missing data and homogeneity test.

3.2.1.1 Estimation of missing data

Several methods have been recommended by WMO (1996) for the estimation of missing records in meteorological time series. In the present study, there were no missing data

3.2.1.2 Data homogeneity using Short –Cut Bartlett Method

In the present study, Short-Cut Bartlett method was used to test the homogeneity of rainfall records. This method was used to ascertain the significance of a break by testing the seasonal rainfall time series for stability of variance.

Short –Cut Bartlett’s test is a test of the hypothesis that all factor standard deviations (or equivalently variances) are equal against the alternative that the standard deviations were not all equal. The sampling distribution of the Bartlett statistic is approximately chi-square when the k factor samples were from independent normal populations. This method is very sensitive to departures from this normality assumption. The method has been used analysis of variance (ANOVA) in a statistical test of the significance of an apparent break in the slope. ANOVA supposes a normal distribution of the data and therefore testing for stability of variance. This method was applied by dividing the time series data into k equal sub periods, where  $k > 2$ . In each of these sub-periods, the sample variance  $S_k$  was given by Equation 1:

$$S_k^2 = \frac{1}{n} \left[ \sum x_i^2 - \frac{1}{n} (\sum x_i)^2 \right] \dots\dots\dots(1)$$

In equation (1) n represented the summations range over the series in the sub-period k. The largest and smallest values of  $S_k^2$  were then selected and denoted as  $S_{max}^2$  and  $S_{min}^2$  respectively. The 95% significant points for the ration  $S_{max}^2 / S_{min}^2$  was obtained by comparing this ration with the values in F-distribution table at 95% significance points. In this method, the null hypothesis is rejected if the F- value calculated is less than tabulated value.

**3.2.2 Wind circulation patterns and its effects on local aerosol distribution**

**3.2.2.1 Determination of anomalous rainfall years**

The major wet and dry years within the study period (1971–2010) were determined from the regional rainfall anomaly indices. The regional rainfall anomaly indices were defined as;

$$\bar{\gamma}_t = \frac{1}{m} \sum_{j=1}^m \frac{100X_{tj}}{\bar{X}_j} \dots\dots\dots (2)$$

Where m is the total number of rainfall stations in the region of study, j is the number of stations used,  $\bar{X}_j$  is the time dependent rainfall index as a percentage of the mean and averaged over all the stations,  $X_{tj}$  represents the time series of individual station for the OND seasonal rainfall and  $\gamma_t$  is the rainfall anomaly index

The wet years have large values of this index (>125%), while the drought years have low values of the index (<75%). The normal years had values of this index between 125% and 75%. The major wet and dry seasons were first be delineated and then averaged (composites) for each category to study the spatial and temporal evolutions of the wind circulation over the region.

**3.2.2.2 HYSPLIT back trajectory analysis**

HYbrid Single-Particle Lagrangian Integrated Trajectory (HYSPLIT) model is a computer-based air pollution modeling package used for Modeling. The HYSPLIT is a system for computing both simple air parcel trajectories and complex dispersion and deposition simulations. In this study, the model calculation method used was a hybrid between the Lagrangian approach, which used a moving frame of reference as the air parcels moved from their initial location, and the Eulerian approach, which used a fixed three-dimensional grid as a frame of reference. The pollutant trajectories were calculated on a fixed grid. Calculations were performed on archived meteorological data from the Global Data Assimilation System ran by United States National Weather Service's National Centers for Environmental Prediction (NCEP) four times a day at 00, 06, 12, and 18 UTC. NCEP post-processing of the GDAS converted the data from spectral coefficient form to 1 degree latitude-longitude (360 by 181) grids and from sigma levels to mandatory pressure levels. HYSPLIT Model output is in GRIB format. The archived data file usually contained the data in synoptic time sequence, without any missing records (Draxler and Rolph, 2012).

### **3.2.2.3 Composite wind analysis**

The composite analysis involved identifying and averaging one or more categories of fields of a variable selected according to their association with key conditions. The results of these composites were then used to generate hypotheses for patterns that were associated with the individual scenarios. The key conditions for the composite analysis in the study were the wet, normal, and dry conditions defined in section 3.2.2.1. Advantages of composite fields are that they are easy to interpret and are dimensional. A number of studies have indicated that the results obtained from composite analysis usually agree closely with those from correlation methods (Ward 1992). The approach has been used in the region by Matarira and Jury (1992) to study the synoptic scale kinematic patterns associated with the dry and wet spells in Zimbabwe. Moreover, the composite method is capable of displaying some features which would otherwise be smoothened out by correlations and many basic climatological and statistical methods.

The anomalously wet and dry years selected using methods in section 3.2.2.1 above were composed in order to isolate the circulation patterns associated with the wet and dry seasons

### **3.2.3 Temporal and spatial variability of atmospheric aerosols**

In this study, the temporal and spatial variability of atmospheric aerosols were investigated. A time series analysis was used to examine the temporal variations of aerosol optical depth measured over land at 550nm and particle mass concentration. Graphical time series analysis was used in the study. It involved plotting of scatter diagrams where various AOD550 and aerosol mass concentrations were plotted against time. The time series graphs were smoothened out with the intention of showing the natural trend of the centre of mass of the data. Smoothing always involves some form of local averaging of data such that the non-systematic components of individual observations cancel out. Graphical method is highly subjective and has the weakness of dependency on visual judgment (Muthama et al., 2008).

Spatial variability of atmospheric AOD550 nm and aerosol mass concentration was represented by spatial maps. These maps were generated based on representative stations data retrieved from MODIS aerosol product. These maps were generated with the aid of SURFER software.



### **3.2.4 Cloud type identification and image classification**

The three standard steps in image classification for cloud detection were followed in this study. These included image pre-processing, image classification and accuracy assessment.

#### **3.2.4.1 Image pre-processing**

The most effective method of identifying individual cloud types is by obtaining a Visible and an IR image of the same scene. Image processing (corrections and calibrations) and clipping the study area from satellite images was performed. The Visible (VIS) channels 1 and 2 of the data were processed for Albedo. The VIS image was used to identify cloud shapes, textures, organizational patterns, and thicknesses. Generally, the thicker the cloud, the higher its albedo and the brighter appears in visible imagery. Thin clouds are often very dark or transparent in visible imagery. Cloud texture referred to its appearance in visible imagery. The Visible satellite data was compared to an Infrared (IR) image in order to determine the height of the clouds.

The selected bands were corrected and geo-referenced. The atmospheric correction was completed the PCIgeomatica software. These images were then geo-referenced using the Surfer8 software. The IR channels 3, 4 and 5 of the data were then processed for brightness temperature. General, the higher the cloud, and the colder it appears in IR imagery. Therefore, lower warmer clouds appeared darker while high, cold clouds appeared brighter.

#### **3.2.4.2 Image classification**

Single date classifications were performed with a per-object approach for both dry and wet OND season. Figure 2 shows a schematic diagram for image classification. Standard stages for image classification as described by Lillesand et al., (2004) were followed. These include image segmentation, training stage and classification stage

##### **3.2.4.2.1 Image segmentation**

The multi-resolution segmentation was selected in the study. It resulted to a condensing of information and a knowledge-free extraction of image objects. In this method, the used AVHRR channels brightness temperatures of band 4 and 5 and cloud height were weighted by 1, whereas the Digital Elevation Model (DEM), LST and SST that showed free cloud areas, were weighted by 0.2 (Göttsche and Olesen, 2005). Since the clouds with medium area and more were important in the study, a fairly medium scale of 50 was chosen for the finest segmentation (level 1 called analysis level).

In this study, image segmentation was carried out using the commercial software eCognition software. The software has been increasingly been applied in different researches as it provides a straightforward set of tools for incorporating the spatial domain through segmentation and therefore appropriate for this study. Additionally, it allows combination of segmentation techniques with fuzzy classifiers (Hay et al., 2003). The eCognition software uses a segmentation procedure based in the computation of a heterogeneity or homogeneity criterion. According to the heterogeneity criterion, pixels are merged into bigger objects starting with one pixel object at any point in the image. Two main elements are used during the segmentation process; the scale parameter and the heterogeneity criterion.

#### **3.2.4.2.2 Training stage**

The algorithm used for the classification requires training areas which are segments representative of different cloud types. They have the same function as the training areas in the pixel based approach. Prior to the classification, a class hierarchy has to be created. The hierarchy contains all the classes to be identified and the description of the classes. The description of classes is achieved by combining different measures such as mean, standard deviation, ratio and bands (Volker, 2003). The feature space tool in the eCognition software was used to find the best feature combination and parameters which were later used by the classifier to differentiate the cloud types during the classification process.

#### **3.2.4.2.3 Classification stage**

The eCognition software uses a multidimensional membership function with the nearest neighbour classifier. The classifier uses fuzzy logic to assign objects to classes. It defines a degree of membership that ranges from 0 when there is no membership to 1 when there is full membership. The intermediate values show a partial degree of membership (Campbell, 2002). It not only allocates the primitive objects to a specific class, but also provides information about the degree of assignment of the objects to the rest of the defined classes. Fuzzy logic systems allow consideration of uncertainties in remote sensing classification process. The resulting classification shows the membership degree of each class in the cloud type map. The lower the membership value the higher the uncertainties about the allocation of the object to a category.

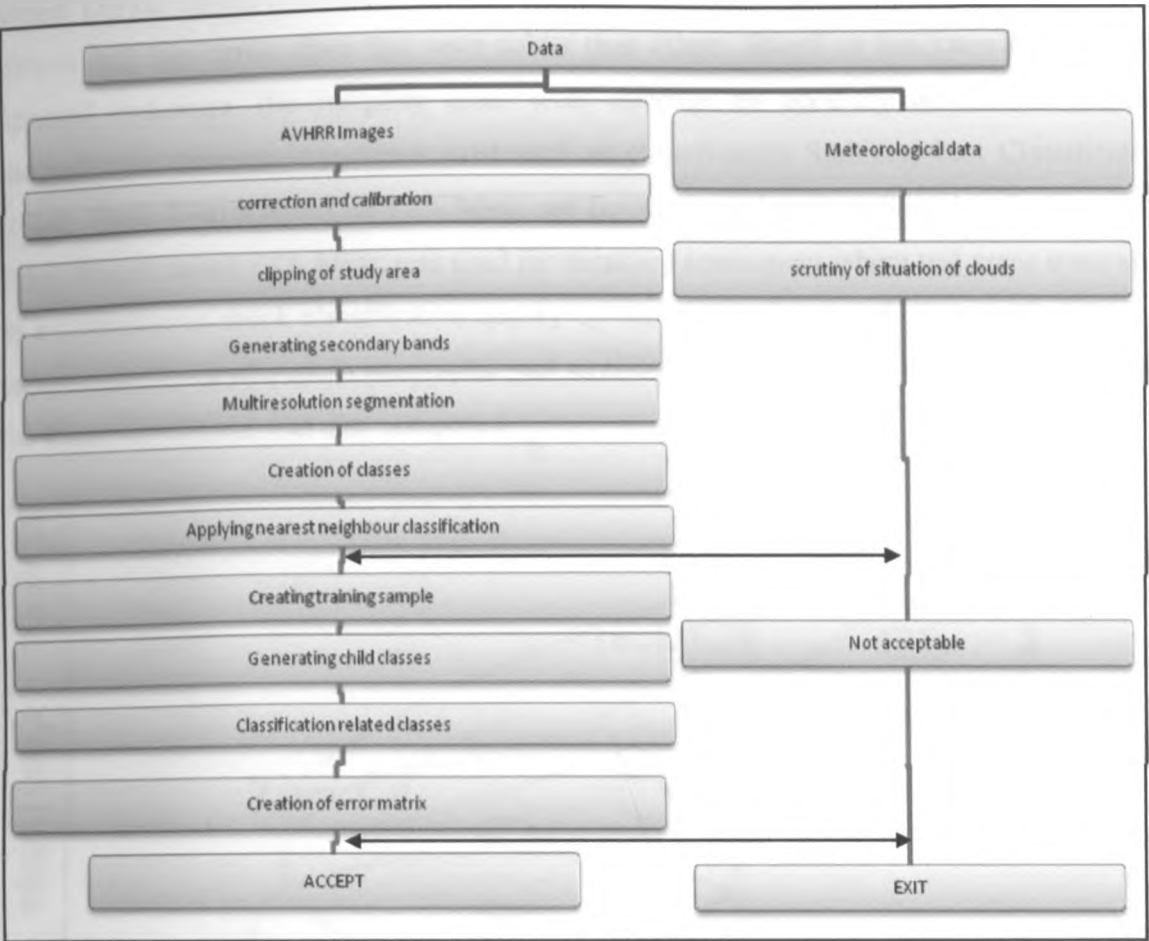


Figure 3: Schematic diagram illustrating steps and type of data used in cloud classification

3.2.4.3 Image classification accuracy assessment

Accuracy assessment methods can produce statistical outputs to check the quality of the classification results. In this study, the principle of bi-spectral technique based on the relationship between cold and brightness temperature of clouds was used to assess the accuracy of object oriented classification (figure 4). It was assumed that there was a probability of other types of clouds existing during the day when the images used in the study was taken. Therefore, it necessitated the collection of control points since accurate assessment could not be guaranteed. The regions which had the most adaptation with bi-spectral cloud classification theories were used as training samples optically. Standard methods for image classification assessment such as overall accuracy, error matrix, producer's and user's accuracy and kappa index have regularly been used.

The NIR and IR channels 3, 4, and 5 of the data were further processed for temperature and brightness. In IR image cold clouds are usually high clouds. The colors typically highlighted

the colder regions mid height clouds with TB below 230k and identified as cumulonimbus cloud. Darker clouds in IR images were associated to warm stratus, Strato-cumulus, cumulus clouds and thin cirrus cloud that were colder than others. Based on this knowledge and bi-spectral technique, the sampling areas were selected for accuracy assessment. Several methods for accuracy assessment exist such as classification Stability, best Classification Result, Error Matrix based on TTA Mask and Error Matrix based on Samples. In this study, Error Matrix based TTA Mask was used for accuracy assessment where test areas were used as a reference to check classification quality by comparing the classification with reference values called ground truth in geographic and satellite imaging based on objects. Furthermore, the kappa coefficient was also computed.

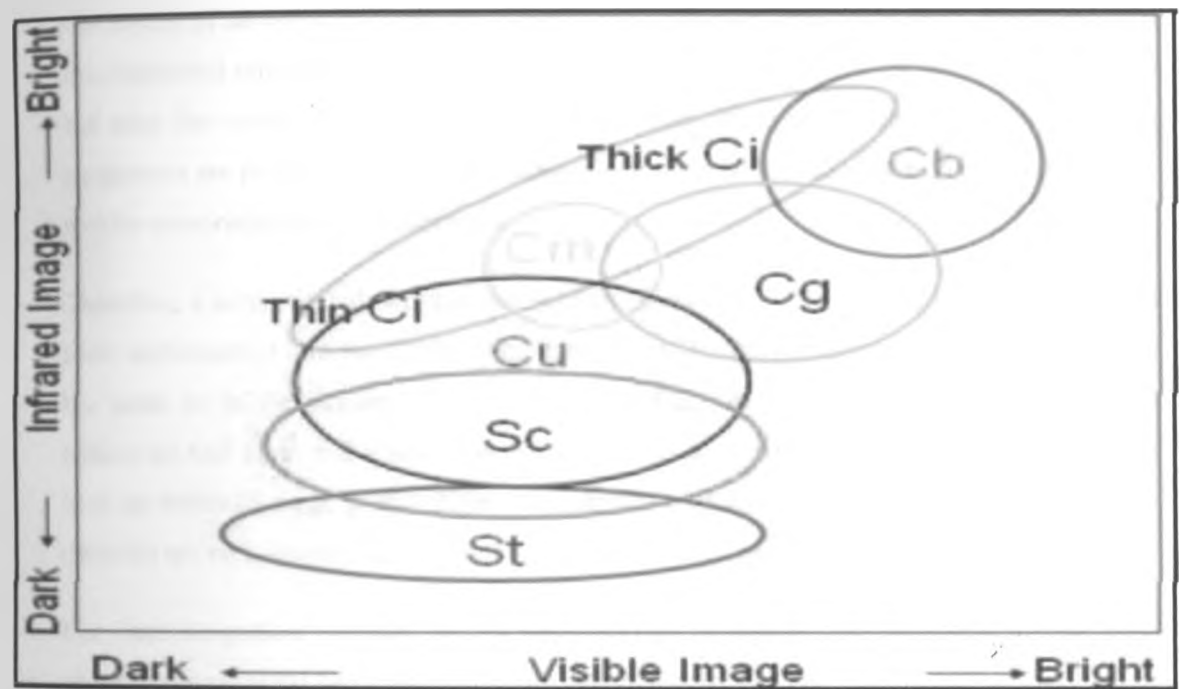


Figure 4: The principle of bi-spectral technique (Ito, 2000)

### 3.2.5 Simulation of aerosol effects on precipitation

#### 3.2.5.1 Overview of the Model system

In this study, the Consortium for Small-Scale Modelling (COSMO) Model was used in numerical weather prediction mode. This is a non-hydrostatic limited-area atmospheric prediction model designed for both operational numerical weather prediction (NWP) and various scientific applications on the meso-B and meso-γ scales. The COSMO-Model is based on the primitive thermo-hydrodynamical equations describing compressible flow in a moist atmosphere. The model equations are formulated in rotated geographical coordinates and a generalized terrain following height coordinates (Steppeler et al., 2003).

A variety of physical processes are taken into account by parameterization schemes for accurate numerical prediction of near surface weather conditions, focusing on clouds, fog, frontal precipitation, and orographically and thermally forced local wind systems. The COSMO-Model provides two kinds of output which can be written in GRIB or in NetCDF output.

The standard COSMO model uses a one moment scheme for cloud physics, i.e. only the bulk masses of the different hydrometeors (cloud droplets, raindrops, cloud ice, snow, graupel) are predicted at each grid point. For the number concentration of the particles or their sizes, certain assumptions have to be made. Therefore, such a scheme is not appropriate to study the impact of aerosols on clouds, as it works via particle numbers and sizes. More advanced microphysical schemes take into account balance equations not only for mass concentrations but also for number concentrations (so called two-moment schemes). In this way, two parameters are predicted in space and time which allowed for reconstruction of hydrometeor spectra comprising the bulk quantities.

Therefore, a sophisticated two-moment scheme developed by Seifert and Beheng (2006) has been implemented into the COSMO model. Originally, the particle types are assumed to be the same as in the standard COSMO scheme. The two important extensions include an additional hail class and a new scheme to parameterize cloud droplet nucleation based on look-up tables by Segal et al., (2006). A multitude of processes and interactions between the particles are considered. For different purposes different configurations are used.

For time integration COSMO uses a time-splitting technique. The time step for the slow processes is set at the beginning of the run which, for the 7 km resolution, amounts to 8 s. For certain fast processes (sound and gravity wave propagation, some microphysical processes) a smaller, and for very slow processes a larger time step is applied. Different time integration schemes can be chosen within COSMO. This study used a two time-level, third order Runge-Kutta method.

### **3.2.5.2 Model setup**

In this study, all simulations were performed with the non-hydrostatic numerical weather prediction model COSMO developed by the German Weather Service for their operational weather forecasts. It is based on the fully compressible Navier-Stokes equations using finite differences with a terrain following grid and rotated spherical coordinates. It allows for a wide range of spatial resolutions, provided that adequate parameterizations for the sub-grid scale processes are considered.

Three dimensional simulations have been performed in order to study the impact of aerosols. COSMO Model with the 2-moment scheme for cloud microphysics has been used with a horizontal resolution of about 7km and a time step of 10 s for the slow processes. Total simulation time was 3 h for each of the three aerosols scenarios.

The size of the model domain is described in section 3.1 (v) of 201 x 193 x 316 and comprises Kenya and adjacent regions. The model was initialized 0600UTC with data from the GME Model. In the model, cloud droplet nucleation was parameterized using the look-up tables given in Segal et al., (2006) where the number of nucleated droplets was determined by vertical velocity at cloud base and aerosol properties represented by CCN number concentration  $N_{ccn}$ , mean radius of the larger aerosol mode  $R_2$  (a bi-modal aerosol distribution is assumed), logarithm of the standard deviation of the size distribution  $\log \sigma$ , and a factor  $\epsilon$  representing the effect of the soluble fraction.

Simulations for three different aerosol scenarios of CCN concentration leading to three different typical maximum cloud droplet concentrations  $N_{drop}$  at cloud base were performed to study the impact of aerosols and thus the possible effects of cloud seeding. These scenarios included; low CCN concentration,  $N_{drop} = 5\text{ugcm}^{-3}$ , intermediate CCN concentration,  $N_{drop} = 10\text{ugcm}^{-3}$  and high CCN concentration,  $N_{drop} = 20\text{ugcm}^{-3}$ . For the control run, low CCN concentration was assumed. The cloud droplet concentrations result from these values depend on the vertical velocities that develop near cloud base and therefore on simulation time. The time it takes to form raindrops out of cloud droplets not only depends on the size of the nucleated droplets but also on the width of the cloud droplet size distribution. In the two moment scheme, a general gamma distribution with four parameters is assumed for all size distributions (with  $x$  = hydrometeor mass)

$$f(x) = Ax^v \exp(-\lambda x^\mu) \dots \dots \dots (3)$$

$A$  and  $\lambda$  are determined by the predicted number and mass densities (the 0<sup>th</sup> and 1st moment of the distribution),  $\mu$  and  $v$  have to be fixed.

4 RESULTS AND DISCUSSION

This results obtained in this study using the methods outlined in the preceding chapter are discussed in this section.

4.1 DATA QUALITY CONTROL

The results are presented in the table 3 and figure 4 for all stations used in the study at 95% significance points. The F statistics value and F critical represented the computed and tabulated F distribution sample variances respectively. In figure 5, the results showed that the ration (F computed statistics) between the highest sample variance and the smallest sample variance were less than the F tabulated statistics for all stations used. These statistics are presented in table 3. This indicated that the variance of rainfall records used in the study were significant at 95% confidence level. Therefore, the null hypothesis which stated that all factor standard deviations (or equivalently variances) were equal was accepted i.e. the rainfall records used were homogeneous against the alternative hypothesis

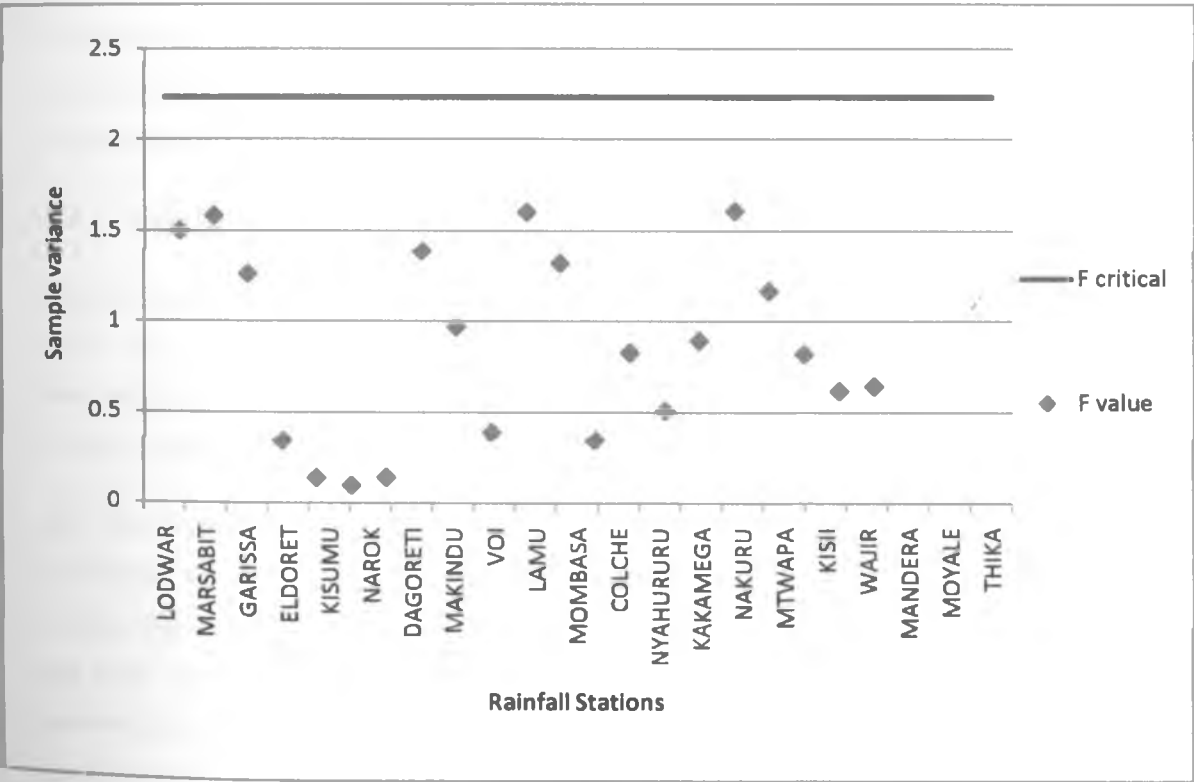


Figure 5: Analysis of variance over selected rainfall stations in Kenya

**Table 3: Short-cut Bartlett test**

STATION	F-value (Computed)	F-critical (Tabulated)	STATION	F-value (Computed)	F-critical (Tabulated)
LODWAR	1.5	2.2326	COLCHE	1.3179	2.2326
MARSABIT	1.5812	2.2326	NYAHURURU	0.3462	2.2326
GARISSA	1.2578	2.2326	KAKAMEGA	0.8278	2.2326
ELDORET	0.3444	2.2326	NAKURU	0.5102	2.2326
KISUMU	0.1392	2.2326	MTWAPA	0.8948	2.2326
NAROK	0.0976	2.2326	KISII	1.6077	2.2326
DAGORETI	0.1432	2.2326	WAJIR	1.1665	2.2326
MAKINDU	1.3857	2.2326	MANDERA	0.8214	2.2326
VOI	0.97	2.2326	MOYALE	0.6186	2.2326
LAMU	0.3906	2.2326	THIKA	0.6459	2.2326
MOMBASA	1.6016	2.2326			

## 4.2 Wind circulation and its effects on local aerosols distribution

The dominant wind direction during the OND season was investigated through composite analysis of wind with similar patterns for both the dry and wet rainfall seasons based on the rainfall anomaly index. The results are presented in the preceding sections.

### 4.2.1 Rainfall anomaly index

Rainfall anomaly indices were computed for OND rainfall seasonal for the period 1971 to 2010. The years delineated as wet, normal and dry are shown in table 4 arranged in descending order of magnitude. The mean spatial distribution of rainfall and the time series of the computed rainfall anomaly index are presented in figure 5 and figure 6 respectively.

The time series for RAI was presented in figure 6. Based on the RAI (table 4), it was established that 17, 8 and 15 years corresponded to the dry, wet and normal rainfall years respectively during the OND season. The RAI indicated that the wettest and driest year over the study region corresponded to 1997 and 2005 respectively. The 1997 wet year had anomalously high RAI of 338% compared to other wet years. Numerous studies on the wet spell observed in 1997 OND rainfall season classified the event as unique and one of the wettest periods of the last 100 years over most of east Africa (WMO, 1998). Furthermore, a detailed study by Okoola et al., (2008) on the anomalous wet spell event of October 1997 attributed this unique event to the general mechanism that causes rainfall during the short rain



season over the region. Moreover, the study by Okoola et al., (2008) established that the circulation features that were common during most of the wet events included weakening or reversal of the east west (walker type) circulation over the Indian ocean; enhanced convergence between the northern and southern hemisphere trade winds and westward moving disturbances in the low level equatorial winds.

In the study, 1997 OND season was considered as an anomalous wet year and not appropriate for further studies. Instead, 2006 was picked to represent the wet OND season while 2005 represented OND seasonal rainfall. Furthermore, wet and dry years during the OND season selected for further analysis of atmospheric aerosols corresponded to years when MODIS atmospheric aerosol products from MODIS Tera satellite were available. Figure 9 shows the long term mean spatial distribution of rainfall over the region of study. It is noted that the western parts of Kenya including Kakamega, Kisumu and Kisii recorded the highest amounts of rainfall of over 250mm during the OND rainfall season. The Northern parts of the study region (Lodwar) and most of the Eastern stations recorded low rainfall totals of less than 120mm.

A plot of pentad rainfall over selected stations to show intra-seasonal distribution of rainfall showed that during dry OND season (figure 7), rainfall was observed over many stations in November. The beginning and end of the dry season recorded depressed rainfall. The distribution of rainfall during wet OND season (figure 9) noted that significant rainfall was observed over most these selected stations throughout the season with highest amount being recorded in November.

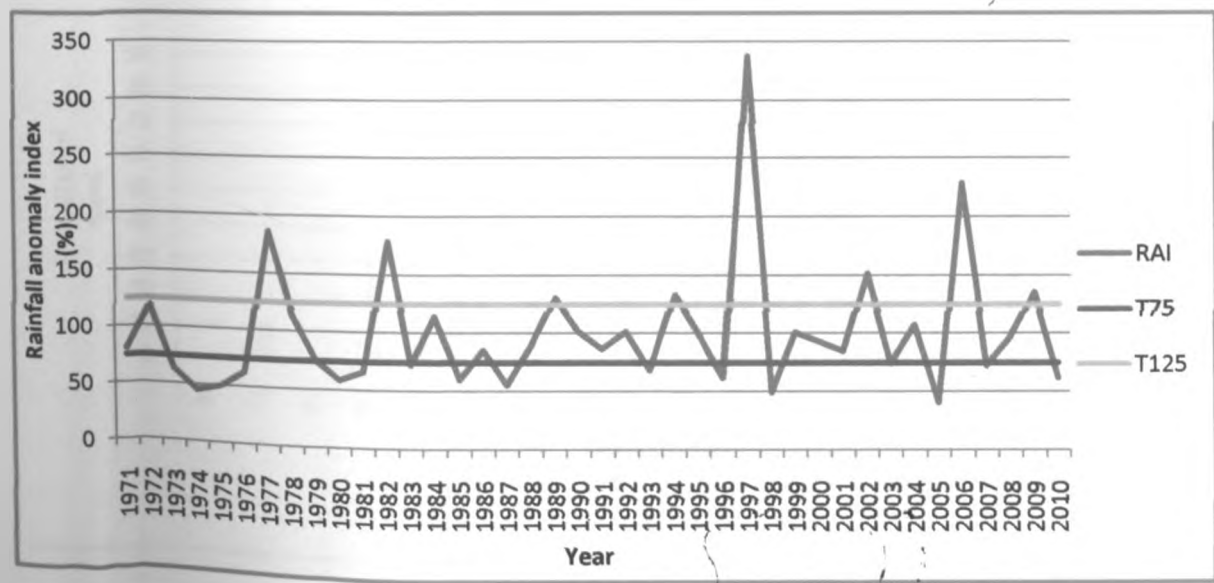


Figure 6: Time series of averaged seasonal rainfall anomaly index (1971-2010)

Table 4: Classification of the dry, normal and wet rainfall anomaly scenarios

Scenario type	Anomaly range (%)	Frequency (n = 40)	Years
DRY	$\chi_t < 75$	17	2005, 1974, 1998, 1975, 1987, 1980, 1985, 2010, 1996, 1976, 1973, 1981, 1993, 2007, 1983, 2003
NORMAL	$75 \leq \chi_t \leq 125$	15	1979, 1971, 2001, 1986, 1991, 1988, 2000, 2008, 1999, 1995, 1992, 1990, 2004, 1978, 1984, 1972
WET	$\chi_t > 125$	8	1997, 2006, 1977, 1982, 2002, 2009, 1994, 1989

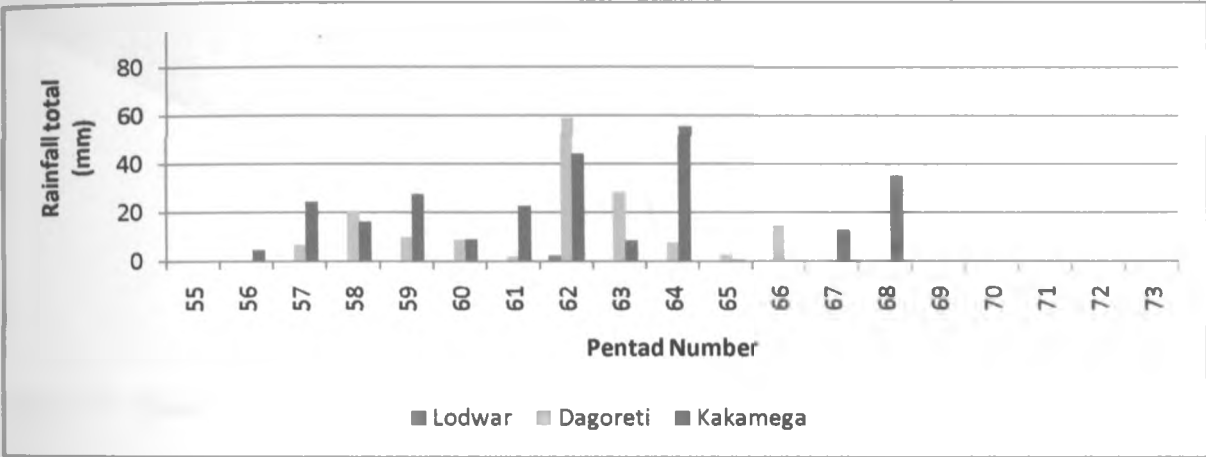


Figure 7: Pentad rainfall during dry (2005) OND season

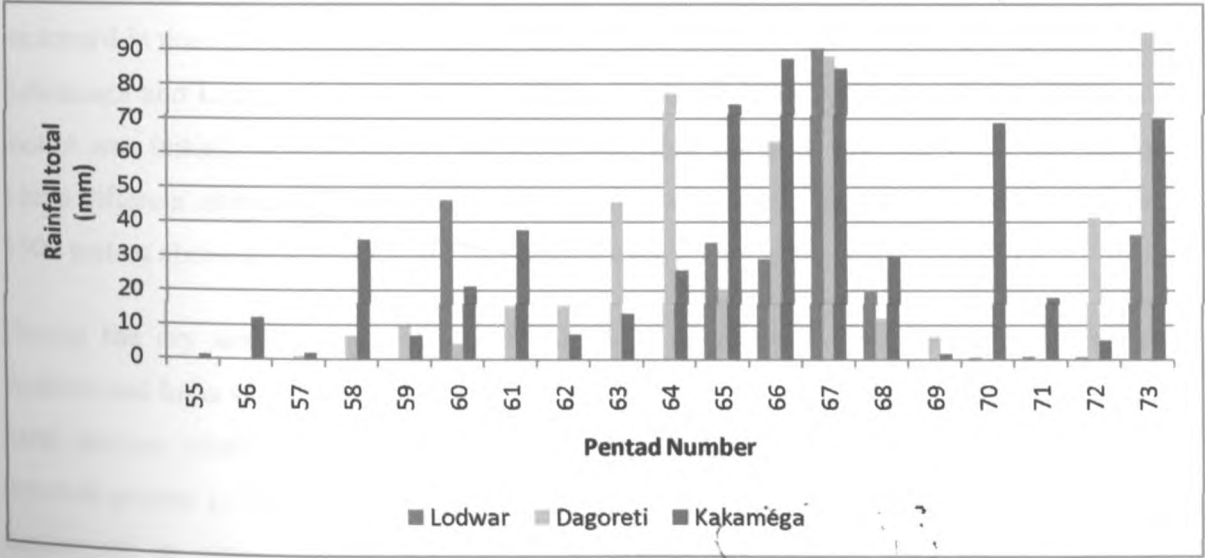
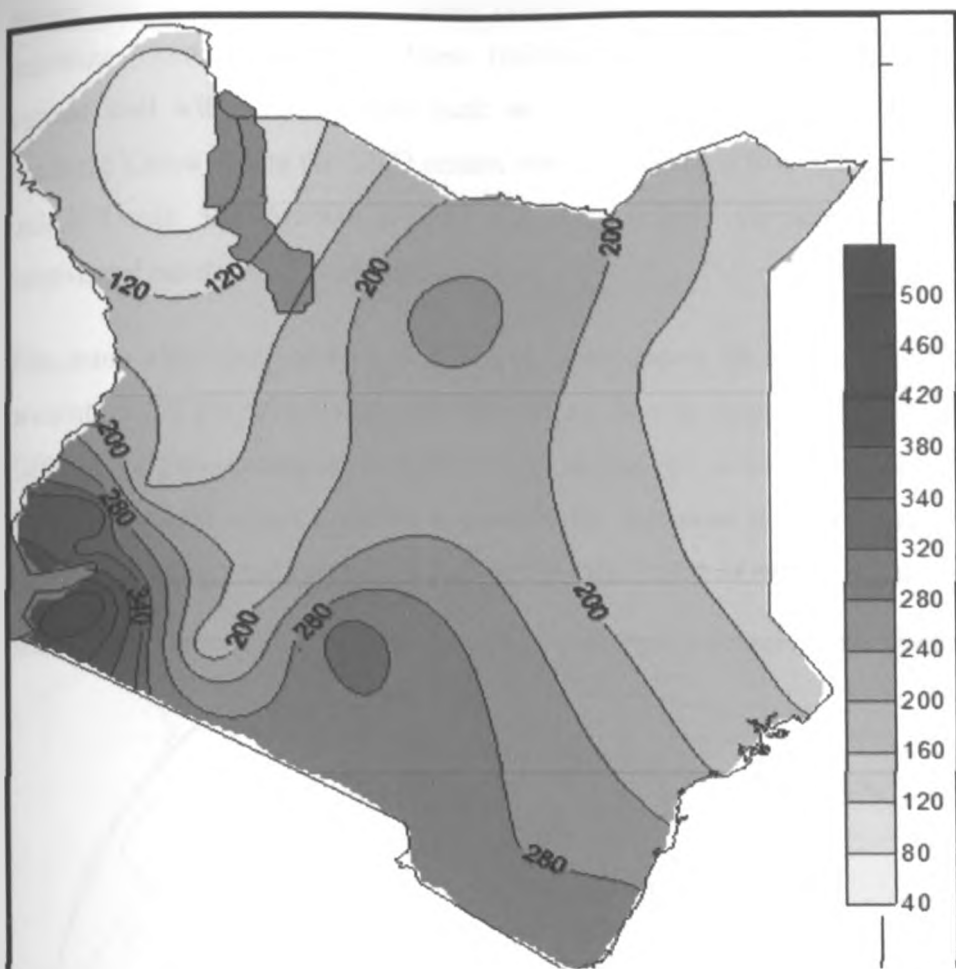


Figure 8: Pentad rainfall during wet (2006) OND season



**Figure 9: Mean spatial distribution of rainfall during OND rainfall season**

**4.2.2 HYbrid Single-Particle Lagrangian Integrated trajectory (HYSPLIT) analysis**

Backward trajectory analysis was done using the HYSPLIT model. The model was run backward in time for five days to identify the sources of atmospheric aerosols over Dagoretti, Kakamega and Lodwar during the wet (2006) and dry (2005) OND season. The HYSPLIT model was initialized at 0000UTC on 15<sup>th</sup> November for both dry and wet OND season. Three different altitudes for the stations considered were used. These were at 500, 1000 and 1500 metres above the ground level. The results were presented in figure 10 and 11.

During the dry season (figure 10), aerosols were observed to have originated from the Arabian and India subcontinent especially at levels above 1000m. At levels below 1000m, the local sources which could either be from natural or anthropogenic sources accounted for aerosols present in the atmosphere. During this period (dry), aerosols were noted to be mainly continental in nature. During the wet season (figure 11) aerosols were mostly from the southwestern parts of the Indian Ocean especially below 1000m above the ground. Above 1000m, few aerosols trajectory were observed to originate from the continental arabian and

indian sub continent region. During this period (wet) aerosols were noted to be mainly maritime (oceanic) in nature. These trajectory analysis for the wet and dry OND season agreed well with other studies such as Gatebe (1999) which had noted that pollutants reaching Kenya during the OND season mainly originated from the south western parts of the Indian Ocean and Arabian regions and were mainly characterised by their oceanic or continental nature of aerosols respectively.

The study also observed that at different levels above the ground, the atmospheric aerosol present in the atmosphere had different origins. It was assumed that these aerosols at from different origins underwent vertical mixing as they got advected inland of the study region. Therefore, these mixed aerosols accounted for enhanced rainfall observed over the central kenya and western regions which had highly mixed type of aerosol composition.

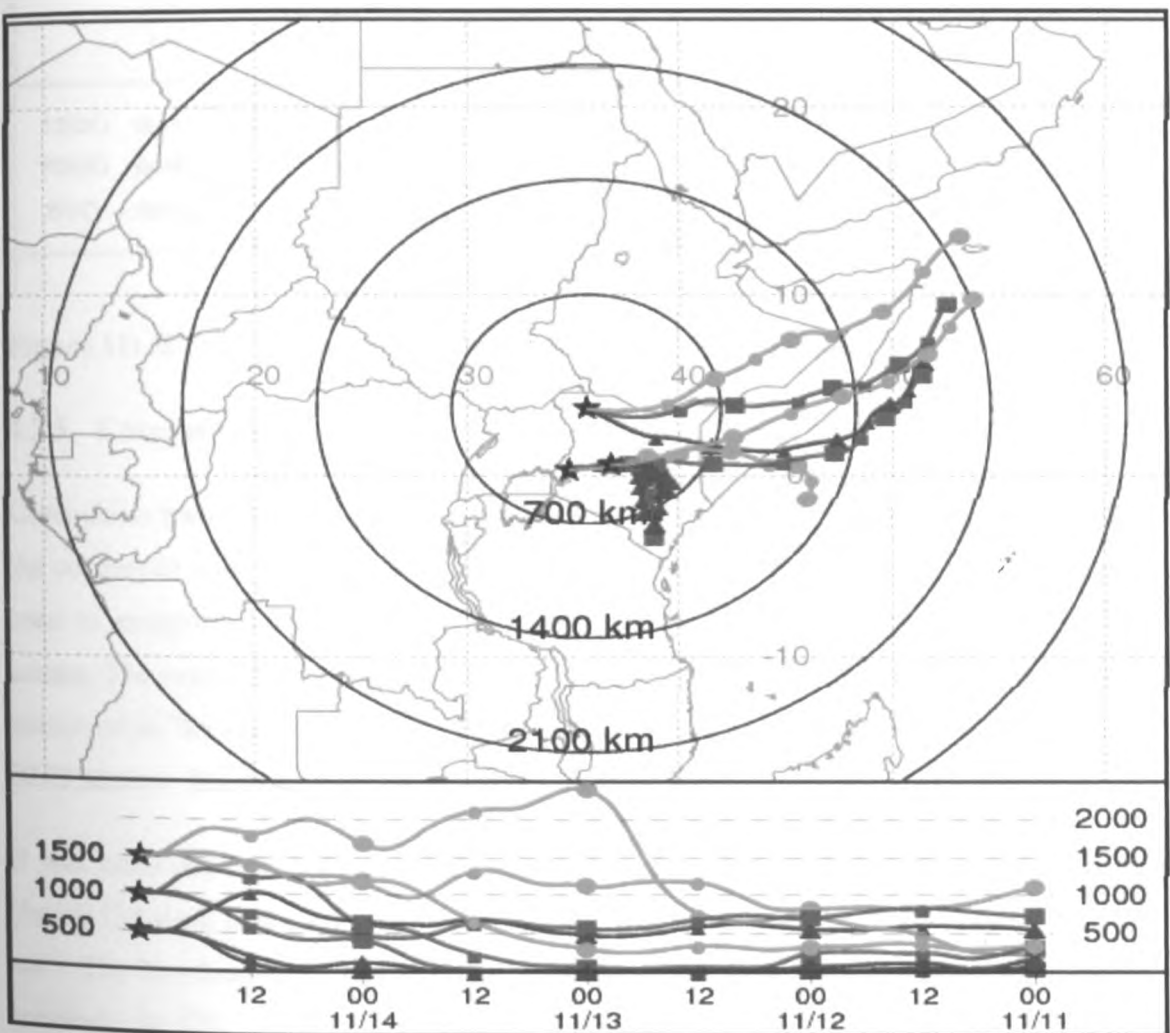


Figure 10: HYSPLIT back trajectory during dry rainfall season (15<sup>th</sup> November 2005)

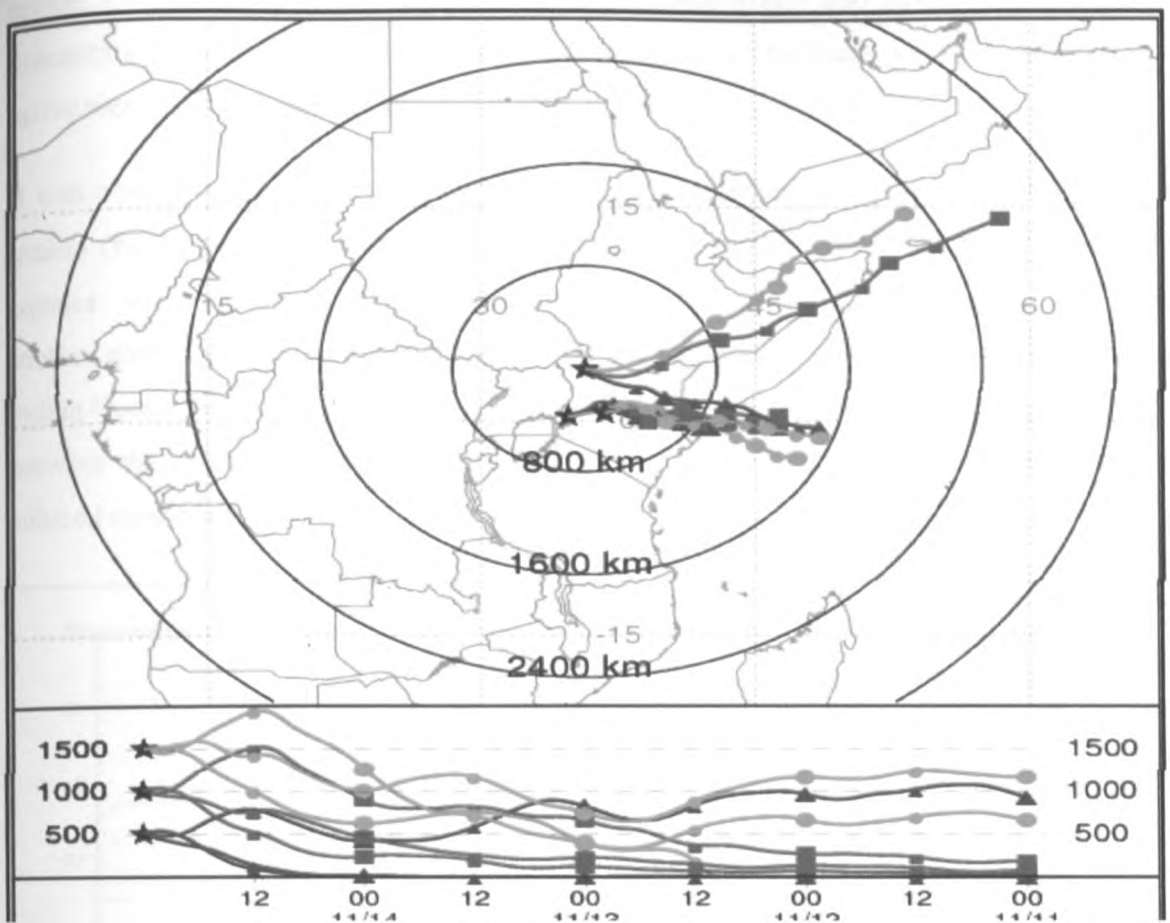


Figure 11: HYSPLIT back trajectory during wet rainfall season (15<sup>th</sup> November 2005)

#### 4.2.3 Composite wind analysis

Composites techniques, based on streamlines and isotach wind analysis were used to derive the composite wind pattern for the dry and wet conditions over the region. Four years were used to composites surface winds at 700hPa pressure levels for both dry and wet OND season. The years 2005, 1974, 1998 and 1975 were used to composite winds during dry OND season while the years 2006, 1977, 1982 and 2002 were used to composite winds during dry OND season. The results are presented in Figure 12 and 13.

It was observed that winds were dominantly north easterlies during the dry OND season (figure 12) along latitude 4<sup>0</sup>N. These winds were relatively weak at 700hPa with less than 1.1 ms<sup>-1</sup>. The Northeasterlies had maximum intensity of about 4.9 ms<sup>-1</sup> along the equator at longitude 34.5<sup>0</sup>E. These North easterlies were noted to have its roots in the high pressure centre over arabia and India. Studies by Anyamba (1983) established that these monsoonal air were mainly continental in origin with moderate sea trajectory, and hence dry. The dominantly shallow and weak winds approaching the equator underwent rising motions in the vicinity of the equator. The convective activities resulted to observed precipitation over the

region. Large scale systems occurring over these region would also have contributed to the precipitation received. In such situations, the normally dry northeast monsoon become very active weatherwise in eastern kenya (Okoola, 1996).

It was observed that winds were dominantly south easterlies during the wet OND rainfall season (figure 13) with increasing wind speeds above the surface at 700hPa along the equator with maximum wind intensity of of about  $6\text{ms}^{-1}$  .The cool and moist southeast/southwest monsoon air flows from the Mascarene Anticyclone in the southern Indian Ocean. The considerable amount of rainfall during this period is attributed to interaction between the south east monsoon current, the congo air mass and the lake victoria thermally induced mesoscale circulation (Kiangi et al., 1981).

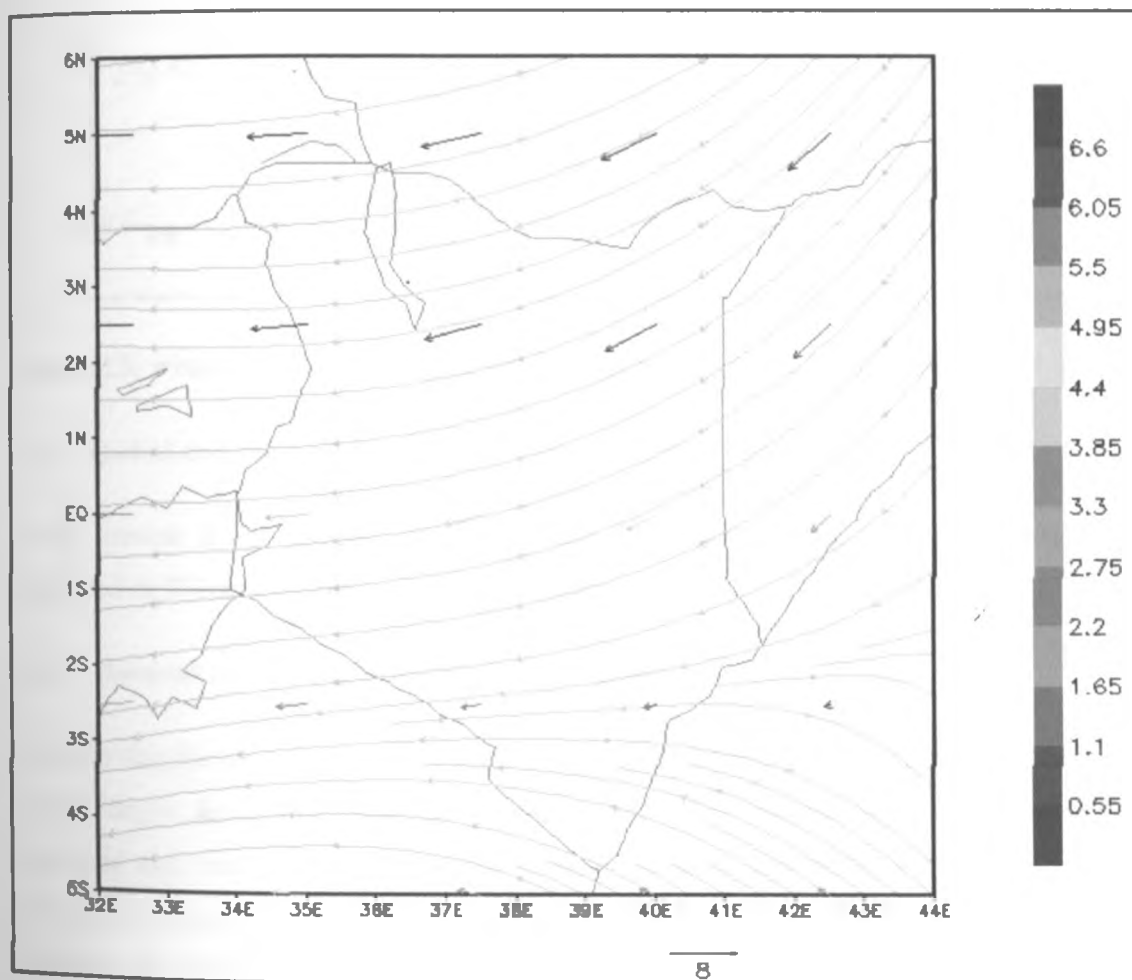


Figure 12: Wind patterns at 700hPa during dry OND season (2005,1974,1998 &1975)

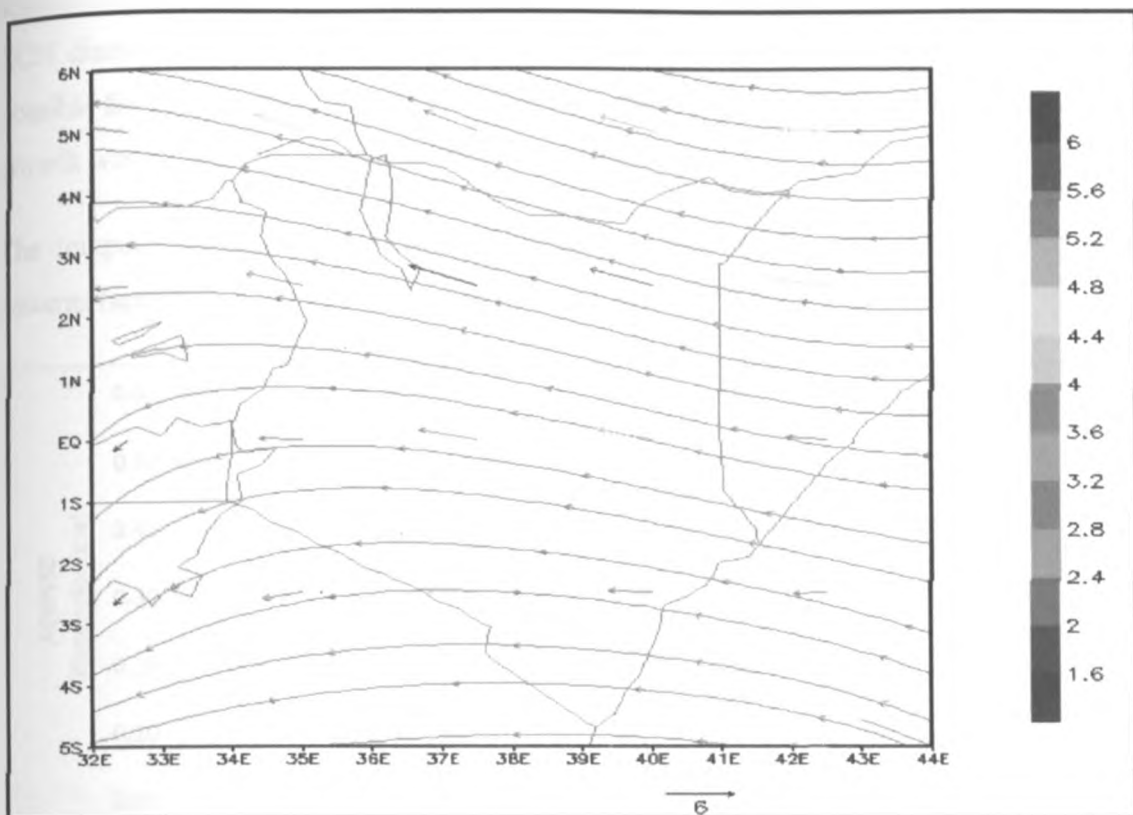


Figure 13: wind patterns at 700hPa during wet years (2006, 1977, 1982, 2002)

### 4.3 Spatial and temporal variability of aerosols over Kenya

In the present study, aerosols properties were investigated using the aerosol optical depth measured at 550nm and mass concentration over land.

#### 4.3.1 Aerosol optical depth at 550 nm over Kenya

The size distribution of aerosol particles was estimated from the spectral variation of aerosol optical depth derived at 550 nm (wavelengths). This wavelength has been considered important and used in numerous global climate modeling and analysis (Remer et al., 2005). The time series showing the intra-seasonal variation of AOD550 for Kakamega, Lodwar and Dogoreti are presented in figures 12-14. Figure 17 showed the spatial distribution of AOD550 over the study region.

Figure 14-16 shows AOD550 in the atmosphere. It was noted that AOD550 during the wet OND season was generally larger than during the dry OND season over all stations used. The spatial pattern of AOD550 during wet OND season showed that aerosols over Northern parts of the area of study had larger diameters with an average value of 0.19 and varied between

0.09 and 0.35 while it varied between 0.07 and 0.22 with a mean of 0.15 during dry OND season. It was noted that the high values of AOD550 over northern Kenya translated to larger CCN diameter. Since these areas have little moisture content in the atmosphere, it was not possible for condensation process to occur even during the wet OND season hence the CCN growth was limited resulting to observed less rainfall.

The temporal variability of AOD550 for stations used in the study also showed similar patterns (appendix B) to stations which had same rainfall characteristics.

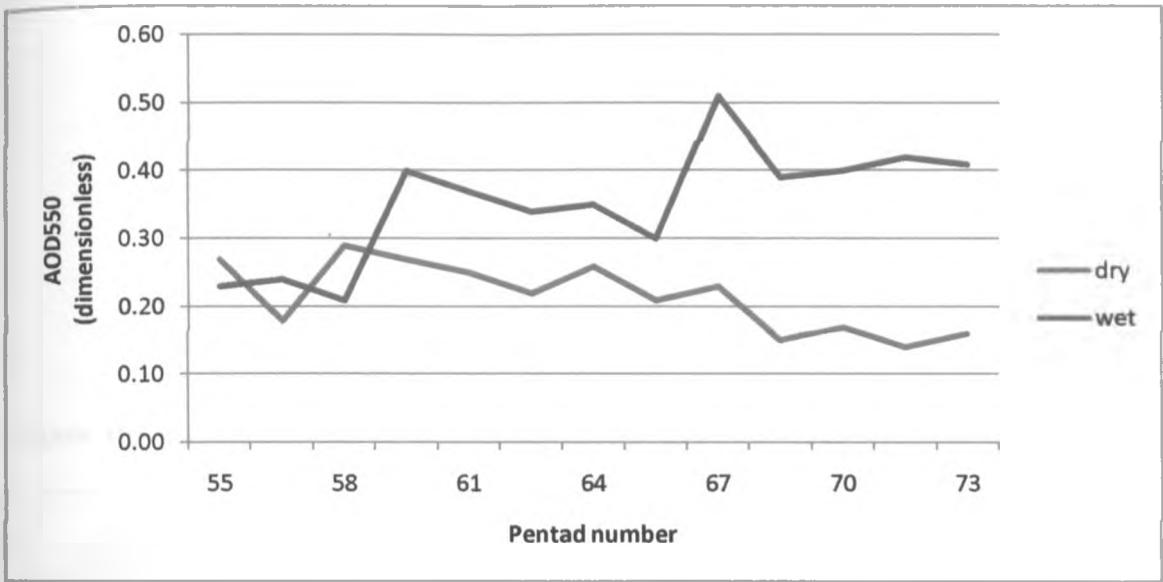


Figure 14: Aerosol optical depth during dry and wet OND season over Lodwar

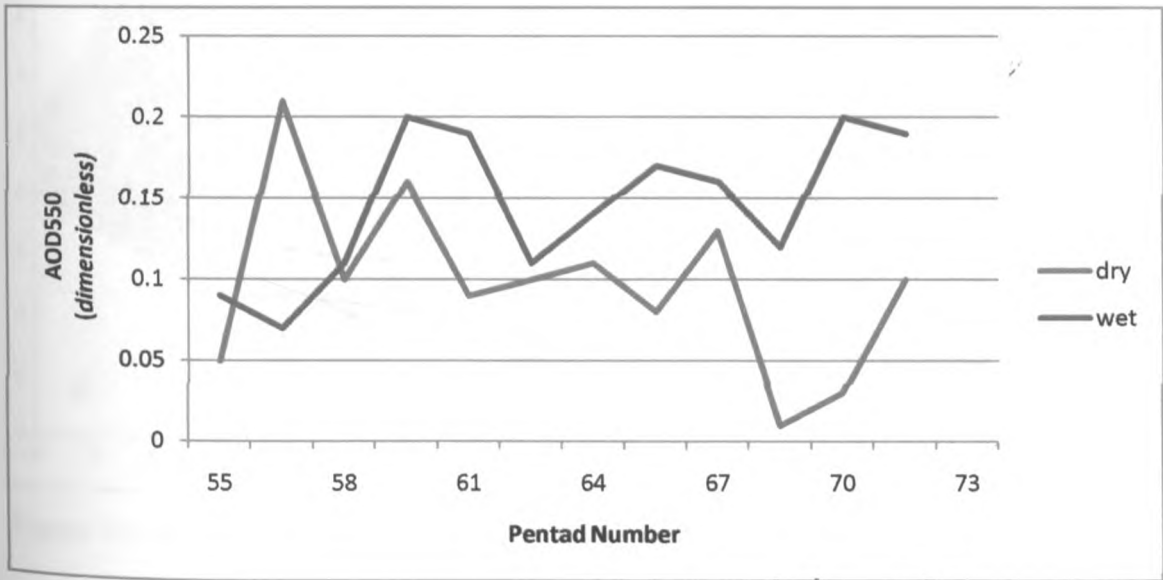


Figure 15: Aerosol optical depth during dry and wet OND season over Kakamega



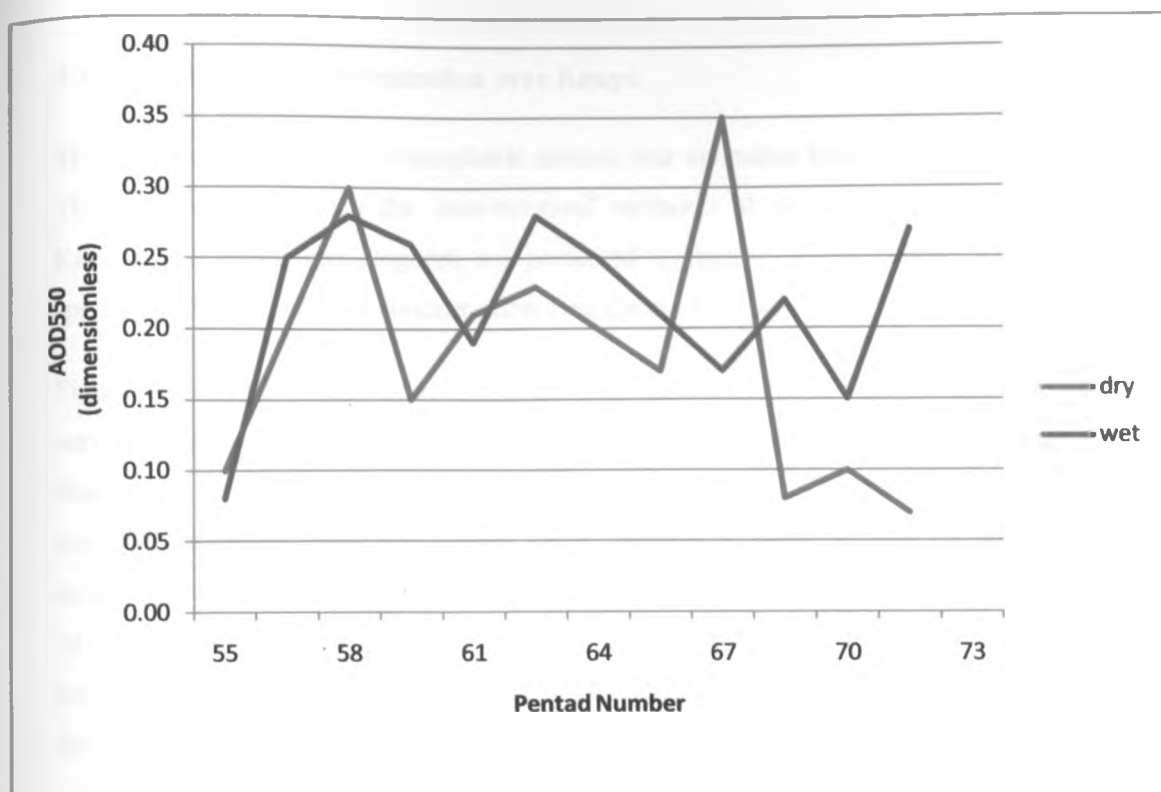


Figure 16: Aerosol optical depth during dry and wet OND season over Dagoretti

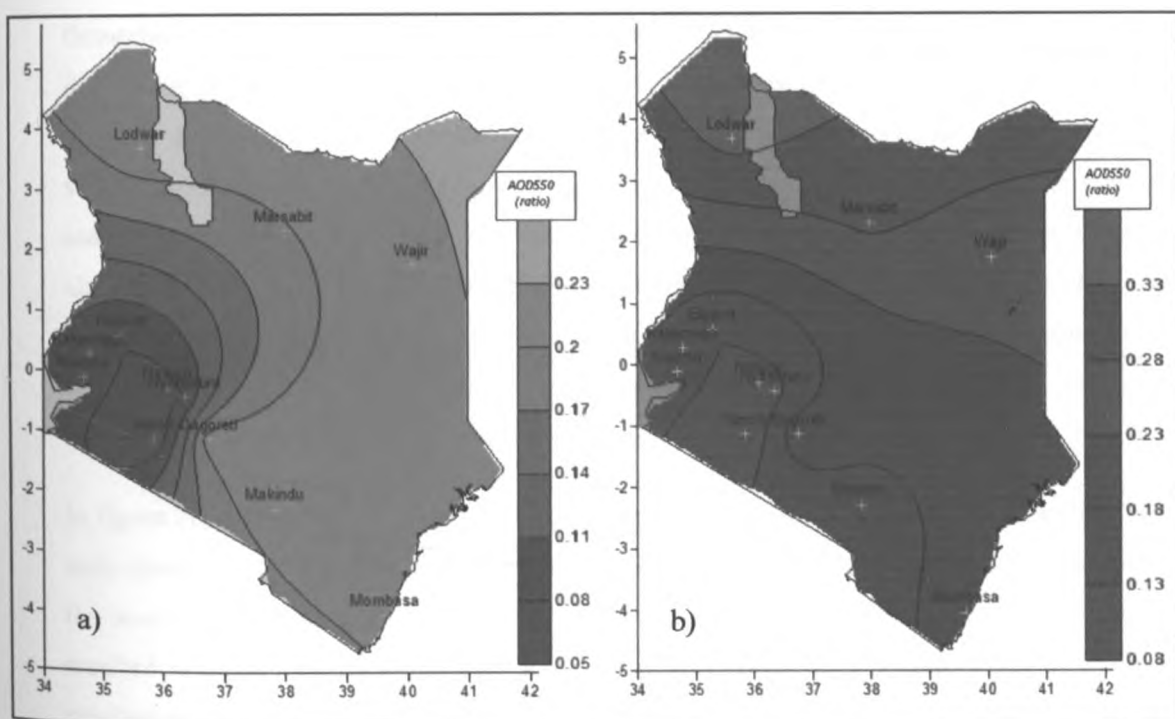


Figure 17: Mean spatial distribution of AOD550 during (a) dry and (b) wet rainfall season

#### 4.3.2 Aerosol mass concentration over Kenya

The mass concentration of atmospheric aerosol was estimated based on a five day average. The time series showing the intra-seasonal variation of aerosol mass concentration for Kakamega, Lodwar and Dogoreti are presented in figures 18-20. Figure 21 showed the spatial distribution of mass concentration over the study region.

Figures 18-20 shows that the temporal pattern of mass concentration in the atmosphere. It was observed that during wet OND season, aerosol mass concentration was generally higher than during the dry rainfall season for all stations used in the study. The total mean particle mass concentrations over land values varied between  $4.55\mu\text{g}/\text{cm}^3$  and  $15.14\mu\text{g}/\text{cm}^3$  with a mean value of  $8.6\mu\text{g}/\text{cm}^3$  during wet rainfall season and between  $5.86\mu\text{g}/\text{cm}^3$  and  $23.22\mu\text{g}/\text{cm}^3$  with a mean of  $10.65\mu\text{g}/\text{cm}^3$  during dry rainfall season. This was accounted by the prevailing direction of aerosols which were mostly oceanic from the southwestern parts of the Indian Ocean especially during the wet rainfall season. Continental aerosols from the Arabia and India sub-continent also contributed during the dry rainfall season.

It was noted that mass concentration during the dry OND season underwent slight variation throughout the season compared to wet OND season. This was attributed to the wet and dry deposition processes of pollutant removal from the atmosphere. It was noted that since aerosols had very short residence time in the atmosphere, it accounted for their high variability observed. The rate of removal of aerosol from the atmosphere during wet rainfall seasons was high due to washout and rainout processes at cloud levels. These aerosols could also have acted as cloud condensation nuclei enhancing formation of clouds resulting to increased precipitation due to reduced mass concentration. During dry rainfall season, mass concentration slightly varied as most of aerosols which were suspended were left to settle due to gravity. Therefore, few aerosols accounted for the cloud formation.

In figure 21, it could be seen that the spatial distribution of aerosols mass concentration in the atmosphere was highly concentrated over the Northern parts of the study region compared to the southern regions. The high mass concentration of aerosols over those areas must have resulted to competition for available limited moisture in the atmosphere. This could have resulted to formation of more clouds which could not undergo rainfall formation processes such as coalescence and Bergeron hence failed to precipitate due to their tiny size of clouds formed.

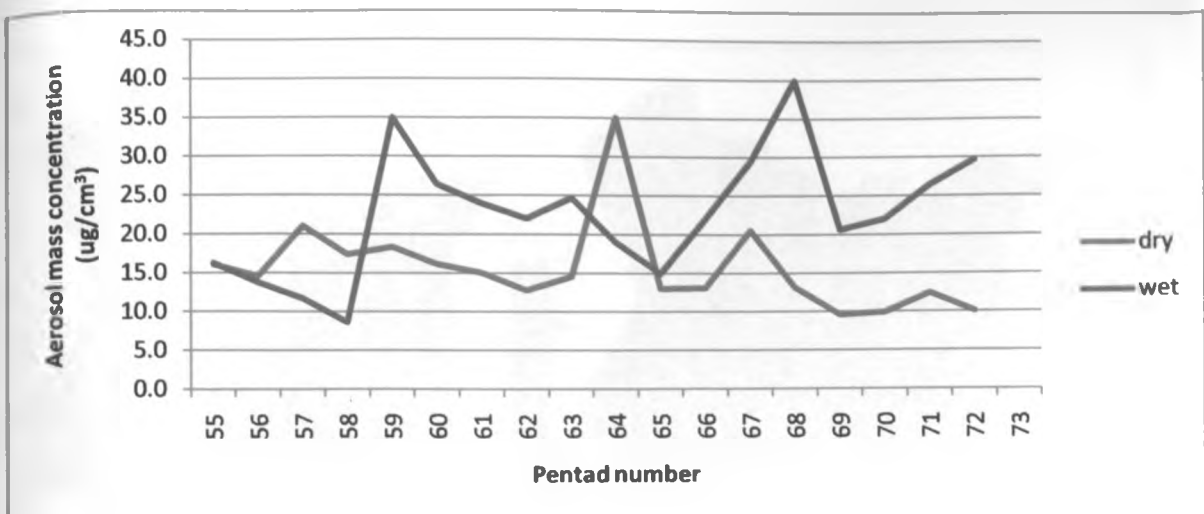


Figure 18: Aerosol mass concentration during dry and wet OND season over Lodwar

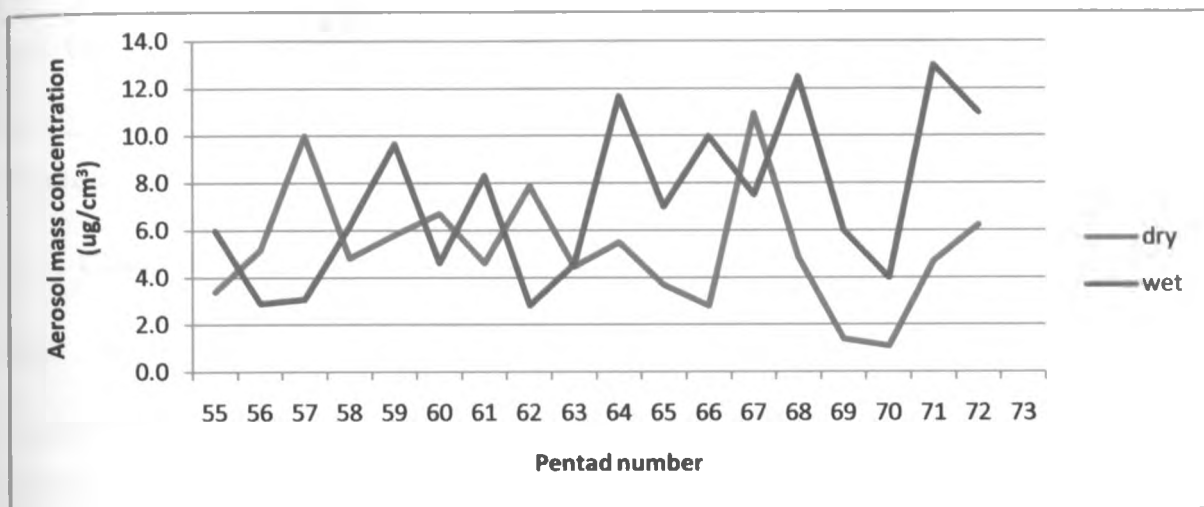


Figure 19: Aerosol mass concentration during dry and wet OND season over Kakamega

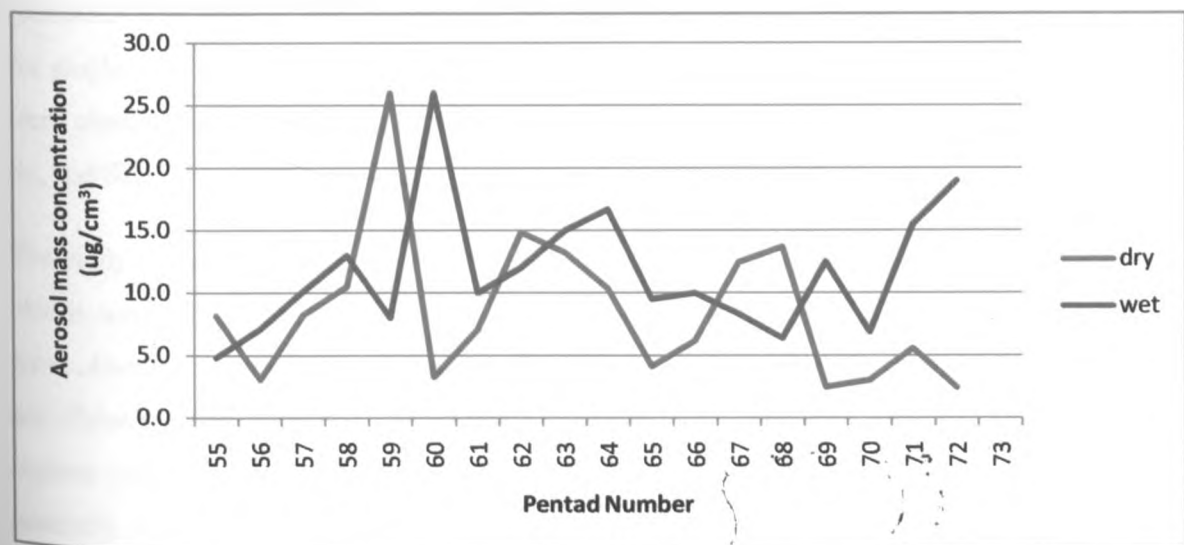


Figure 20: Aerosol mass concentration during dry and wet OND season over Dagoretti

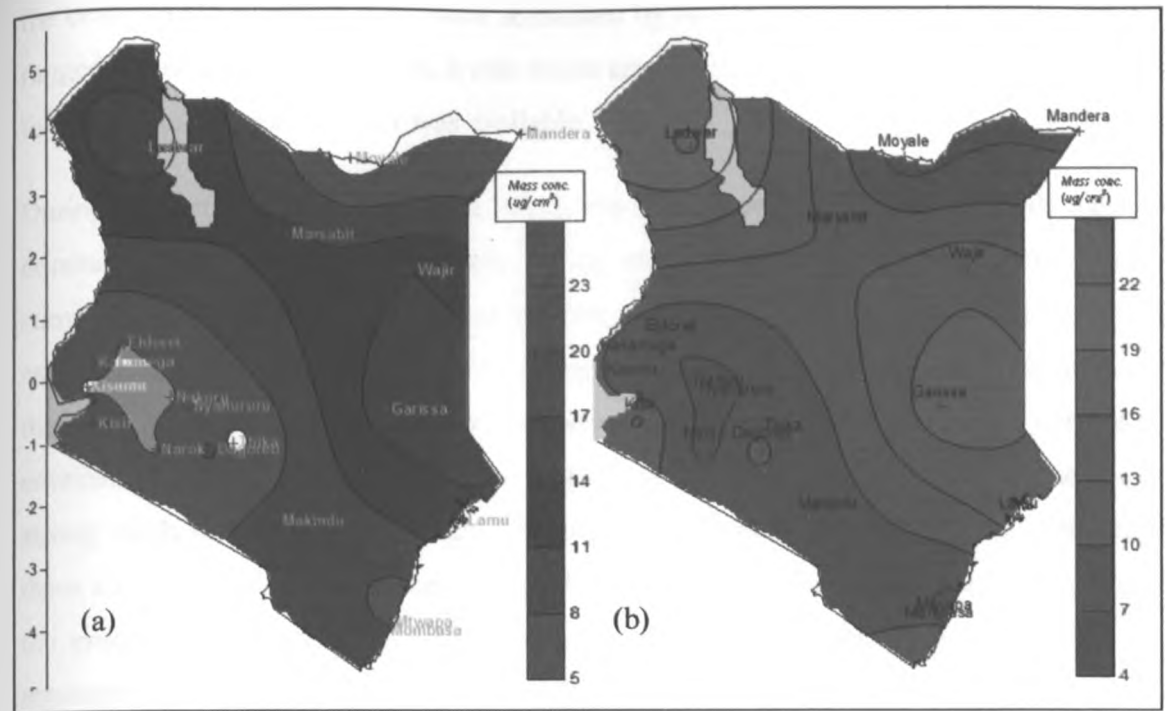


Figure 21: Mean spatial distribution of AMC during (a) dry and (b) wet rainfall season

#### 4.4 Clouds detection and classification

##### 4.4.1 Image processing and cloud classification

Satellite imagery from NOAA/AVHRR3 taken during a typical the wet and dry rainfall season (316<sup>th</sup> Julian date) was used in the study to detect and classify clouds over the region of study. Classification was carried out after scrutinizing the mean, standard deviation, shape (area and density) and texture (homogeneity, contrast and entropy). The results were presented in figures 22 and 23 showing the distribution of cloud types over the area of study for single date analysis during dry and wet rainfall season. Eight classes were identified that were classified as non-cloud classes (sea and terrain) and 7 cloud classes (Ns, Ci, Cb, Cu, Cg, Sc, and St).

The study noted that during the dry OND season (figure 22), it was noted that strato cumulus clouds were very dominant over the Northeastern parts of the study region. Stratus clouds were observed over the western parts of the study region especially in Kakamega, Kisumu and Eldoret. Cumulonimbus and cumulus congestus were observed over Voi and Mt. Kenya regions respectively. These were accounted for by the north easterlies winds which were generally weak and dry undergoing vertical motions over these regions. The limited moisture available over northern parts of Kenya and the high concentration of aerosols observed



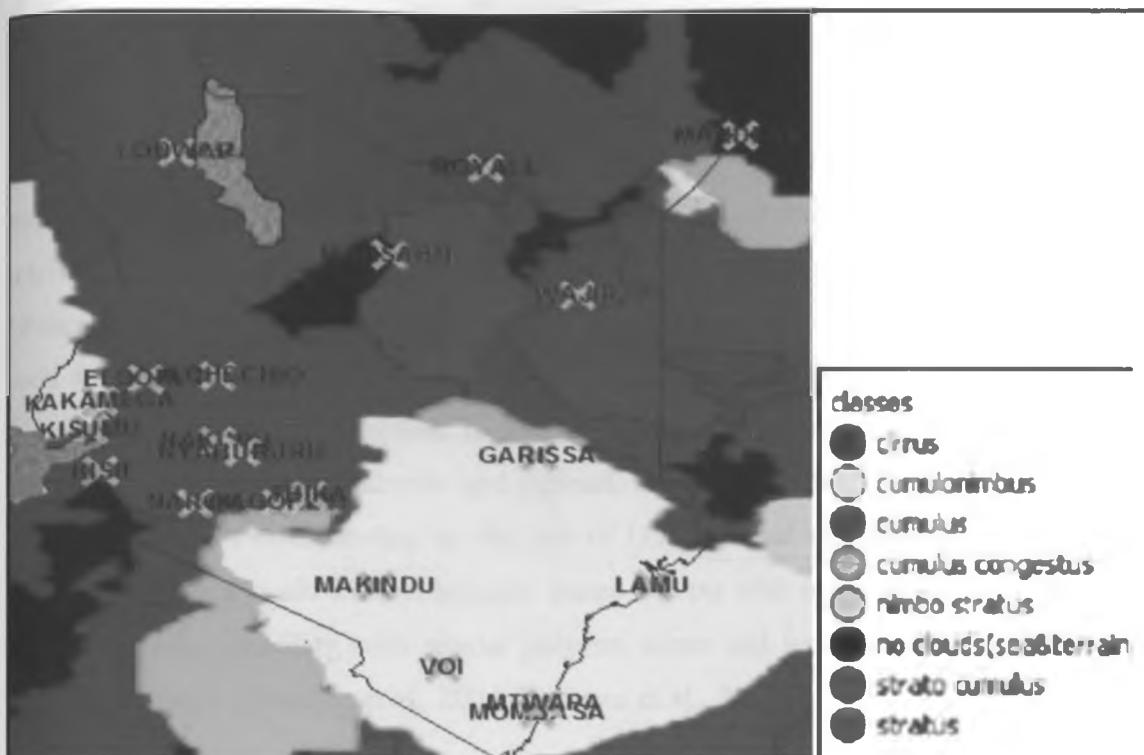


**Figure 23: Classified clouds with eCognition during the wet OND rainfall season**

#### 4.4.2 Accuracy assessment

The bi-spectral cloud classification technique was used to assess the accuracy of object oriented image classification. In this study, error matrix based on TTA mask method for accuracy assessment was used. A series of error matrices with the producer's (eCognition classification) and user's (Observations) accuracy and kappa coefficients for the 8 cloud types classified are presented. The error matrix based on TTA Mask presented in figure 24 and 25 for dry and wet rainfall season respectively. A graphical representation of user class against reference class is plotted in Figure 26 and 27

In the study, the per object classification of November miscalculations for dry OND season resulted mainly from confusion between cumulonimbus and cirrus, cumulus and cirrus, cumulonimbus and cumulus congestus, cumulus and stratocumulus, cumulus and stratus, nimbostratus and stratus, stratus and cumulus, stratus and stratocumulus, stratus and no clouds. The per object classification of November miscalculations for dry OND season resulted mainly from confusion between cirrus and cumulus, cirrus and cumulus congestus, cirrus and cumulus and stratus, cumulonimbus and stratus, cumulus congestus and cirrus, nimbostratus and stratus, stratus and cumulus stratus and stratocumulus, stratus and no clouds.

It was noted that the lowest user's and producer's accuracies during dry OND season was found in stratus clouds with about 78% and 77% respectively. Similarly, lowest user's and producer's accuracies during the wet OND season were found in stratus class with about 81% and 82% accuracy respectively. In all classes during the dry and wet OND season, the user's and producer's accuracy were found to be high with values above 77% accuracy. This was attributed to the sensors high spatial resolution and where image objects were evident (Zalazar, 2006). In this study, the image objects appeared to be quite delineated and agree well with other studies which established high accuracies using object based classification of high resolution imagery compared to other classification methods such as per pixel based classification approach (Whiteside and Ahmad, 2005; Willhauck, 2000). Furthermore, the study agrees with other studies on the use of Object based classification on the ease of interpretation as it deals with meaningful image objects with maps obtained in the analysis providing more appealing with regular polygon edges and less speckled results like other research findings (Blaschke et al., 2004; Stuckens et al., 2000)

The error matrix showed that the overall accuracy for the dry and wet OND season exceeded 90% and kappa coefficient of over 0.8. The kappa coefficient and the overall accuracy statistics agreed well with previous study by Lewinski (2004). Therefore, it was concluded that the accuracy of the image classification was very high.

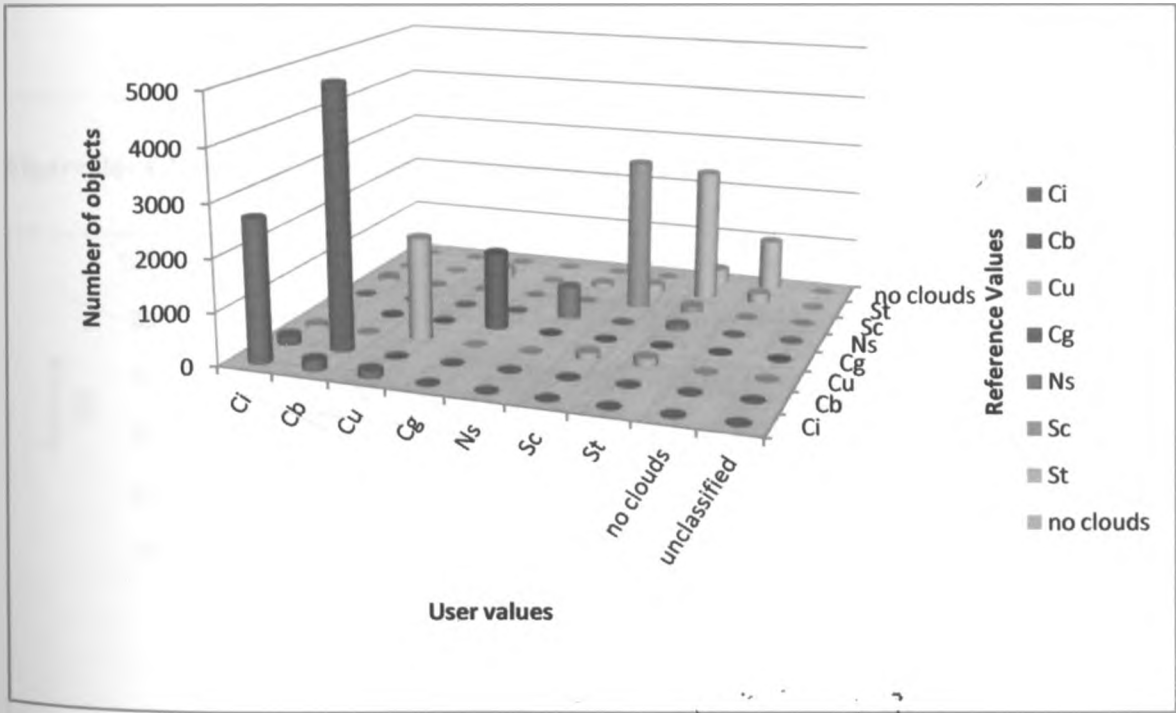


Figure 24: Error Matrix based on TTA Mask for dry OND season

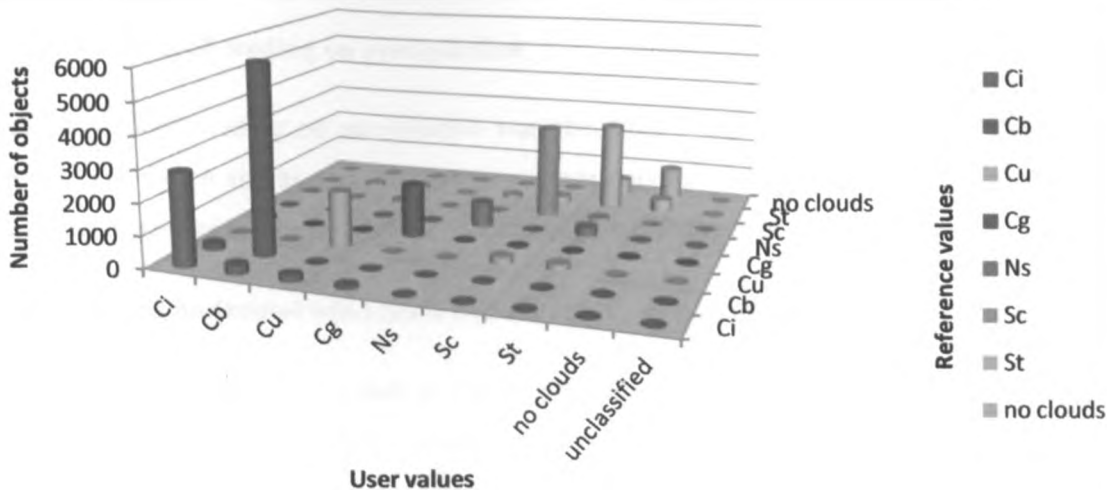


Figure 25: Error Matrix based on TTA Mask for wet OND season

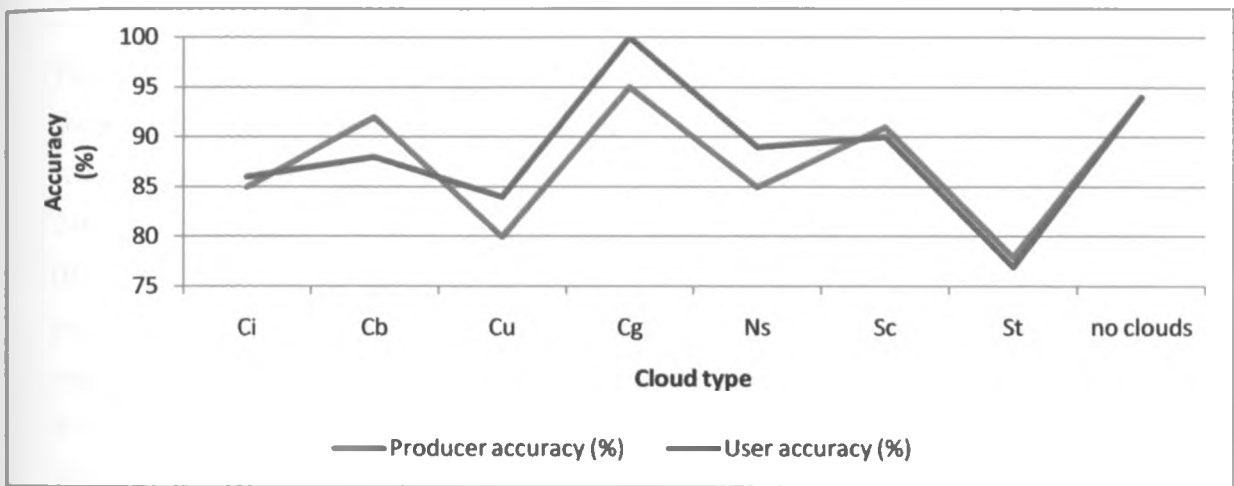


Figure 26: Cloud type class accuracy during dry OND season

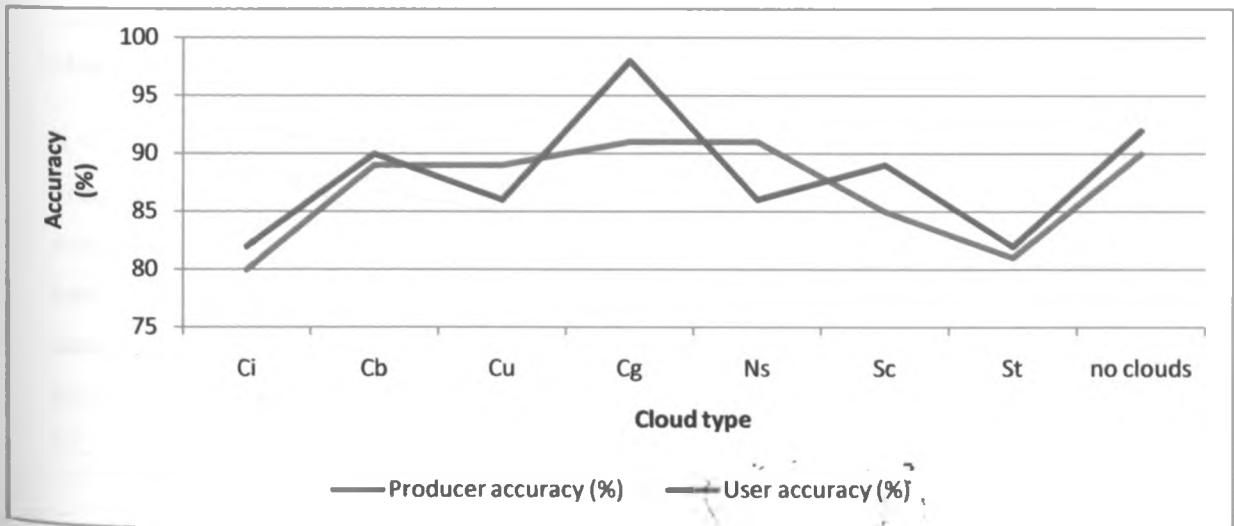


Figure 27: Cloud types accuracy during wet OND season



## **4.5 Effects of cloud seeding on precipitation**

The effect of cloud seeding on precipitation was simulated using a cloud resolving Model. The Model simulation and its accuracy assessments are presented in the sub sections below. Three different aerosol scenarios of CCN concentration were simulated were performed.

### **4.5.1 Simulated horizontal wind fields and accumulated precipitation**

COSMO Model simulation of winds and total precipitation was performed for the three aerosols scenarios. Model simulation results are presented in figures 28-30 for horizontal wind fields at 10m agl and accumulated precipitation after 3 hours of simulation time. This time was equivalent to 24 hour model forecast for aerosols scenarios over the domain of study. Figure 31 presents the time series of accumulated precipitation

Figure 28 showed that model simulation for control simulation (low CCN concentration) showed more precipitation received over the western parts of Kenya around Kisumu, Kakemga and Kitale regions with magnitudes of about 5 to 15 mm received during the 24hour forecast period. Model simulation for intermediate CCN concentration scenario (figure 29) showed an enhanced precipitation over the western parts of Kenya with magnitudes of about 10 to 20mm received during the 24 hour forecast period while model simulation showed a decreased precipitation (figure 30) received over the western parts of Kenya with magnitudes of less than 10mm. The rest of the areas were observed to be generally dry for the three aerosols scenarios simulations. Simulated horizontal wind field were observed to be generally south easterlies with magnitudes of approximately 5 to 10 m/s and weakening towards the western parts of Kenyan for all aerosols simulation. The highly variable surface winds accounted for low level convergence over the region which resulted to observed spatial distribution of precipitation over the domain of study.

It was further noted that precipitation over the model domain (figure 31) was observed to occur after 45 minutes of simulation time and displayed an exponential increase in accumulated precipitation. Moreover, the study noted that an increase in CCN concentration hardly affected the total accumulated precipitation as all the low, intermediate and high CCN scenarios increased exponentially at almost the same rate. Accumulated precipitation was observed to be higher under intermediate CCN concentration scenario than in low and high CCN aerosol scenarios.

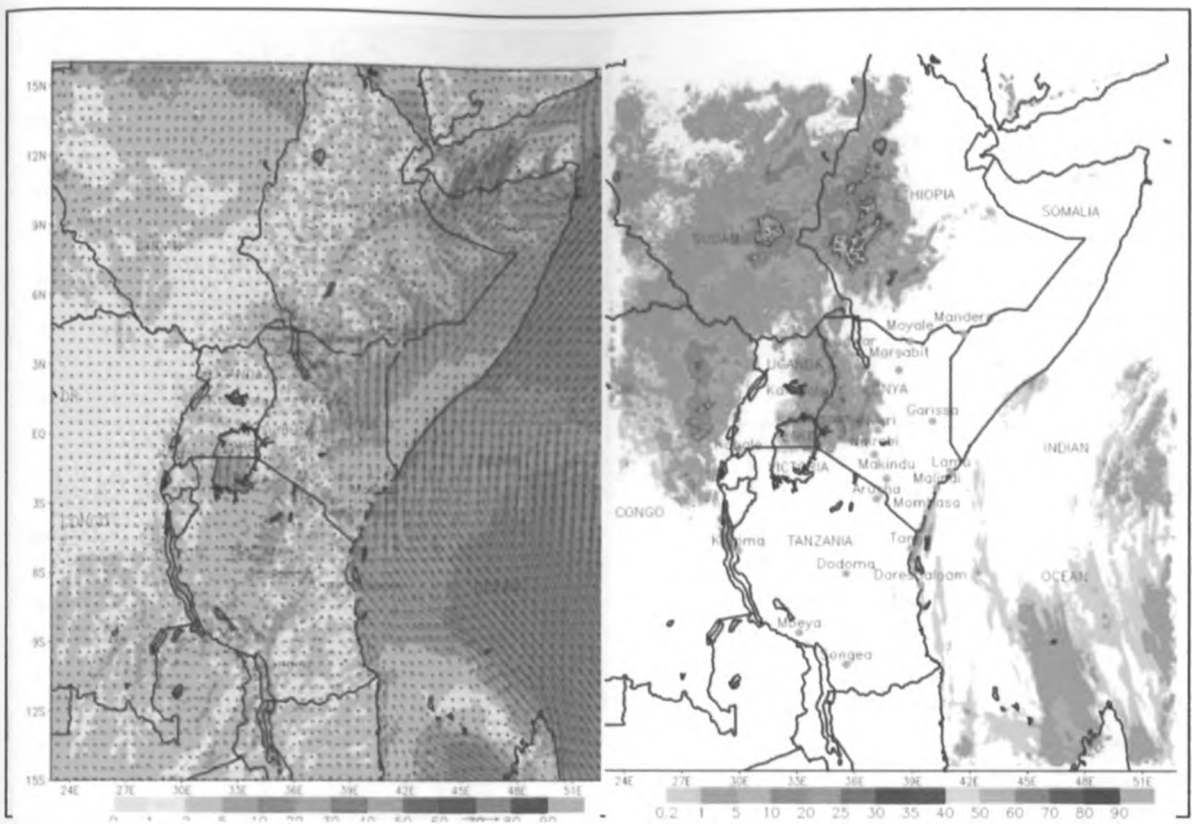


Figure 28: Simulated horizontal wind (m/s) and accumulated precipitation ( $\times 10^3 \text{ m}^3$ ) for low CCN concentration

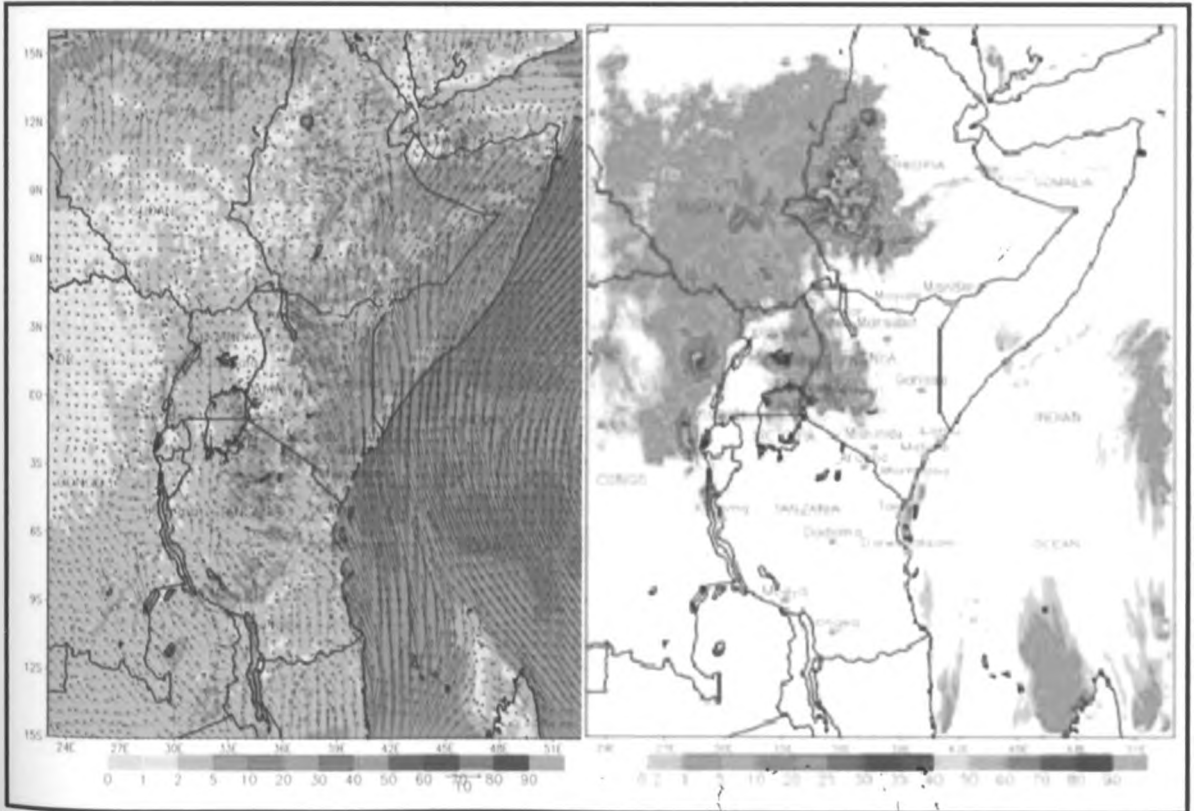


Figure 29: Simulated horizontal wind (m/s) and accumulated precipitation ( $\times 10^3 \text{ m}^3$ ) for intermediate CCN concentration

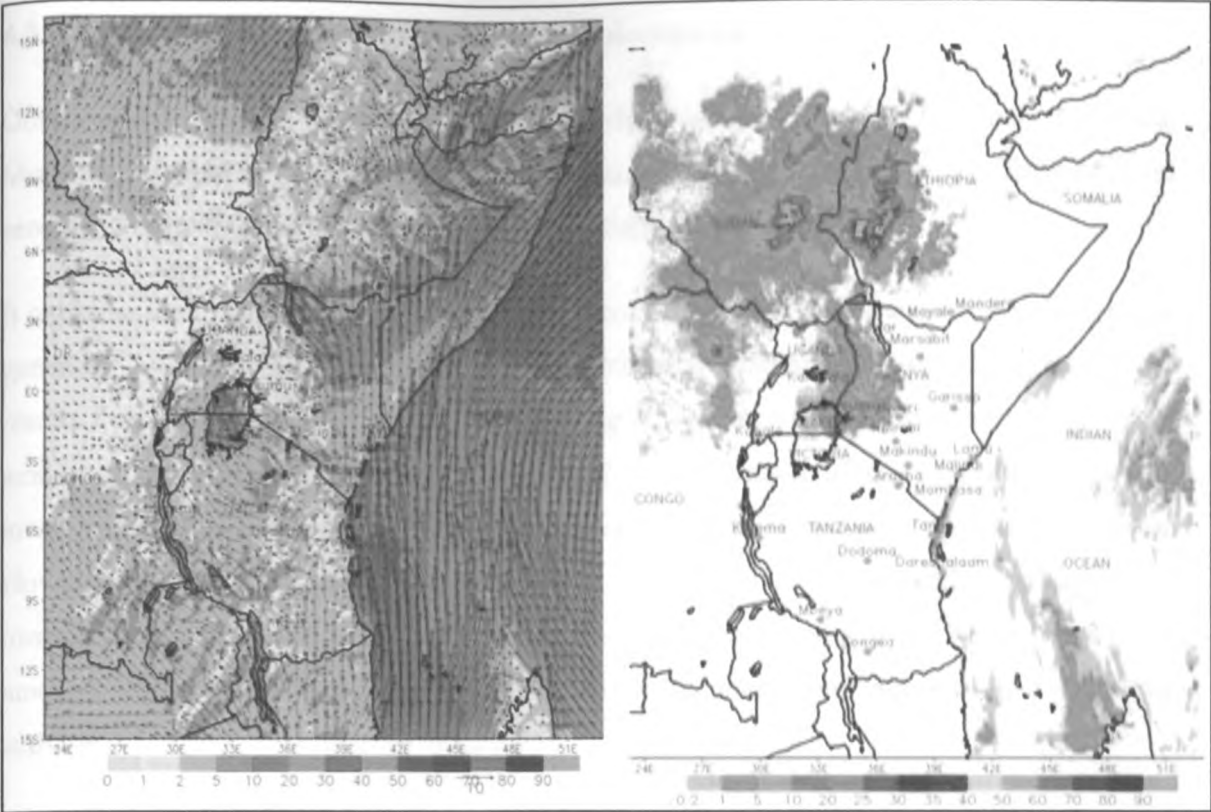


Figure 30: Simulated horizontal wind (m/s) and accumulated precipitation ( $\times 10^3 \text{ m}^3$ ) for high CCN concentration

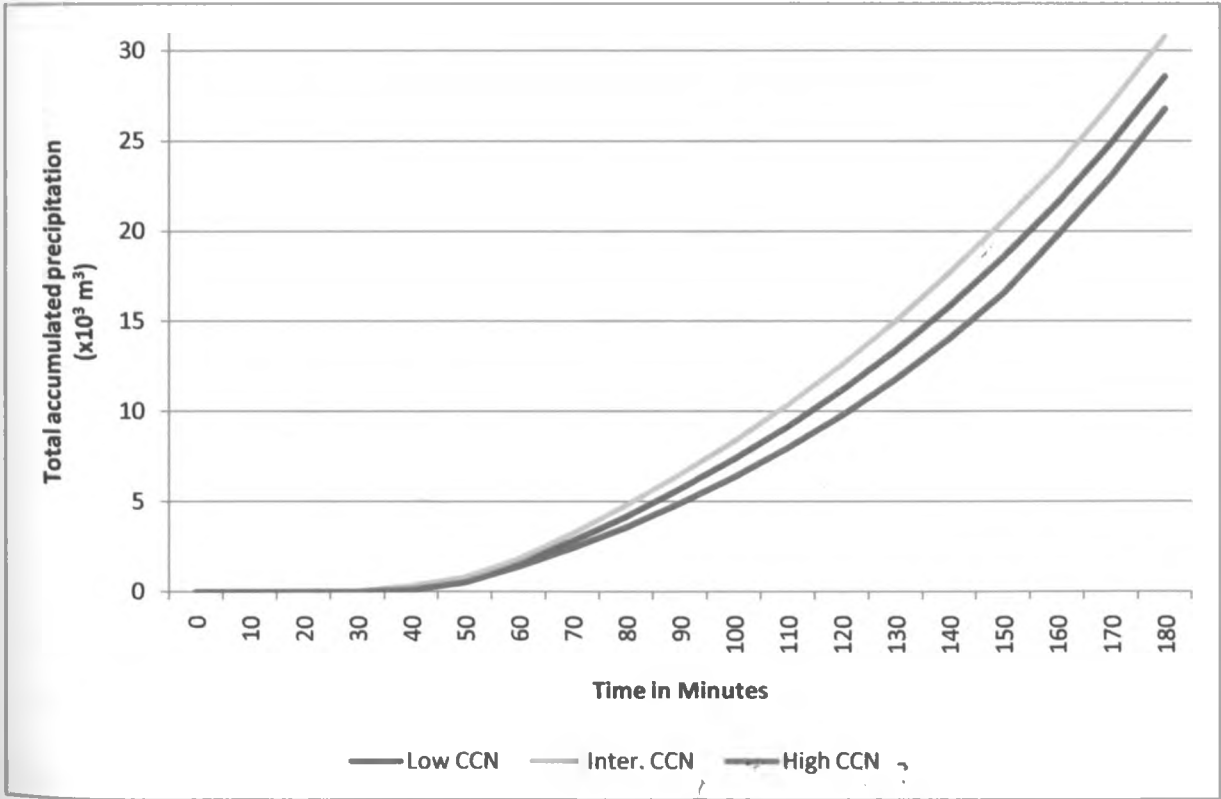


Figure 31: Time series of total accumulated precipitation for different Model runs

4.5.2 Assessment of effects of cloud seeding simulation

Observed daily rainfall over selected stations which included Lodwar, Dagoretti, Makindu, Mombasa, Nyahururu, Kakamega, Wajir and Kisumu were used to assess the effects of cloud seeding simulation. The results are presented in figure 32.

It could be seen from figure 32 that the daily rainfall observed over the selected stations was generally lower than all the aerosols scenarios model simulations. It is noted that simulation results from intermediate CCN scenario were higher over stations which received significant amount of observed 24 hour rainfall. Under high CCN scenario, all the stations selected had lower values than other model output and observed precipitation over the 24 hour period. However, the control scenario (Low CCN) showed higher values than other scenarios and observations. This would be attributed to an urban environment which contributed significant amounts of aerosols from anthropogenic activities such as road transport and industrial activities.

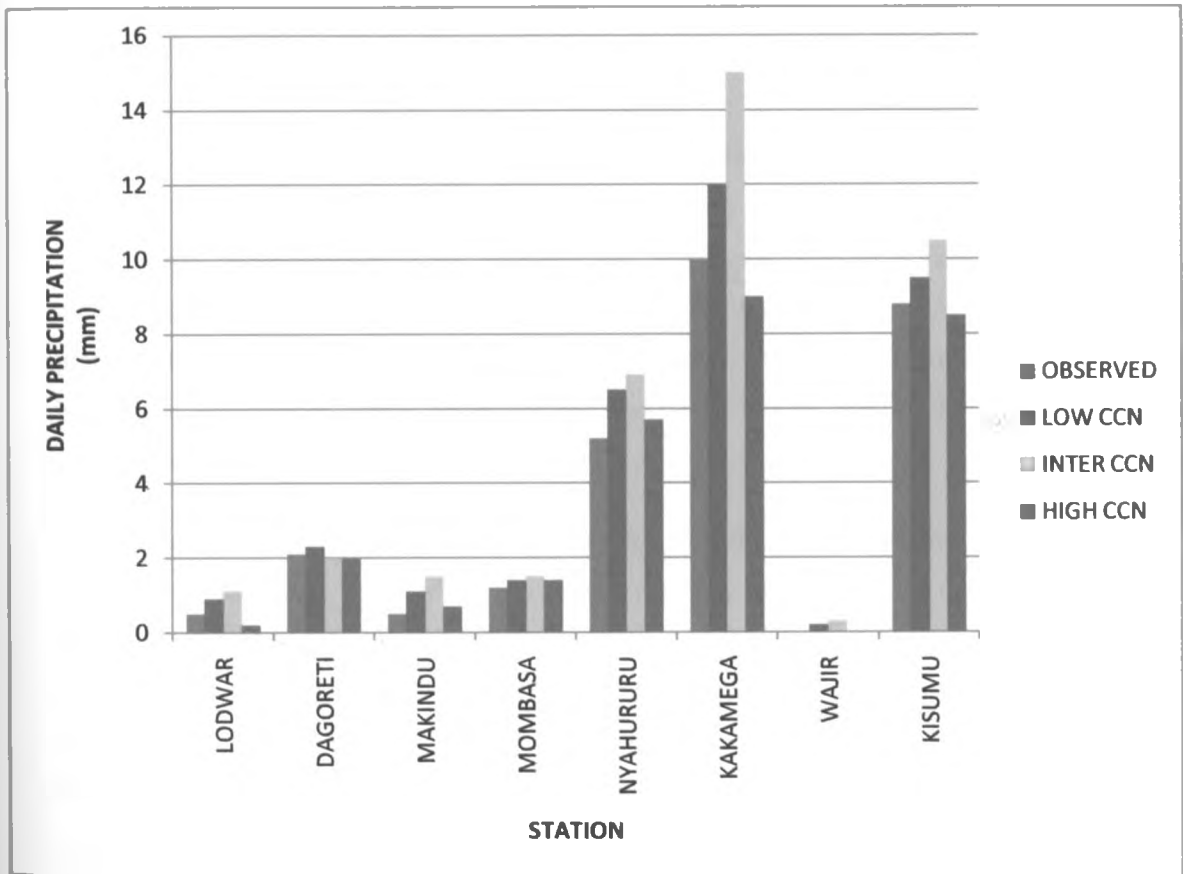


Figure 32: Comparison of 24 hour simulated and observed rainfall

## CHAPTER FIVE

### 5 SUMMARY, CONCLUSIONS AND RECOMMENDATIONS

This chapter gives the summary, major conclusions that were drawn from the various results of the study together with recommendations for future research work for a better understanding of enhancing rainfall through weather modification.

#### 5.1 Summary

Many socio economic activities over Kenya are rain dependent. However the rainfall over Kenya displays both spatial and temporal variability bringing to question its reliability. The occurrence of extreme rainfall events have been associated with losses of life and property which can be reduced through possible enhancement or suppression of precipitation. Rainfall enhancement, a component of weather modification program has been identified in Kenya's vision 2030 as one of the flagship projects aimed at making the country globally competitive and prosperous with a high quality of life to all its citizens in a clean and secure environment by 2030

The main objective of the present study was to investigate the potential of enhancing rainfall through weather modification. The specific objects were aimed at determining the seasonal wind pattern; investigation of the temporal and spatial variation of atmospheric aerosols; identification of the cloud types and simulation of the effects of cloud seeding on precipitation. The study focused on enhancing rainfall during the months of October – November –December which constitute the short rain season due to the easiness of its prediction.

The datasets used included daily and monthly rainfall from the Kenya Meteorological Department; daily and monthly NCEP global wind reanalyses datasets from the National centre for environmental and prediction; daily mean atmospheric aerosol optical depth measured over land at 550nm and mass concentration from MODIS terra aerosol products; satellite imagery from the Advanced Very High Resolution Radiometer sensor onboard the National Oceanic and atmospheric administration satellite series 18 and the initial and boundary conditions from the GME Model of the German weather service. Rainfall and wind reanalysis datasets extended within the period 1970 -2010 while MODIS terra aerosols products extended within the period dry (2005) and wet (2006) OND season. The AVHRR satellite imagery covered the 316<sup>th</sup> Julian date for both 2005 and 2006 OND season.

Several methods were used in achieving the objectives of the study. These included rainfall anomaly index, composite analysis, time series analysis, HYSPLIT backward trajectory analysis, object oriented image classification and COSMO model simulation.

The study picked 2005 and 2006 OND season to represent the dry and wet years respectively during the OND season. These two years were subjected for further analysis. The pentad rainfall distribution indicated peak values mid-season during both dry and wet years. HYSPLIT backward trajectory indicated that most aerosols were continental in origin during dry year and oceanic origin during wet year. The low level winds were observed along the equator to be dominantly north easterlies with maximum wind speeds of  $4.9 \text{ ms}^{-1}$  during dry season and south-easterlies with maximum wind speeds of  $6 \text{ ms}^{-1}$  during the wet OND season.

The aerosol optical depth and mass concentration in the atmosphere during the wet rainfall season was generally higher than during the dry rainfall season over all stations used and more concentrated over Northern parts of the study area. The mean AOD550 values varied between 0.09 and 0.35 with a mean value of 0.19 during wet rainfall season and between 0.07 and 0.22 with a mean of 0.15 during dry rainfall season. The mean particle mass concentrations over land values varied between  $4.55 \mu\text{g}/\text{cm}^3$  and  $15.14 \mu\text{g}/\text{cm}^3$  with a mean value of  $8.6 \mu\text{g}/\text{cm}^3$  during wet rainfall season and between  $5.86 \mu\text{g}/\text{cm}^3$  and  $23.22 \mu\text{g}/\text{cm}^3$  with a mean of  $10.65 \mu\text{g}/\text{cm}^3$  during dry rainfall season. The spatial pattern of AOD550 and mass concentration were accounted by the oceanic aerosols carried by the south easterlies from the southwestern parts of the Indian Ocean during wet OND season and the continental aerosols from the Arabian and India sub continent during the dry OND season.

During a typical dry OND season it was noted that strato cumulus clouds were very dominant over the Northeastern parts of the study region. Stratus clouds were observed over the western parts of the study region especially in Kakamega, Kisumu and Eldoret while Cumulonimbus and cumulus congestus were observed over Voi and Mt. Kenya regions respectively. During atypical the wet OND season, it was noted that cumulonimbus clouds were very dominant over the southeastern parts while the cumulonimbus and cumulus clouds dominating the region of study.

Simulation results from the COSMO Model indicated that seeding with intermediate CCN concentration lead to significant increase in total accumulated precipitation while high CCN concentration lead to reduced precipitation. The observed rainfall was noted to be lower than simulated intermediate CCN scenario.

## **5.2 Conclusions**

The low level winds were predominantly north easterlies/easterlies during the dry/wet OND season. Thus, during dry years, the winds would have continental trajectory characterized by dry conditions while during the wet years, the winds would have maritime trajectory injecting moisture over land. Furthermore, trajectory showed that aerosols present over the area of study during dry years at mainly originated from the Arabian and India subcontinent and were dominantly observed to be suspended at levels above 1000 meters above the ground while during the wet years, the aerosols originated from the south western parts of the Indian Ocean and were dominantly suspended at levels below 1000 meters above the ground.

The study found that the amount of aerosols in the atmosphere were varied both in time and space. It was noted that Northern parts of Kenya had high values of both mass concentration and size distribution of aerosols in the atmosphere suggesting that the aerosols reduced rainfall. However, since the Northern parts of Kenya receive less rainfall than the rest of the country, it could be noted that aerosols alone would not explain the occurrence of rainfall over the region. Nevertheless, CCN which was approximated by AOD550 and mass concentration were considered significant factors in cloud formation in the atmosphere.

Classification of cloud types established that areas which had recorded the highest amount of rainfall between the 64<sup>th</sup> and 65<sup>th</sup> pentad during the wet or dry OND season were highly dominated by the cumulonimbus clouds. Therefore, these clouds were highly associated with high amounts of rainfall received. Therefore, the process that leading to the vertical development of clouds was responsible for much of the rainfall over the region.

Finally, it was observed that variability in total accumulated precipitation from model simulation showed non linear dependency in the amount of cloud condensation nuclei used for seeding. Thus, the study indicated that in order to get desired effects of significant increase in precipitation over the area of study, low to intermediate CCN concentrations should be considered. The understanding of possible effects of intentional cloud seeding on clouds and precipitation would be important towards development of operational program for weather modification program.

## **5.3 Recommendations**

In this study, monthly rainfall totals for OND season were used to determine the wet and dry rainfall years used in the study. This was based on the magnitude of received precipitation over the stations used. Further studies should investigate both the intraseasonal and

interseasonal variation of rainfall in order to determine the distribution of wet and dry spell and their causes.

The study used single date analysis for object based classification. A combination of image classification methods such as per pixel based and objects based approach could have increased both the user's and producer's accuracy. Furthermore, single dates and multi temporal approach could be combined to increase the overall accuracy of image classification.

In the present study, assumed that cloud seeding was done over the whole model domain while the initial and boundary conditions used were for a single date. Further studies of the effect of cloud seeding on precipitation should be restricted to certain areas in order to facilitate cloud seeding results. Model simulations should also be performed using initial and boundary conditions for several days. Sufficient number of days would enable statistics to be generated.

Quantification of the feedback processes between aerosols and the state of the atmosphere on regional scale should be investigated using more sophisticated models such as COSMO ART and results used to determine the threshold values to be considered for different atmospheric aerosols scenarios .

Results from the present study indicated that there existed a possibility of enhancing rainfall through cloud seeding with known wind pattern; temporal and spatial variability of atmospheric aerosols and dominant cloud types over the area of study under certain CCN scenarios. Information from the study should used to form basis for future cloud seeding assessments and weather modification programs in the country towards achievement of Vision 2030



## REFERENCES

- Anyamba, E. K., 1983: On the monthly mean lower tropospheric circulation and anomalous circulation during the 1961/62 floods in East Africa. *M.Sc. thesis, Department of Meteorology, University of Nairobi*, 240 pp.
- Bell, T. L., D. Rosenfeld, K.-M. Kim, J.-M. Yoo, M.-I. Lee, and M. Hahnenberger, 2008: Midweek increase in U.S. summer rain and storm heights suggests air pollution invigorates rainstorms, *J. Geophys. Res.*, 113,
- Bangert, B, C. Kottmeier, B. Vogel, and H. Vogel, 2011: Regional scale effects of the aerosol cloud interaction simulated with an online coupled comprehensive chemistry model. *Atmos. Chem. Phys. Discuss.*, 11, 1–37.
- Blanchard, D. C. and Woodcock, A. H., 1980: The production, concentration, and vertical distribution of the sea salt aerosol. *Ann. New York Acad. Sci.* 338, 330-347.
- Blaschke, T., Lang, S., Lorup, E., Strobl, J. and Zeil, P., 2004: Object oriented image processing in a GIS/remote sensing environment and perspectives for environmental applications. *In Environmental Information for Planning, Politics, and the Public*, 2, A. Cremers and K. Greve (Eds), pp. 555–570
- Bruintjes, R. T., 1999: A review of cloud-seeding experiments to enhance precipitation and some new prospects. *BAMS* 80, 803–820.
- Campbell, J.B., 2002: Introduction to remote sensing. *Taylor and Francis*, 621 pp
- Chen B, Z. Deping, G. Fujiu, W. Jihong, and Geng S., 2005: AgI-Seeding modeling study on the 12 July 2002 cold vortex precipitation in Shenyang. *J. Nanjing Inst. Meteor.*, 28, 483-491.
- Chu, D.A., Kaufman, Y.J., Zibordi, G., Chern, J.D., Mao, J., Li, C., Holben, B.N., 2003: Global monitoring air pollution over land from the earth observing system-terra moderate resolution imaging spectro-radiometer (MODIS). *Journal of Geophysical Research* 108, D21.doi:10.1029/2002JD003179
- Cooper, W.A., R.T. Bruintjes, and G.K. Mather., 1997: Some calculations pertaining to hygroscopic seeding with ares. *J. Appl. Met.*, in press.

- Cotton, W.R., and R.A. Pielke., 1995: Human Impacts on Weather and Climate. *Cambridge Univ. Press*, 288 pp.
- Camberlin, P., and Wairoto, J., 1997: Intraseasonal wind anomalies related to the wet and dry spells during the long and short rainy seasons in Kenya. *Theor. Appl. Climatology.*, 58, 57-69
- Centella, A., Gutiérrez, T., Limia, M. and Rivero, J. R., 1999: Climate change scenarios for impact assessment in Cuba Institute of Meteorology, *Apartado 17032, CP 11700 Habana 17, Cuba.*
- Curie M., Janc D and Vuckovic V., 2007b: Cloud seeding impact on precipitation as revealed by cloud-resolving mesoscale model. *Meteorol. Atmos. Phys.*, 97 179-193.
- Dey, S., Tripathi, S.N., Singh, R.P., Holben, B.N., 2005: Seasonal variability of aerosol parameters over Kanpur, an urban site in Indo-Gangetic basin. *Advances in Space Research* 36, 778-782
- Draxler, R.R. and Rolph, G.D., 2012: HYSPLIT (HYbrid Single-Particle Lagrangian Integrated Trajectory) Model access via NOAA ARL READY Website (<http://ready.arl.noaa.gov/HYSPLIT.php>). *NOAA Air Resources Laboratory, Silver Spring, MD*
- Folland. C.K., 1983: Regional scale inter-annual variability of climate. A North-West European perspective. *Met. Mag.*, 112, 163-187.
- Gatebe C. K., P. D. Tyson, H. Annegarn, S. Piketh and Helas. G., 1999: A seasonal air transport climatology for Kenya. *Journal of geophysical research*, vol. 104, no. d12, pp. 14,237-14,244
- Gottsche Frank-M. and Olesen Folke S., 2005: Classification of clouds and weather situations in meteorological satellite data using Definiens eCognition
- Government of Kenya, 2007: Kenya Vision 2030: A globally competitive and prosperous Kenya. Nairobi: *Ministry of Planning and National Development and the National Economic and Social Council.*
- Griffith, D.A., M.E. Solak and D.P. Yorty., 2007: A level II weather modification feasibility study for winter snowpack augmentation in the Salt River and Wyoming ranges in Wyoming. *Journal of Weather Modification*, 39:23-37

- Gupta, P., Christopher, P.A., Wang, J., Gehring, R., Lee, Y., Kumar, N., 2008: Satellite remote sensing of particulate matter and air quality assessment over global cities. *Atmospheric Environment* 40, 5880-5892
- Hobbs, P.V, J.S. Reid, R. A. Kotchermruther and Ferek R. J., 1997: Direct Radiative Forcing by Smoke from Biomass Burning. *Vol. 275 no. 5307 pp. 1777-1778*
- Hay, G.J., T. Blaschke, D.J. Marceau and A. Bouchard, 2003: A comparison of three Image object methods for the multiscale analysis of landscape structure. *Photogrammetry Remote Sensing*, 57: 327-345.
- Ito M., 2000: Analysis and Use of Meteorological Satellite Images, First Edition, Chapter 2, Meteorological Satellite Center, *Japan Meteorological Agency*,
- Ininda, J.M, Muhati.F.D and F.J Opijah., 2007: Relationship between ENSO parameters and the trends and periodic fluctuations in east African rainfall. *J. Kenya Met.*, 1, 20-43.
- IPCC, 2007: Climate change 2007: The physical science basis. In Contribution of Working Group I to the Fourth Assessment Report of the Intergovernmental Panel on Climate Change, Solomon S, Qin D., Manning M., Chen Z., Marquis M., Averyt K. B., Tignor M., Miller H.L., *Eds, Cambridge University Press: Cambridge, New York.*
- Jury, W.A., and J. Vaux, 2007: The emerging global water crisis: Managing scarcity and conflict between water and users. *Advances in Agronomy* 95: 1 -6
- Kalnay, E., and R. Jenne., 1996: The NCEP/NCAR 40-year reanalysis project, *Bull. Am. Meteorol Soc.*, 77, 437-471.
- Khain, A. P., 2009: Notes on state-of-the-art investigations of aerosol effects on precipitation: a critical review, *Environ. Res. Lett.*, 4, 015004, doi: 10.1088/1748-9326/4/1/015004.
- Khain, A. P., M. Ovtchinnikov, M. Pinsky, A. Pokrovsky, and H. Krugliak., 2000: Notes on the state-of-the-art numerical modeling of cloud microphysics, *Atmos. Res.*, 55, 159-224.
- Kiangi, P.M.R., Kavishe, M. M. and Patnaik, J. K., 1981: Some aspects of mean tropospheric motion field in East Africa during the long rains season. *Kenya Journal of sci. and Techn. (A)*, 2, 91-103

- Lewinski S, Zarenski K., 2004: Examples of object-oriented classification performed on high-resolution satellite images. *Miscellanea Geographica*. 11: 349-358.
- Li X, Sui CH, and Lau K. M., 2002b: Dominant cloud microphysical processes in a tropical oceanic convective system: A 2-D cloud resolving modelling study. *Mon Wea Rev* 130:2481–2491
- Lillesand, T.M., Kiefer, R.W. and Chipman, J.W., 2004: Remote sensing and image interpretation. *Wiley and sons*, 763pp
- Lohmann U. and Schwartz S. E., 2009: Aerosols and Clouds in Chemical Transport Models and Climate Models, *MIT Press, Cambridge MA*, pp. 531-555. ISBN 978-0-262-01287-4.
- Matarira, C. H., and M. R. Jury, 1992: Contrasting meteorological structure of intraseasonal wet and dry spells in Zimbabwe. *J. Climatol.*, 12, 165–176.
- Mather, G.K., D.E. Terblanche, F.E. Stevens., 1996b: Results of the South African cloud seeding experiments using hygroscopic flares. Preprints, 13th Conf. on Planned and Inadvertent Weather Modification, January 28 - February 2, 1996, Atlanta, GA, *AMS, Boston, MA*, 121-128.
- Maritinsson, B. C., 1999: Droplet nucleation and growth in orographic clouds in relation to the aerosol population, *Atmos. Res.*, 50, 289– 315.
- Muhlbauer A. and U. Lohmann., 2009: Aerosol-cloud-precipitation interactions on mixed-phase orographic precipitation, *J. Atmos. Science*, 10.1175/2009JAS3001.1.
- Muthama, N. J., Manene, M. M. and Ndetei, C. J., 2008: Simulation of decadal precipitation over Nairobi. *Kenya. J. Scie.*, Vol 13, 43-54 pp
- Nakajima, T., Higurashi, A., Kawamoto, K., and Penner, J. E., 2001: A possible correlation between satellite-derived cloud and aerosol microphysical parameters, *Geophys. Res. Lett.* 28, 1171–1174.
- Ogallo, L. J., 1989: The spatial and temporal patterns of East African rainfall derived from principal component analysis; *Int. J. Climatol.*, Vol 9, 145–167 pp.

- Okoola, R. E., 1996: Space – Time characteristics of the ITCZ over equatorial East Africa during anomalous rainfall years. *PhD. thesis, Department of Meteorology, University of Nairobi, Kenya*
- Okoola, R. E., 1999: Mid-tropospheric circulation patterns associated with extreme dry and wet episodes over equatorial eastern Africa during the northern hemisphere spring. *J. Appl. Meteor.*, 38, 1161 – 1169
- Okoola R. E., J. M Ininda and P. Camberlin., 2008: Wet periods along the east African coast and the extreme wet spell event of October 1997. *J. Kenya Met soc.*, Vol 2, 67-83pp
- Orville H. D., 1996: A review of cloud modeling in weather modification. *Bull Amer Meteor Soc* 77: 1535–1555
- Prasad, A.K., Singh, R.P., 2007: Comparison of MISR-MODIS aerosol optical depth over the Indo-Gangetic basin during the winter and summer seasons (2000-2005). *Remote Sensing of Environment* 107, 109-119
- Ranjan, R.R., Joshi, H.P., Iyer, K.N., 2007: Spectral variation of total column aerosol optical depth over Rajkot: a tropical semi-arid Indian station. *Aerosol and Air Quality Research* 7, 33-45
- Reid, H. and Huq, S., 2007: Community-based adaptation: A vital approach to the threat climate change poses to the poor, *International Institute for Environment and Development*, London.
- Remer, L.A., Kaufman, Y.J., Tanré, D., Mattoo, S., Chu, D.A., Martins, J.V., Li, R.R., Ichoku, C., Levy, R.C., Kleidman, R.G., Eck, T.F., Vermote, E., Holben, B.N., 2005: The MODIS aerosol algorithm, products and validation. *Journal of Atmospheric Science* 62, 947-973
- Rosenfeld, D., U.Lohmann, G.Raga, C.D. O'Dowd, M.Kulmala, S. Fuzzi., A Reissell and M.O. Andrea., 2008: Flood or Drought: How Do Aerosols Affect Precipitation? *Science*. Vol. 321 no. 5894 pp. 1309-1313
- Rosenfeld, D., Woodley, W.L., Axisa, D., Lahav, R., Bomar, G., 2005: On the Documentation of Microphysical structures Following the Base-Seeding of Texas Convective Clouds Using Salt Micro-Powder. *16th Conference on Planned and Inadvertent Weather Modification*, San Diego

- Savtchenko, A., D. Ouzounov, S.Ahmad, J. Acker, G. Leptoukh, J. Koziana & D. Nickless., 2004: Terra and Aqua MODIS products available from NASA GES DAAC. *Advances in space research*, 34, 710-714
- Segal, Y., and Khain, A., 2006: Dependence of droplet concentration on aerosol conditions in different cloud types: Application to droplet concentration parameterization of aerosol conditions. *J. Geophys. Res.*, 111, D15240, doi: 10.1029/2005JD006561
- Seifert, A., Beheng, K.D., 2006: A two-moment cloud microphysics parameterization for mixed phase clouds. Part 1: Model description. *Meteorol. Atmosph. Phys.*, 92, 45–66
- Stuckens, J., Coppin, P.R. and Bauer, M.E., 2000: Integrating contextual information with per-pixel classification for improved land cover classification. *Remote Sensing of Environment*, 71, pp. 282–298.
- Steppeler, J., Doms, G., Schattler, U., Bitzer, H., Gassmann, A., Damrath, U., and Gregoric, G., 2002: Meso gamma scale forecasts using the nonhydrostatic model LM, *Meteorol. Atmos. Phys.*, 82, 75–96
- Volker, W., 2003: Object-based classification of remote sensing data for change detection, *ISPRS Journal of Photogrammetry & Remote Sensing*, 58, pp. 225– 238.
- Ward, M. N., 1992: Provisionally corrected surface wind data, worldwide ocean–atmosphere surface fields and Sahelian rainfall variability. *J. Climatol.*, 5, 454–475.
- Willhauck, G. 2000: Comparison of object oriented classification techniques and standard image analysis for the use of change detection between SPOT multispectral satellite images and aerial photos. *Proceedings of the XIX ISPRS Congress on Comparison of Object Oriented Classification Techniques and Standard Image Analysis for the Use of Change Detection between SPOT Multispectral Satellite Images and Aerial Photos*, pp. 1-8. ISPRS, Amsterdam
- Whiteside, T. and Ahmad, W., 2005: A comparison of object-oriented and pixel-based classification methods for mapping land cover in northern Australia. *Proceedings of Spatial Intelligence, Innovation and Praxis: The National Biennial Conference of the Spatial Sciences Institute*, pp. 1225-1231. *Spatial Sciences Institute, Melbourne*
- WMO, 1998: World meteorological organisation settlement on the status of the global climate in 1997. *Geneva, Switzerland, WMO/TD 877, 12P*

WMO. 1996. Guide to Meteorological Instruments and Methods of Observation (<sup>h</sup>6<sup>th</sup> edition), WMO-No.8. World Meteorological Organization, Geneva.

[www.gov.ns.ca/geonova/gif/maps/pdf/AFR\\_KN\\_THEM\\_Physical.pdf](http://www.gov.ns.ca/geonova/gif/maps/pdf/AFR_KN_THEM_Physical.pdf) (Accessed on 10<sup>th</sup> May 2012)

Yin, Y., Z. Levin, T. G. Reisin, and S. Tzivion., 2001: A numerical evaluation of seeding with hygroscopic flares: Sensitivity to seeding time, seeding height, seeding amounts, size of particles and environmental shear. *Proc. Seventh WMO Scientific Conference on Weather Modification*, Chiang Mai, Thailand, WMO Rep. No. 31, 69–72.

Zalazar Viviana Laura, 2006: Comparison of classification approaches for land cover mapping in the Wielkoposka, Poland. *M.sc. thesis, International institute of geo-information science and earth observation*

Zhan, Q., Molenaar, M., Tempfli, K. and Shi, W., 2005: Quality assessment for geospatial objects derived from remotely sensed data. *International journal of remote sensing*, 26: 2953-2974.

Zhang Jie, Zhang Qiang, TianWenshou, and He Jinmei., 2006c: Remote sensing retrieval and analysis of optical character of cloud in Qilian Mountains. *J. Glacio. Geocryo*, 28, 722-727.

**APPENDIX A: Pentad calendar**

PENTAD NO.	MON	DATES	PENTAD NO.	MON	DATES	PENTAD NO.	MON	DATES
1	JAN	1 – 5	25	MAY	1 – 5	49	AUG-SEP	29 – 2
2	-	6 - 10	26	-	6 – 10	50	-	3 – 7
3	-	11– 15	27	-	11 – 15	51	-	8 – 12
4	-	16 - 20	28	-	16 – 20	52	-	13 – 17
5	-	21 – 25	29	-	21 – 25	53	-	18 – 22
6	-	26 – 30	30	-	26 – 30	54	-	23 – 27
7	JAN-FEB	31 – 4	31	MAY-JUN	31 – 4	55	SEP-OCT	28 – 2
8	-	5 – 9	32	-	5 – 9	56	-	3 – 7
9	-	10 – 14	33	-	10 – 14	57	-	8 – 12
10	-	15 – 19	34	-	15 – 19	58	-	13 – 17
11	-	20 – 24	35	-	20 – 24	59	-	18 – 22
12	FEB-MAR	25 – 1	36	-	25 – 29	60	-	23 – 27
13	-	2 – 6	37	JU-JUL	30 – 4	61	OCT-NOV	28 – 1
14	-	7 – 11	38	JUL	5 – 9	62	-	2 – 6
15	-	12 - 16	39	-	10 – 14	63	-	7 – 11
16	-	17 – 21	40	-	15 – 19	64	-	12 – 16
17	-	22 – 26	41	-	20 – 24	65	-	17 – 21
18	-	27 – 31	42	-	25 – 29	66	-	22 – 26
19	APR	1 – 5	43	JUL-AUG	30 – 3	67	NOV-DEC	27 – 1
20	-	6 – 10	44	AUG	4 – 8	68	-	2 – 6
21	-	11 – 15	45	-	9 – 13	69	-	7 – 11
22	-	16 – 20	46	-	14 – 18	70	-	12 – 16
23	-	21 – 25	47	-	19 – 23	71	-	17 – 21
24	-	26 – 30	48	-	24 – 28	72	-	22 – 26
						73	-	27 – 31

Courtesy of Okoola (1996)



APPENDIX B: Temporal variation of atmospheric aerosols.

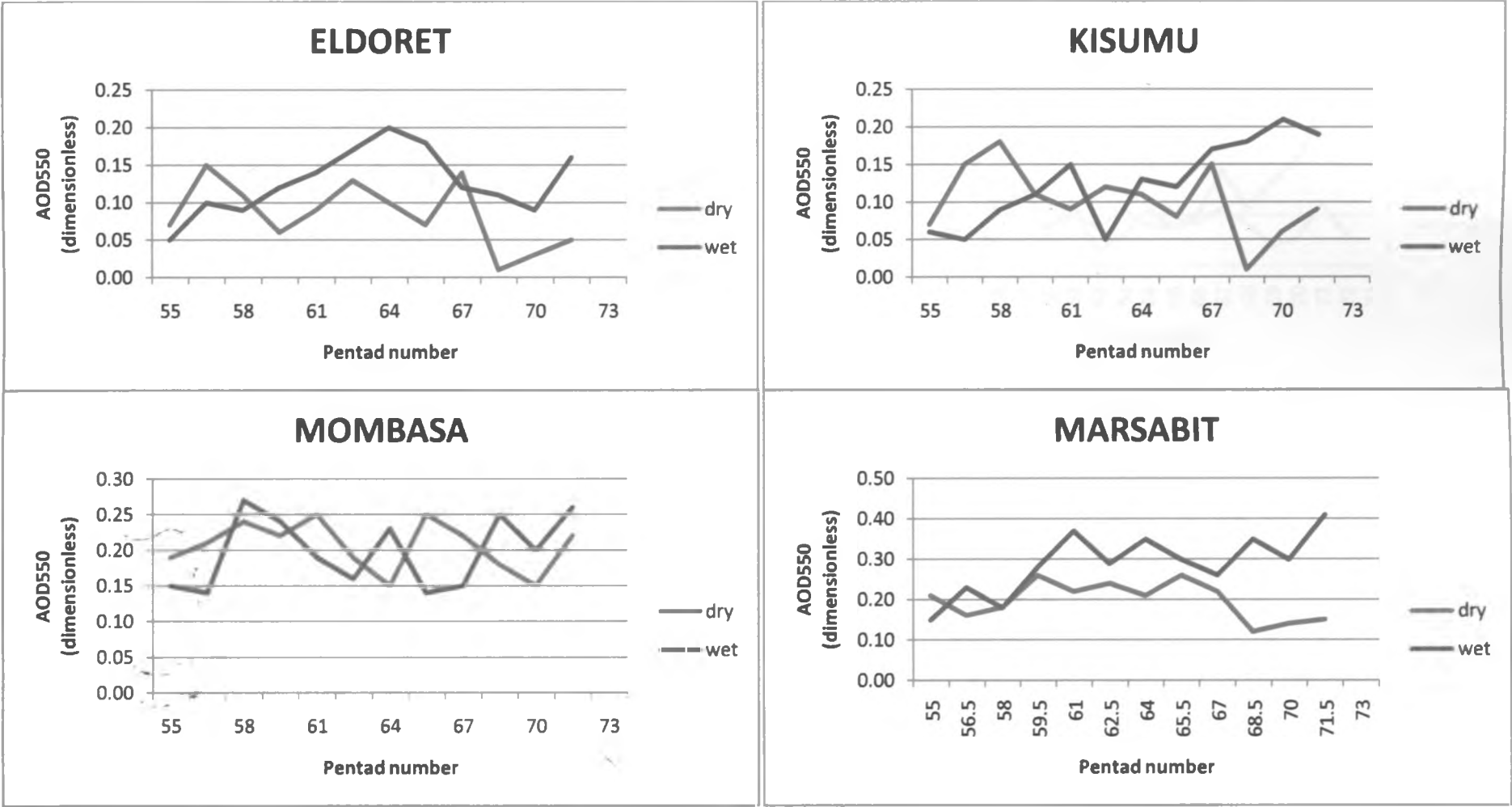


Figure 33: Atmospheric optical depth during wet and dry OND season.

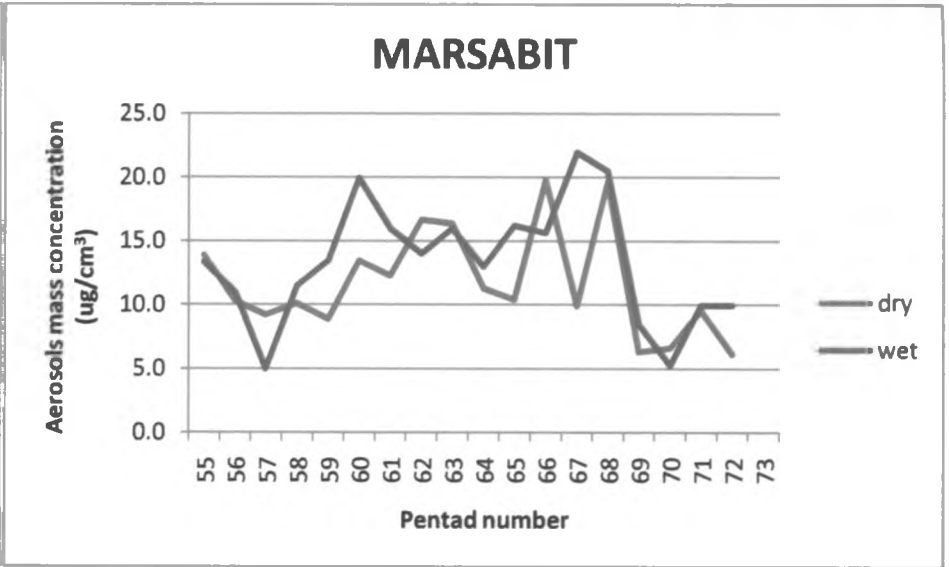
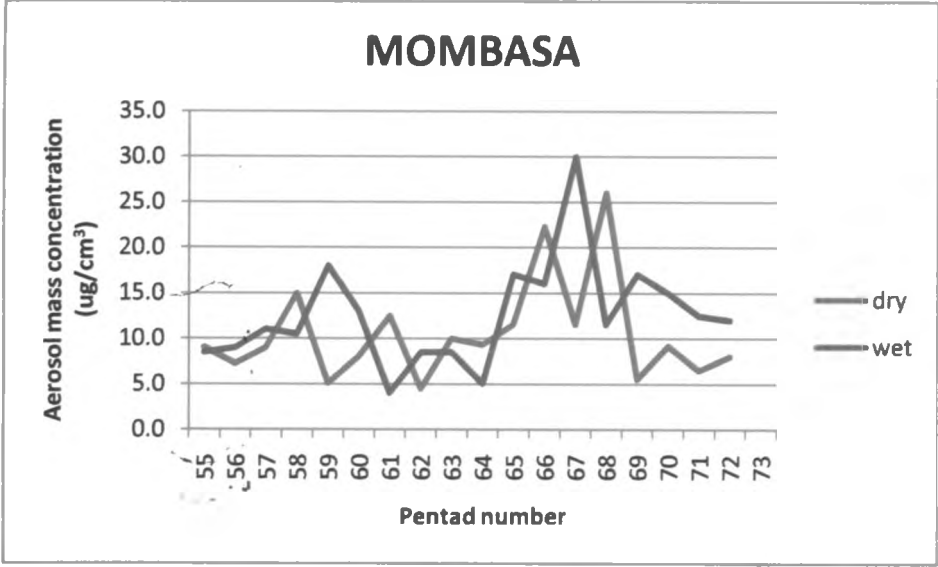
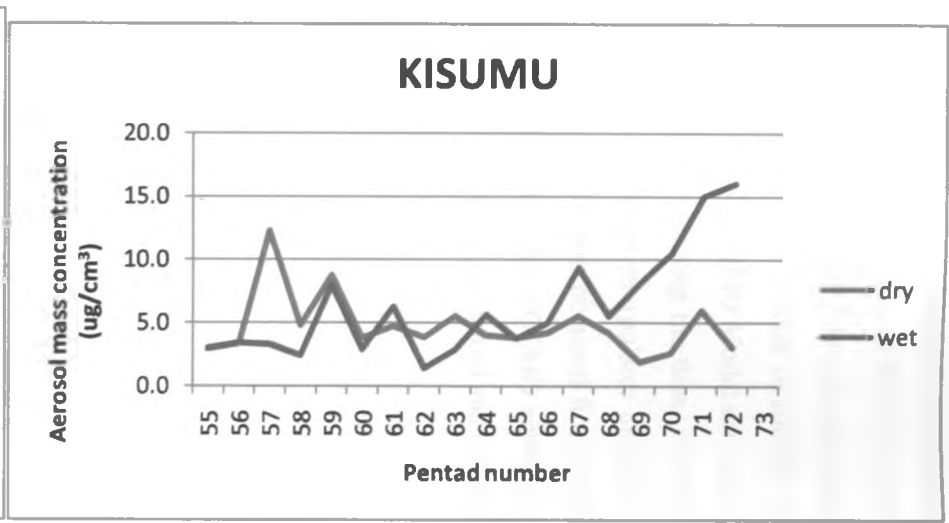
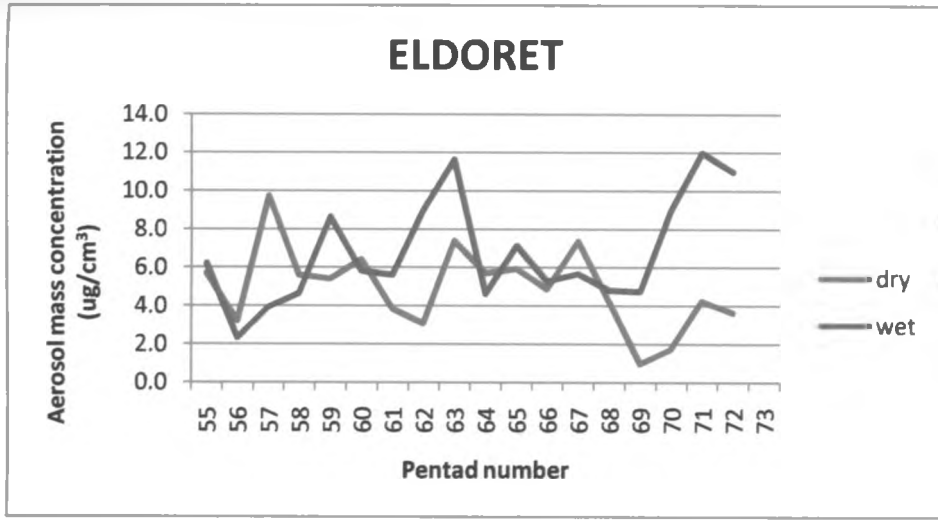


Figure 34: Atmospheric mass concentration during wet and dry OND season.

## **APPENDIX C: Procedure for obtaining precipitation simulation from COSMO Model**

The domain was set to 15.0° S to 23.0°N and 90.0°E to 180.0°W which is the greater horn of Africa (GHA). The forecast hours required was set to 24 and resolution of 7 km on a work station computer, Linux operating system (OpenSUSE 11.3), FORTRAN compilers (gcc-fortran) and COSMO Model source codes were installed. The libraries were compiled and the binaries for running the data, *tstint2lm* and *tstint\_lm* obtained. An interface program called *INT2LM* which interpolates analysis and forecast data of the global model GME to any COSMO grid was obtained from DWD. The interpolated data served as an initial and lateral boundary data for COSMO simulation. *INPUT\_INT2LM* converts topographical data from GME analysis to the initial and boundary data used by the COSMO model.

## APPENDIX D: The INPUT\_INT2LM Namelist used in this study

```
#!/bin/ksh
#
# The GME2COSMO Job
#
rm -f gme2cosmo_job
#####
# number of processors
#####
NPX=1
NPY=1
NPIO=0
NP1=`expr $NPX \* $NPY`
NP=`expr $NP1 + $NPIO`
N1=`expr $NP + 15`
NODES=`expr $N1 \ / 16`

DATE=2012053106
LM_EXT=/home/cosmo/const
IN_EXT=/home/cosmo/const
IN_DIR=/home/cosmo/source/GME_2012053106_grib1
LM_DIR=/home/cosmo/source/COSMO_RUN_input_2012053106
cat > gme2eu_job << ****
#####
# batch commandos
#####
#PBS -q normal
#PBS -l cpunum_job=$NP
#PBS -b $NODES
#####PBS -T mpisx
#PBS -j o
#PBS -N gme2eu
# change to working directory
cd /home/cosmo/source/int2lm_110311_1.18
# @ shell=/usr/bin/ksh
```

```

# @ output=gme2eu.out
# @ error=gme2eu.out
# @ job_type=parallel
# @ class=np
# @ initialdir=.
# @ network.MPI=sn_all,shared,us
# @ notification=never
# @ ec_smt=no
# @ node=$NODES
# @ total_tasks=$NP
# @ queue
#####
# cat together the INPUT-file
#####
cat > INPUT << end_input
&CONTRL
  ydate_ini='$DATE', ydate_bd='$DATE',
  hstart=0.0, hstop=6.0, hincbound=1.0,
  linitial=.TRUE., lboundaries=.TRUE.,
  nprocx=$NPX, nprocy=$NPY, nprocio=$NPIO, lreorder=.FALSE.,
! lgme2lm=.TRUE., lec2lm=.FALSE, llm2lm=.FALSE., lum2lm=.FALSE.,
  yinput_model='GME',
  ltime_mean=.TRUE.,
  lfilter_oro=.TRUE., eps_filter=0.1,
  ilow_pass_oro=1, ilow_pass_xso=0, rxso_mask=0.0,
  lfilter_pp=.FALSE., lbalance_pp=.FALSE., norder_filter=5,
  luvcor=.TRUE.,
  lmulti_layer_in=.TRUE., lmulti_layer_lm=.TRUE.,
  lprog_qi=.TRUE., lprog_qrqs=.TRUE.,
  lprog_rho_snow=.TRUE.,
  lsso=.TRUE., lforest=.TRUE., llake=.FALSE., lbdclim=.FALSE., lt_cl_corr=.TRUE.,
  itype_ndvi=0, idbg_level=2,
/
&GRID_IN
  ni_gme = 256, i3e_gme = 60, kcontrol_fi=15, ke_soil_in=7,

```

/

## &LMGRID

```
startlat_tot = 15.0, startlon_tot = 23.0,  
pollat=90.0,    pollon=-180.0,  
dlon=0.0625,    dlat=0.0625,  
ielm_tot=201,    jelm_tot=193,    kelm_tot=316,  
ke_soil_lm=7,  
ivctype=2, irefatm=2, delta_t=75.0, h_scal=10000.0,
```

/

## &DATABASE

/

## &DATA

```
ie_ext=201, je_ext=193,  
ylmext_lfn='lm_d5_07000_965x773.sso.mol.gl',  
ylmext_cat='$LM_EXT',  
yinext_lfn='invar.i314a',  
yinext_form_read='ncdf',  
yinext_cat='$IN_EXT',  
yin_form_read='grbl',  
yin_cat='$IN_DIR',  
! ybitmap_cat='$IN_DIR',  
! ybitmap_lfn='bitmap516',  
ylm_cat='$LM_DIR',  
nprocess_ini = 131, nprocess_bd = 132,  
nl_soil_in=2, nl_soil_lm=2,  
l_ke_in_gds=.TRUE.,
```

/

## &PRICTR

```
igp_tot = 36, 40, 48, 44, 48, 85, 77  
jgp_tot = 30, 94, 38, 26, 26, 96, 12  
lchkin=.TRUE., lchkout=.TRUE.,  
lprps=.FALSE.,
```

/

## end\_input

```
# ivctype=1, vcflat=0.220,
```

```
# vcoord_d = 0.020, 0.032, 0.050, 0.065, 0.080, 0.095, 0.110, 0.125, 0.140,
#      0.155, 0.170, 0.185, 0.200, 0.230, 0.260, 0.290, 0.320, 0.350,
#      0.382, 0.414, 0.446, 0.478, 0.510, 0.542, 0.574, 0.606, 0.638,
#      0.670, 0.702, 0.732, 0.760, 0.786, 0.810, 0.832, 0.852, 0.870,
#      0.886, 0.901, 0.915, 0.929, 0.943, 0.957, 0.970, 0.982, 0.992, 1.000
#      'PLCOV  ', 'LAI  ', 'ROOTDP  ', 'VIO3  ',
#      'HMO3  ', 'U  ', 'V  ', 'W  ',
#      'T  ', 'QV  ', 'QC  ', 'PP  ',
#      'T_SNOW  ', 'T_S  ', 'T_M  ', 'QV_S  ',
#      'W_SNOW  ', 'W_I  ', 'W_G1  ', 'W_G2  '
# yvarini='PLCOV  ', 'ROOTDP  ', 'LAI  ', 'VIO3  ',
#      'HMO3  ', 'T_CL  ', 'W_CL  ', 'HSURF  ',
#      'FR_LAND  ', 'W_CL  '
# ymode_write='a ',
# ybitmap_cat='/home/cosmo/const',
# ybitmap_lfn='bitmap516',
```

```
#####
```

```
# run the program
```

```
#####
```

```
export LIBDWD_BITMAP_TYPE=ASCII
```

```
export
```

```
GRIB_DEFINITION_PATH=/home/cosmo/int2lm_110311_1.18/TABLES_1.9.5_COSMO/
definitions.edzw:/home/cosmo/int2lm_110311_1.18/TABLES_1.9.5_COSMO/definitions
```

```
#export MPIPROGINF=yes
```

```
export MPIPROGINF=ALL_DETAIL
```

```
export MPISUSPEND=on
```

```
#export F_FTRACE=yes
```

```
export F_ERRCNT=0
```

```
export F_ERROPT1=255,255,0,0,2,2,2,2
```

```
export F_ERROPT2=253,253,0,0,0,0,2,2
```

```
export GRIB_API_IO_BUFFER_SIZE=67108864
```

```
export MPIEXPORT="GRIB_API_IO_BUFFER_SIZE F_ERROPT1 F_ERROPT2
F_ERRCNT MPIPROGINF F_PROGINF LIBDWD_MPIEXPORT"
```

```
#mpirun -np $NP /usr/local/pkg/for0adm/abs/int2lm
#mpirun -np $NP
./tstint2lm
ftrace -all -f ftrace.out* -fmt l
rm -f mon.out.* ftrace.out.*
#machine specific for IBM
#export MP_LABELIO=yes
#export MP_SHARED_MEMORY=yes
#export MP_WAIT_MODE=poll
##export MP_INFOLEVEL=2
#export MP_TASK_AFFINITY=mcm
#export MEMORY_AFFINITY=mcm
#export MP_SINGLE_THREAD=yes
#
#poe
./tstint2lm
#####
# cleanup
#####
rm INPUT
****
chmod u+x gme2cosmo_job
nqsub gme2cosmo_job
rm gme2cosmo_job
```



## APPENDIX E: The runtime control parameters of the COSMO Model

```
#!/bin/ksh
#
# The LM Job
#
rm -f cosmo_eu_job
#####
# number of processors
#####
NPX=1
NPY=16
NPIO=0
NNP=4
NP1=`expr $NPX \* $NPY`
NP=`expr $NP1 + $NPIO`
N1=`expr $NP + 15`
NODES=`expr $N1 \ / 16`
NN=`expr $NPY \ / $NNP`

DATE=2012053106
INIDIR=/home/cosmo/COSMO_EU_input_$DATE
BD_DIR=/home/cosmo/COSMO_EU_input_$DATE
OBSDIR=/home/cosmo/COSMO_EU_mld_$DATE
OUTPUT=/home/cosmo/COSMO_EU_output
RESTAR=/home/cosmo/COSMO_EU_output
cat > cosmo_eu_job << ****
#####
# batch commandos
#####
#PBS -q normal
####PBS -l cpunum_job=$NPY
####PBS -b $NODES
#PBS -l cpunum_job=$NNP
#PBS -b $NN
#PBS -T mpisx
```

```

#PBS -j o
#PBS -N cosmo_eu_test
cd /home/cosmo_110525_4.18
# for IBM in Reading
# @ shell=/usr/bin/ksh
# @ output=cosmoeu.out
# @ error=cosmoeu.out
# @ job_type=parallel
# @ class=np
# @ initialdir=.
# @ network.MPI=sn_all,shared,us
# @ notification=never
# @ ec_smt=no
# @ node=$NODES
# @ total_tasks=$NP
# @ queue

#####
# global settings
#####

rm -f YU* M_*
rm -f $OUTPUT/1*
rm -f $RESTAR/1*

#####
# cat together the INPUT*-files
#####

cat > INPUT_ORG << end_input_org

&LMGRID

startlat_tot = 15.0, startlon_tot = 23.0,
pollat=40.0,    pollon=-170.0,
dlat=0.0625,   dlon=0.0625,
ie_tot=665,    je_tot=657,    ke_tot=40,
startlat_tot = 15.0, startlon_tot = 23.0,
pollat=90.0,    pollon=-180.0,
dlon=0.0625,    dlat=0.0625,
ielm_tot=201,   jelm_tot=193,   kelm_tot=316,

```

```

ke_soil_lm=7,
/
&RUNCTL
hstart = 0.0, hstop = 1.0, dt = 66.0, ydate_ini='$DATE',
nprocx = $NPX, nprocy = $NPY, nprocio = $NPIO,
lphys = .TRUE., luse_rttov = .TRUE., luseobs = .FALSE., leps = .FALSE.,
lreorder = .FALSE., lreproduce = .TRUE., itype_timing = 4,
ldatatypes = .FALSE., ltime_barrier = .FALSE., ncomm_type=3,
nboundlines=3, idbg_level = 2, lartif_data=.FALSE,
ldfi=.TRUE.,
/
&TUNING
c_soil = 1.0,
clc_diag = 0.5,
crsmin = 150.0,
qc0 = 0.0,
q_crit = 4.0,
qi0 = 0.0,
rat_can = 1.0,
rat_lam = 1.0,
tur_len = 500.0,
v0snow = 25.0,
wichfakt = 0.0,
/
end_input_org
cat > INPUT_INI << end_input_ini
&INICTL
ndfi = 1,
nfilt = 1,
tspan = 3600.0,
dtbak = 60.0,
dtfwd = 60.0,
taus = 3600.0,
/
end_input_ini

```

```

#cat > INPUT_SAT << end_input_sat
#&SATCTL
#itype_rtov=9,
#num_sensors=1,
#sat_input_01='MSG' ,2,'SEVIRI',8,.TRUE.,.TRUE.,.TRUE.,.TRUE.,
#nchan_input_01=1,2,3,4,5,6,7,8
#lcon_clw=.TRUE., extrp_type=2, iwc2effdiam=1, iceshape=1,
/
#end_input_sat
cat > INPUT_IO << end_input_io
&IOCTL
  lasync_io=.FALSE., l_ke_in_gds=.TRUE., ngribout=1,
! nsma_stat=20,
! nhour_restart=5,6,1
! ydir_restart='$RESTAR',
! ytunit_restart='f',
! ytrans_in='/gtmp/uschaett/LM_TEST/LMQ_input/ready/',
! ninccwait=30,
! nmaxwait=2400,
/
&DATABASE
/
&GRIBIN
  lan_t_so0=.TRUE., lan_t_cl=.TRUE., lan_w_cl=.TRUE., lan_vio3=.TRUE.,
  lan_hmo3=.TRUE., lan_plcov=.TRUE., lan_lai=.TRUE., lan_rootdp=.TRUE.,
  lan_t_snow=.TRUE., lan_w_i=.TRUE., lan_w_snow=.TRUE., lan_rho_snow=.TRUE.,
  hincbound=1.0,
  lchkini=.TRUE., lchkbd=.TRUE., lbdana=.FALSE.,
  lana_qi=.TRUE., llb_qi=.TRUE., lana_rho_snow=.TRUE.,
  lana_qr_qs=.TRUE., llb_qr_qs=.TRUE.,
  ydirini='$INIDIR',
  ydirbd='$BD_DIR',
/
&GRIBOUT
  hcomb=0,78,1.,

```

```

lanalysis=.false.,
lcheck=.true.,
lwrite_const=.true.,
l_p_filter=.true.,
l_z_filter=.true.,
ysystem='file',
yvarml='U      ','V      ','W      ','T      ',
      'QV      ','QC      ','QI      ','P      ',
      'TKE      ','CLC      ',
      'PS      ','T_SNOW      ','T_S      ','W_SNOW      ',
      'QV_S      ','W_I      ','RAIN_GSP      ','SNOW_GSP      ',
      'RAIN_CON      ','SNOW_CON      ','U_10M      ','V_10M      ',
      'T_2M      ','TD_2M      ','TMIN_2M      ','TMAX_2M      ',
      'VMAX_10M      ','TCM      ','TCH      ','CLCT      ',
      'CLCH      ','CLCM      ','CLCL      ','ALB_RAD      ',
      'ASOB_S      ','ATHB_S      ','ASOB_T      ','ATHB_T      ',
      'APAB_S      ','ASWDIR_S      ','ASWDIFD_S      ','ASWDIFU_S      ',
      'TOT_PREC      ','Z0      ','AUMFL_S      ','AVMFL_S      ',
      'ASHFL_S      ','ALHFL_S      ','BAS_CON      ','TOP_CON      ',
      'HTOP_DC      ','RUNOFF_S      ','RUNOFF_G      ','PMSL      ',
      'T_G      ','HTOP_CON      ','HBAS_CON      ','HZEROCL      ',
      'CLCT_MOD      ','CLDEPTH      ','TDIV_HUM      ','TWATER      ',
      'AEVAP_S      ','CAPE_CON      ','TQI      ','TQC      ',
      'TQV      ','TQR      ','TQS      ','T_SO      ',
      'W_SO      ','W_SO_ICE      ','FRESHSNW      ',
      'SNOWLMT      ','RHO_SNOW      ','H_SNOW      ',
      'RELHUM_2M      ','ZHD      ','ZTD      ','ZWD      ',
      'CAPE_ML      ','CIN_ML      ',
      'T_MNW_LK      ','T_WML_LK      ','T_BOT_LK      ','C_T_LK      ',
      'H_ML_LK      ','T_ICE      ','H_ICE      ',
yvarpl='T      ','RELHUM      ','U      ','V      ',
      'FI      ','OMEGA      ',
yvarzl='T      ','RELHUM      ','U      ','V      ',
      'P      ','W      ',
yvars1='SYNMSG',

```

```

    zlev=500.0,1000.0,1500.0,2000.0,3000.0,5000.0,
    ydir='$OUTPUT',
/
end_input_io
cat > INPUT_DYN << end_input_dyn
&DYNCTL
    betasw=0.4,
    epsass=0.15,
    hd_corr_p_bd=0.0,
    hd_corr_p_in=0.0,
    hd_corr_q_bd=0.0,
    hd_corr_q_in=0.0,
    hd_corr_t_bd=0.0,
    hd_corr_t_in=0.0,
    hd_corr_u_bd=0.25,
    hd_corr_u_in=0.25,
    hd_dhmax=250.,
    iadv_order=3,
    irk_order=3,
    irunge_kutta=1,
    itype_bbc_w=2,
    itype_hdiff=2,
    itype_outflow_qrsg=1,
    l2tls=.true.,
    lcond=.true.,
    ldyn_bbc=.true.,
    ldiabf_lh=.true.,
    lexp_lbc=.true.,
    y_scalar_advect='SL3_MF',
    lspbc=.true.,
    nrdtau=5,
    rlwidth=85000.0,
    xkd=0.1,
/
end_input_dyn

```

```

cat > INPUT_PHY << end_input_phy
&PHYCTL
  lgsp=.TRUE.,
  lprogprec=.TRUE.,
  ltrans_prec=.TRUE.,
  itype_gscp=3,
  lrad=.TRUE.,
  nradcoarse=1,
  lradf_avg=.FALSE.
  hincrad=1.0,
  lforest=.TRUE.,
  itype_aerosol=0
  ltur=.TRUE.,
  ninctura=1,
  lexcor=.FALSE.,
  ltmpcor=.FALSE.,
  lprfcor=.FALSE.,
  lnonloc=.FALSE.,
  lcpfluc=.FALSE.,
  itype_turb=3,
  imode_turb=1,
  itype_tran=2,
  imode_tran=1,
  itype_wcld=2,
  icldm_rad =4,
  icldm_turb=2,
  icldm_tran=0,
  itype_synd=2,
  limpltkediff=.TRUE.,
  lsoil=.TRUE.,
  itype_evsl=2,
  itype_trvg=2,
  lmulti_layer=.TRUE.,
  lmelt=.TRUE.,

```

```

lmelt_var=.TRUE.,
ke_soil = 7,
czml_soil = 0.005, 0.02, 0.06, 0.18, 0.54, 1.62, 4.86, 14.58,
llake=.TRUE.,
lseoice=.TRUE.,
lconv=.TRUE.,
nincconv=4,
itype_conv=0,
lcage=.FALSE.,
lsso=.TRUE.,
/
end_input_phy
cat > INPUT_DIA << end_input_dia
&DIACTL
n0meanval=0, nincmeanval=1,
lgplong=.TRUE., lgpsort=.FALSE., lgpspec=.FALSE.,
n0gp=0, hincgp=1.0,
end_input_dia

cat > INPUT_EPS << end_input_eps
&EPSCTL
iepsmem=0, iepstyp=55, iepstot=15,
/
end_input_eps
cat > INPUT_ASS << end_input_ass
&NUDGING
lnudge =.true.,
itype_obfile = 2,
ycdfdir='$OBSDIR/',
hnudgsta = 0.0, hnudgend = 4.0, tconbox = 240.0,
lverif =.true.,
llhn =.false., llhnverif=.false., lhn_wweight=.true.,
rqrgmax= 0.4,
radar_in='./',
hversta = 0.001, hverend = 4.0,

```



```

khumbal = 100,
mruntyp = 2,
ntpscor = 1, ptpstop=400.0, luvgor=.TRUE.,
ltpol =.TRUE., tipolmx = 3.0, wtukrsa = 3.0, wtukrse = 1.0,
ltipsu =.TRUE., tipmxsu = 1.0, wtuksua = 1.5, wtuksue = 0.5,
                wtukara = 1.5, wtukare = 0.5,
msrpar = 1, msrpsu = 0,
gnudg  = 0.0006, 0.0012, 0.0006, 0.0006,
gnudgsu = 0.0006, 0.0012, 0.0000, 0.0006,
gnudgar = .0006, .0000, .0006, .0000,
vcorls = .333 , .333 , .04 , .04 , vcutof = 0.75, 0.75, 1.0 , 1.0 ,
vcorlsu = .013 , .013 , .002 ,.00001, vcutosu = 0.75, 0.75, 4.0 ,0.001,
vcsnisu = 2500., 2500., 9. , 9. ,
                rhvfac = 1.0 , 0.0 , 0.83, 0.83,
rhinfl = 0., 70., 0., 0., rhtfac = 1.3 , 1.43, 1.3 , 1.3 ,
rhiflsu = 70., 70., 100., 70., rhtfsu = 1.0 , 1.43, 1.0 , 1.0 ,
fnondiv = 0.8 , cnondiv = 0.1 , cutofr = 3.5 , 3.5 , 3.5 , 3.5 ,
tnondiv = 1.1 ,                cutofsu = 2.0 , 3.5 , 2.0 , 2.0 ,
topobs = 849., 1099., 799., 699.,
botmod = 1099., 1099., 1099., 899.,
lscadj =.TRUE.,.TRUE.,.TRUE.,.FALSE.,
dtqc  = 720.,                qcvf  = 5.00, 1.00,10.00, 1.00,
qcc  = 0.00,500.00, 0.00, 0.00,
qccsu = 12., 500., 12., .7,
lsynop =.true.,
laircf =.true.,
ldribu =.true.,
ltemp  =.true.,
lpilot =.true.,
lcd132 =.true., lcd133=.false., lcd136=.false.,
maxmlo = 1600, maxsgo = 5000, maxuso = 5000, nolbc = 5,
altopsu = 100., 5000., 5000., 5000., thairh = 20.,
exnlat = 90., exslat =-90., exwlon = -180., exelon = 180.,
lsurfa =.false.,
lt2m  =.false., ht2a = 0., ht2i = 1.,

```

```

lrh2m =.false., hh2a = 0., hh2i = 1.,
lprec =.false., hprc = 0., raintp = 12.,
lpraof =.false., lprodr =.true. , ldiasa =.true., noctrq = 9,
dinlat = 55., dislat = 45., diwlon = 7., dielon = 14.,
ionl =167, jonl=103, ionl2 =167, jonl2 =103,
lff10m =.true., hffa=0., hffi=1.,

```

```
/
```

```
end_input_ass
```

```
#####
```

```
run the program
```

```
#####
```

```
./tstint_lm
```

```
#####
```

```
# machine specific for NEC
```

```
rm -f mon.out.* ftrace.out.*
```

```
export MPIPROGINF=yes
```

```
#export MPISUSPEND=on
```

```
export MPIPROGINF=ALL_DETAIL
```

```
#export F_FTRACE=yes
```

```
export F_ERROPT1=255,255,0,0,2,2,2,2
```

```
#export F_ERROPT2=253,253,0,0,0,0,2,2
```

```
export F_ERRCNT=0
```

```
#export C_SETBUF_VERBOSE=YES
```

```
export C_SETBUF=48M
```

```
export MPIEXPORT="F_ERRCNT F_ERROPT1 F_ERROPT2 MPIPROGINF
```

```
F_PROGINF $LIBDWD_MPIEXPORT C_SETBUF C_SETBUF_VERBOSE"
```

```
#mpirun -nn $NN -nnp $NNP lmparbin_all
```

```
./tstint_lm
```

```
ftrace -all -f ftrace.out* -fmtl
```

```
rm -f mon.out.* ftrace.out.*
```

```
#####
```

```
# machine specific for IBM
```

```
#export MP_LABELIO=yes
```

```
#export MP_SHARED_MEMORY=yes
```

```

#export MP_WAIT_MODE=poll
##export MP_INFOLEVEL=2
#export MP_TASK_AFFINITY=mcm
#export MEMORY_AFFINITY=mcm
#export MP_SINGLE_THREAD=yes
#poe ../../lmbin
#####
#####
# cleanup
#####
rm -f INPUT_ORG INPUT_IO INPUT_DYN INPUT_DIA INPUT_PHY INPUT_INI
rm -f INPUT_ASS INPUT_SAT INPUT_EPS
****
chmod u+x cosmo_eu_job
nqsub cosmo_eu_job
#lsubmit cosmo_eu_job
rm cosmo_eu_job

```